

NASA
Reference
Publication
1274

February 1992

Propagation Effects
for Land Mobile
Satellite Systems:
Overview of Experimental
and Modeling Results

Julius Goldhirsh
and Wolfhard J. Vogel

NASA

**NASA
Reference
Publication
1274**

1992

**Propagation Effects
for Land Mobile
Satellite Systems:
Overview of Experimental
and Modeling Results**

Julius Goldhirsh
*The Johns Hopkins University
Applied Physics Laboratory
Laurel, Maryland*

Wolfhard J. Vogel
*The University of Texas
Electrical Engineering Research Laboratory
Austin, Texas*

NASA

National Aeronautics and
Space Administration
Office of Management
Scientific and Technical
Information Program

Acknowledgments

The authors are grateful to the following individuals who reviewed the preliminary text (formerly titled, "Propagation Handbook for Land-Mobile-Satellite Systems"). The reviewers, listed in alphabetic order, offered useful and constructive comments which are addressed in this revised manuscript.

John Butterworth
Department of Communications
Communications Research Centre
3701 Carling Ave
P. O. Box 11490, Station H
Ottawa, Ontario K2H 1S8
Canada

Faramaz Davarian
Jet Propulsion Laboratory
Mail Stop: 161-228
4800 Oak Grove Drive
Pasadena, California 91109

Kim Dinh
MOBILESAT
Austrian National Satellite System (AUSSAT)
54 Carrington Street
Sydney, 2000, Australia

Gary C. Hess
Land Mobile Products Sector Research
1301 E. Algonquin Road, Room 2240
Schaumburg, IL 60196

Peter Kinman
Jet Propulsion Laboratory
Mail Stop: 161-228
4800 Oak Grove Drive
Pasadena, California 91109

Chun Loo
Department of Communications
Communications Research Centre
3701 Carling Avenue
P.O. Box 11490, Station H
Ottawa, Ontario K2H 8S2

Mario Sforza
European Space Agency (ESA)
European Space Research and Technology Centre
Electromagnetic Division
Postbus 299
NL-2200 AG Noordwijk

Ernest K. Smith
NASA Propagation and Information Center
Dept. of Electrical and Computer Engineering
Campus Box 425
University of Colorado
Boulder, CO 80309-0425

Harry Smith
University of Bradford
Department of Electrical Engineering
Bradford, West Yorkshire
BD7 1DP, United Kingdom

Warren L. Stutzman
Virginia Polytechnic Institute and State University
The Bradley Department of Electrical Engineering
Virginia Tech Satellite Communications Group
Blacksburg, Virginia 24061-0111

The authors are particularly grateful to John Kiebler, Faramaz Davarian, and Ernest Smith for their sustained guidance and support during the writing of this text. The preparation of this text and much of its background research was funded by the Communications and Information Systems Division of NASA Headquarters and the NASA Office of Commercial Programs for the Johns Hopkins University (Contract #N00039-89-C-0001), and by The Jet Propulsion Laboratory for the University of Texas (Contract #JPL956520).

Foreword

This NASA Reference Publication has been prepared through the joint efforts of Dr. Julius Goldhirsh of The Johns Hopkins University Applied Physics Laboratory and Dr. Wolfhard J. Vogel of The University of Texas Electrical Engineering Research Laboratory . It was developed under NASA's Radio Science and Support Studies Program, which with its predecessor programs, has been involved for two decades in the study of radiowave propagation over earth-space paths.

Much work has been carried out during the last 10 years to measure and model the impairments to which communications via land-mobile satellites are subjected due to propagation effects. This topic was given the highest priority for NASA supported propagation studies in the United States for several years. Significant contributions have also been made by researchers in a number of other countries. International cooperation has facilitated the acquisition of propagation measurements using actual satellite paths. The authors' Australian campaign, for example, relied on the use of Japan's ETS-V satellite, INMARSAT's Pacific satellite, and the participation of the AUSSAT organization. Measurements taken in Maryland were achieved through the cooperation of INMARSAT, this time through use of the MARECS B-2 satellite.

The objective of this document is to distill the important results pertaining to the measurements and analyses of propagation as relevant to land-mobile satellite systems and to present them in a single reference. Beyond this objective, a need was perceived to present the information in a form that would be most useful for engineers concerned with the design of land-mobile satellite systems.

This publication takes its place along side of the two NASA handbooks on propagation, Propagation Effects on Satellite Systems at Frequencies Below 10 GHz - A Handbook for Satellite Systems Design, NASA Reference Publication 1108 (02), 1987 and Propagation Effects Handbook for Satellite Systems Design - A Summary of Propagation Impairments on 10 to 100 GHz Satellite Links With Techniques for System Design, NASA Reference Publication 1082 (04), 1989. As in the case of the handbooks, comments regarding this document are welcome.

John W. Kiebler
NASA Headquarters
Office of Commercial Programs

Contents

1	Introduction	1
1.1	Why This Text?	1
1.2	Background	2
1.3	Objectives	2
2	Attenuation Due to Individual Trees: Static Case	5
2.1	Background	5
2.2	Attenuation and Attenuation Coefficient	7
2.3	L-Band Versus UHF Attenuation Scaling Factor: Static Case	11
2.4	Effects on Attenuation Caused by Season and Path Elevation Angle	12
3	Attenuation Due to Roadside Trees: Mobile Case	15
3.1	Background	15
3.2	Time-Series Fade Measurements	16
3.3	Empirical Roadside Shadowing Model	16

3.4	Validation of the Empirical Roadside Shadowing Model	23
3.5	L-Band Versus UHF Attenuation Scaling Factor: Dynamic Case	27
3.6	Seasonal Effects on Attenuation – Dynamic Case	28
3.7	Fade Reduction Due to Lane Diversity	29
4	Signal Degradation for Line-of-Sight Communications	34
4.1	Background	34
4.2	Multipath for A Mountain Environment	35
4.3	Multipath Due to Roadside Trees	37
5	Fade and Non-Fade Durations and Phase Spreads	40
5.1	Background	40
5.2	Experimental Aspects	41
5.3	Cumulative Distributions of Fade Durations	41
5.4	Cumulative Distributions of Non-Fade Durations	46
5.5	Cumulative Distributions of Phase Fluctuations	48
6	Propagation Effects Due to Cross Polarization, Gain, and Space Diversity	51
6.1	Background	51
6.2	Frequency Re-Use	52
6.3	Distributions from Low and High Gain Receiving Antennas	52
6.4	Diversity Operation	55

6.4.1	Joint Probabilities	56
6.4.2	Diversity Improvement Factor, DIF	56
6.4.3	Diversity Gain	58
7	Investigations from Different Countries	61
7.1	Measurements in Australia	63
7.2	Measurements In Canada	63
7.3	PROSAT Experiment-Belgium	68
7.4	Measurements Performed in England	68
7.5	Measurements Performed in the United States	71
7.6	Measurements Performed in Japan	72
8	Modeling for LMSS Scenarios	74
8.1	Background	74
8.2	Background Information Associated with Model Development	76
8.2.1	Diffusely Scattered Waves	76
8.2.2	Faraday Rotation	77
8.2.3	Ground Specular Reflection	77
8.3	Empirical Regression Models	78
8.3.1	Large Scale - Small Scale (LS-SS) Coverage Model	79
8.3.2	Empirical Roadside Shadowing Model	85

8.4	Probability Distribution Models	86
8.4.1	Density Functions Used In Propagation Modeling	87
8.4.2	Loo's Distribution Model	90
8.4.3	Total Shadowing Model	93
8.4.4	Lognormal Shadowing Model	95
8.4.5	Simplified Lognormal Shadowing Model	97
8.4.6	Models With Fade State Transitions	100
8.5	Geometric Analytic Models	103
8.5.1	Single Object Models	103
8.5.2	Multiple Object Scattering Models	109
8.6	General Conclusions	112
8.7	Recommendations and Follow-On Efforts	113
	References	115
	Index	120

List of Figures

2.1	LMSS propagation path shadowed by the canopies of one or two trees in which the attenuation path length is relatively well defined.	6
2.2	Low elevation propagation through a grove of trees giving rise to ambiguity in attenuation path length.	7
2.3	Least square linear fits of attenuation versus elevation angle for propagation through the canopy of a Callery Pear Tree at 870 MHz for a LMSS Configuration.	13
3.1	Time-series of fades (a) and phases (b) over a one second period at a sampling rate of 1 KHz in a flat rural region where the line-of-sight was unshadowed. .	17
3.2	Time-series of fades (a) and phases (b) over a one second period at a sampling rate of 1 KHz in a suburban region with roadside trees where the line-of-sight was shadowed.	18
3.3	Cumulative fade distributions at 1.5 GHz for family of path elevation angles derived from the Empirical Roadside Shadowing model.	21
3.4	L-Band fade exceeded versus path elevation angle for family of indicated constant percentages (ERS model).	23
3.5	Comparison of Australian fade distribution comprising 15 runs with ERS model.	25
3.6	ERS and Australian fade distributions for different elevation angles from measurements obtained with INMARSAT Pacific (40°) and ETS-V (51°).	26

3.7	Mobile-satellite configurations depicting (a) larger intersecting path length with tree canopy when vehicle is driven in the right lane, and (b) smaller intersecting path length when vehicle is driven in the left lane.	30
3.8	Best fit fade reduction at 1.5 GHz versus equi-probability attenuation at path elevation angles of 30°, 45°, and 60°.	32
3.9	Best fit fade reduction at 870 MHz versus equi-probability attenuation at path elevation angles of 30°, 45°, and 60°.	33
4.1	Best fits power curve cumulative fade distributions of form (4.1) for line of sight distributions in which multipath fading dominates for mountainous terrain.	36
4.2	Best exponential fit cumulative fade distributions of the form (4.2) for line of sight distributions in which multipath fading dominates for tree-lined roads.	39
5.1	Best fit exponential fade distributions of the form (5.3) derived from measurements in South-Eastern Australia along road-types classified as “moderate” and “extreme”. Measurements were made at a path elevation of 51°.	43
5.2	Best fit log-normal distribution (5.1) depicting fade durations for a 5 dB threshold. The distribution encompasses road types which exhibit “moderate” and “extreme” shadowing. The distribution is plotted on logarithmic scales for convenience.	45
5.3	Best fit power curves (5.6) depicting non-fade durations for a 5 dB threshold for road types which exhibit “moderate” and “extreme” shadowing.	47
5.4	“Best polynomial fit” (5.8) cumulative phase distributions for road types which exhibit “moderate” and “extreme” shadowing for a 5 dB fade threshold.	50
6.1	Cross-polarization isolation (CPI) as a function of co-polarization fade.	53
6.2	Fade measured by high gain receiver system versus fade measured by low gain system at equi-probability levels.	54

6.3	Single and joint probability fade distributions for mobile communications operating in a space diversity mode with antennas separated by the distance, d	57
6.4	Diversity Improvement Factors (DIF) as a function of fade depth for a family of antenna separation distances.	59
6.5	Diversity gain versus antenna separation distance for a family of single terminal fade levels.	60
7.1	Cumulative fade distributions at various elevation angles derived by Bundrock and Harvey [1988] for Melbourne Australia at 1.55 GHz for a tree lined road having a 85% tree incidence.	64
7.2	Cumulative fade distributions at UHF, L-Band, and S-Band derived by Bundrock and Harvey [1988] for Melbourne Australia at an elevation angle of 45°	65
7.3	Cumulative fade distribution at UHF (870 MHz) in Ottawa, Ontario, Canada derived from helicopter measurements in a rural region (35% woodland) [Butterworth, 1984b].	66
7.4	Cumulative fade distribution at L-Band (1.5 GHz) in Ottawa, Ontario, Canada derived from MARECS A satellite measurements in rural and suburban regions at 19° elevation [Butterworth, 1984a].	67
7.5	Fade distribution for a rural region at 1.5 GHz derived from measurements in Belgium in January 1984 [Jongejan et al., 1986].	69
7.6	Fade distributions (L-Band) for tree shadowed environments in England for different elevation angles [Renduchintala et al., 1990; Smith et al., 1990]. . .	70
7.7	Fade distributions at L-Band for two expressways and an "old road" in Japan [Saruwatari and Ryuko, 1989].	73
8.1	Probability distributions for LS-SS model for family of elevation angles and indicated small scale probabilities P_s	84

-
- 8.2 Typical fade distributions calculated from the Simplified Lognormal Shadowing Model for light (L), and heavy (H) shadowing, and for infrequent (I; $S = 0.25$), moderate (M; $S = 0.5$), and frequent (F; $S = 0.75$) shadowing occurrences. 98
- 8.3 Typical fade distributions calculated from the Simplified Lognormal Shadowing Model for medium shadowing (M), and for infrequent (I; $S = 0.25$), moderate (M; $S = 0.5$), and frequent (F; $S = 0.75$) shadowing occurrences. . 99
- 8.4 Propagation geometry for single object scattering in which a vehicle traveling at a speed v carries an antenna with a given pattern along the x-axis 104
- 8.5 Measured L-Band signal level and phase fluctuations as a function of time relative to arbitrary reference as receiving vehicle passes by a wooden utility pole with a metal cross bar. The vehicle closest approach to the pole occurs at 540 ms. 106
- 8.6 Calculated L-Band signal level and phase fluctuations as a function of time for geometry of Figure 8.4 107
- 8.7 Calculated Doppler spectrum due to single multipath reflector averaged over one second, while the vehicle is driving past the scatterer. 111

List of Tables

1.1	Land-mobile propagation measurement campaigns of EERL, University of Texas, and APL, The Johns Hopkins University.	4
2.1	Summary of Single Tree Attenuations at $f = 870$ MHz	9
2.2	Summary of Experimental Parameters Associated with Source and Receiver System Platforms	10
3.1	Coefficients M and N As a function of θ for Equation (3.1)	20
3.2	Listing of parameter values $\alpha(P)$, $\beta(P)$, and $\gamma(P)$ in equation (3.5)	23
3.3	Summary of Pertinent Transmitter-Receiver System Parameters for Australian Campaign [Vogel et al., 1991].	24
3.4	Fades at the 1% and 10% levels derived from the multifrequency measurements of Bundrock and Harvey [1988]. Also shown in parentheses are the predicted levels employing frequency scaling and the UHF values.	28
3.5	Coefficients of fade reduction formulation (3.9) for lane diversity at $f = 1.5$ GHz.	31
3.6	Coefficients of fade reduction formulation (3.9) for lane diversity at $f = 870$ MHz.	31

4.1	Coefficients a and b in formulation (4.1) describing best fit cumulative fade distribution for multipath in mountainous terrain	37
4.2	Coefficients u and v in formulation (4.2) describing best exponential fit cumulative fade distributions for multipath for tree-lined roads.	38
5.1	Best fit exponential cumulative fade distributions parameters u and v from form (5.3) derived from measurements on roads exhibiting “extreme” and “moderate” shadowing for a path elevation angle of 51°	42
5.2	RMS deviations relative to log-normal fit ($\alpha = 0.22, \sigma = 1.215$) of cumulative distributions of fade durations (threshold of 5 dB) for various runs exhibiting moderate and extreme shadowing [Equation (5.1)].	44
5.3	Non-fade duration regression values of β and γ satisfying the power expression (5.6) at a 5 dB threshold for road-types exhibiting “moderate” and “extreme” shadowing at a path elevation angle of 51°	46
5.4	Listing of polynomial coefficients characterizing phase fluctuation distributions of the form (5.8) for road types exhibiting “moderate” and “extreme” shadowing and a 5 dB fade threshold	49
6.1	Summary of pertinent characteristics for high and low gain receiver antennas used during the Australian campaign [Vogel et al., 1991]	55
7.1	Comparison of L-Band fade levels at 1% and 10% probabilities derived from cumulative distributions in different countries.	62
8.1	Parameter Definition and Values for Hess Model	81
8.2	Coefficients In LS-SS Fade Model	82
8.3	Parameters for Loo’s Model	91
8.4	Typical Parameters for Total Shadowing Model of Lutz et al. [1986]	95

LIST OF TABLES

8.5 Parameter Values for the Lognormal Shadowing Model 96

8.6 Parameters for 2-State Model 101

Chapter 1

Introduction

1.1 Why This Text?

During the period 1983-88, a series of experiments (Table 1.1) were undertaken by the Electrical Engineering Research Laboratory of The University of Texas and the Applied Physics Laboratory of The Johns Hopkins University in which propagation impairment effects were investigated for Land Mobile Satellite Service (LMSS) configurations. Other significant LMSS propagation investigations were performed in the United States [Hess, 1980], in Canada [Butterworth, 1984a; 1984b], and in Europe [Jongejans et al., 1986]. More recently, LMSS propagation measurements were reported from Australia [Bundrock, 1988], and England [Renduchintala et al., 1990].

The results described here are mostly derived from systematic studies of propagation effects for LMSS geometries in the United States associated with rural and suburban regions. Descriptions of these efforts have appeared in a number of technical reports, conference proceedings and publications. The rationale for the development of this text was to locate the salient and useful experimental and modeling results in one single document for use by communications engineers, designers of planned LMSS communications systems, and modelers of propagation effects. This text should complement the Handbook by Flock [1987], where fundamental propagation effects are described for satellite systems operating at frequencies below 10 GHz.

Where applicable, the authors have also liberally drawn from the results of the other related investigations. The results are presented in a “user friendly style” in the form of graphs, tables, and “best fit” analytic functions.

1.2 Background

Propagation experiments were performed by the authors in the Southern United States (New Mexico to Alabama), Virginia, Maryland, Colorado, and South-Eastern Australia. These experiments were executed with transmitters on stratospheric balloons, remotely piloted aircraft, helicopters, and geostationary satellites (MARECS B-2, Japanese ETS-V, and INMARSAT Pacific). The earlier experiments were performed at UHF (870 MHz), followed by simultaneous measurements at L-Band (1.5 GHz) and UHF. The satellite measurements were performed only at L-Band. During these experiments, the receiver system was located in a van outfitted with the UHF and L-Band antennas on its roof, and receivers and data acquisition equipment in its interior.

1.3 Objectives

The general objectives of the above tests were to assess the various types of impairments to propagation caused by trees and terrain for predominantly rural and suburban regions where terrestrial cellular communication services are presently non-existent and commercially impractical. Data acquired from the above experiments and other investigations have provided insight into the following LMSS propagation related characteristics described in this text:

- Attenuation and attenuation coefficients due to various tree types for non-mobile cases and their relation to elevation angle and frequency (Chapter 2).
- Attenuation statistics for mobile cases of roadside trees, including angular, seasonal, and frequency effects (Chapter 3).
- Attenuation statistics for mobile cases of mountainous and roadside tree environments, where line-of-sight propagation is maintained (Chapter 4).

Table 1.1: Land-mobile propagation measurement campaigns of EERL, University of Texas, and APL, The Johns Hopkins University.

Date	Source	Location	Freq.	Objectives	Ref
10/83	Balloon	East Texas to Louisiana	UHF	First U.S. data set for forested and rural roads (600 km), 15°–35°	V and H; 198
1/84	Balloon	East Texas	UHF	150 km, 15°–30°	V and H; 198
11/84	Balloon	East Texas to Alabama	UHF, L	Freq. comparison, variety of roads and terrain, 30°–50°	
6/85	Remotely piloted aircraft	VA	UHF	Single tree attenuation, stationary receiver	V and G; 198
10/85	Helicopter	Central MD	UHF	Systematic roadside tree sampling, single tree attenuation in fall foliage	G and V; 198
3/86	Helicopter	Central MD	UHF	Systematic roadside tree sampling, no foliage	G and V; 198
7/86	Balloon	East Texas to New Mexico	UHF, L	Open terrain, optical sensor, scatter model, 20°–60°	V and H; 198
8/86	Helicopter	Colorado	UHF, L	Mountain roads, canyons, multipath limits	V and G; 198
6/87	Helicopter	Central MD	UHF, L	Systematic roadside tree sampling, full foliage	G and V; 198
12/87	MARECS-B2	Central MD	L	Systematic roadside tree sampling, ERS model	V and G; 1990
10/88	ETS-V and INMARSAT	S.E. Austral.	L	Systematic roadside tree sampling, fade durations, diversity, cross polarization	V et al.; 1991 H et al.; 1991

- Fade duration, non-fade duration and phase characteristics for road-side tree environments (Chapter 5).
- Effects on fade statistics employing different gain antennas, feasibility of frequency re-use, and space diversity modeling (Chapter 6).
- Modeling of propagation effects (Chapter 8).

Also included for completeness are comparisons of fade distribution measurements obtained from various experimenters from different countries (Chapter 7).

We emphasize L-Band since The World Administrative Radio Conference for Mobile Services (WARC-MOB-87) in 1987 had allocated frequencies in this band for both the uplink and downlink modes. In particular, the agreed uplink and downlink bands are: [1] 1631.5 to 1634.5 MHz and 1530 to 1533 MHz, respectively, and [2] 1656.5 to 1660.5 MHz and 1555 to 1559 MHz, respectively, where the first set of bands are to be shared with the maritime mobile satellite service [Bell, 1988].

The results and methods described here deal with propagation for mobile satellite geometries in suburban and rural environments for elevation angles generally above 15°. Results “not” covered are associated with measurements performed in urban environments which may efficiently be serviced by cellular communications. Also, not examined here are measurements which pertain to channel effects associated with wide bandwidth modulated signals; with the exception of fade and non-fade durations and phase spreads (Chapter 5).

Chapter 2

Attenuation Due to Individual Trees: Static Case

2.1 Background

A typical scenario in which fading occurs is depicted in Figure 2.1 which shows a vehicle receiving satellite transmissions. The vehicle, which has an antenna mounted on its roof, is presumed to be at a distance of 10 - 20 m from the roadside trees, and the path to the satellite is generally above 20° in elevation. The antenna is to some extent directive in elevation such that multipath from lower elevation (i.e., near zero degrees and below) is filtered out by the antenna gain pattern characteristics. Although there exist azimuthal multipath contributions, shadowing from the canopies of one or two trees gives rise to the major attenuation contributions. That is, the signal fade for this case is due primarily to scattering and absorption from both branches and foliage where the attenuation path length is the interval within the first few Fresnel zones intersected by the canopies.

This geometry is in contrast to the configuration in which the transmitter and receiver are located near the ground and propagation takes place through a grove of trees as shown in Figure 2.2. The attenuation contribution for this configuration is a manifestation of the combined absorption and multiple scattering from the conglomeration of tree canopies and trunks. An estimation of the attenuation coefficient from attenuation measurements

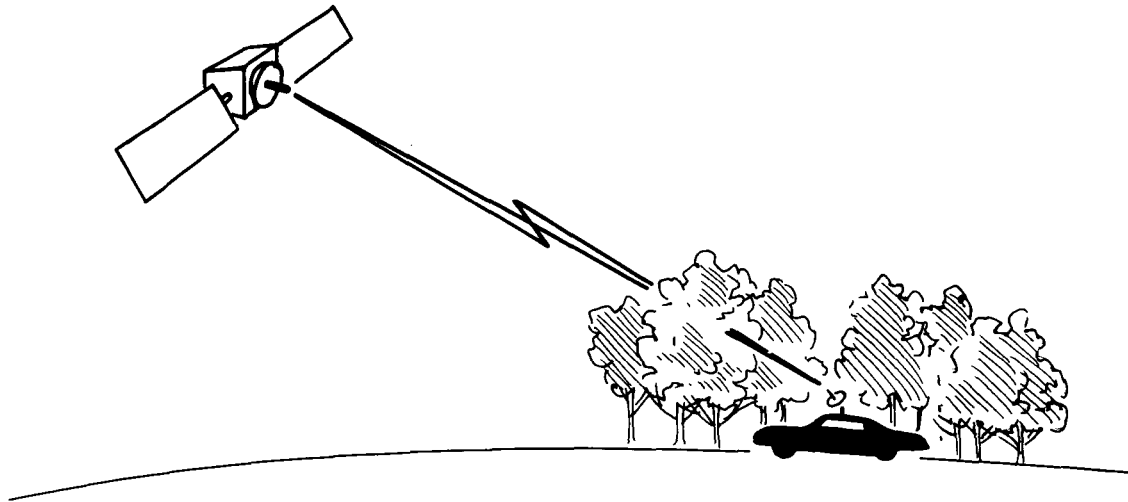


Figure 2.1: LMSS propagation path shadowed by the canopies of one or two trees in which the attenuation path length is relatively well defined.

requires a knowledge of the path length usually estimated to be the “grove thickness”. This thickness may encompass a proportionately large interval of non-attenuating space between the trees. Hence attenuation coefficients as derived for groves of trees [Weissberger, 1982] may underestimate the attenuation coefficient vis a vis those derived for path lengths intersecting one or two contiguous canopies for LMSS scenarios.

Static measurements of attenuation due to isolated trees for LMSS configurations have been systematically performed by only few investigators in the 800 MHz band; namely, Butterworth [1984b], Vogel and Goldhirsh [1986], and Goldhirsh and Vogel [1987]. Ulaby et al. [1990] measured the attenuation properties at 1.6 GHz associated with attenuation through a canopy of foliage comprised of closely spaced trees. Yoshikawa and Kagohara [1989] report briefly on ETS satellite transmissions at 1.5 GHz through a “shade” of trees.

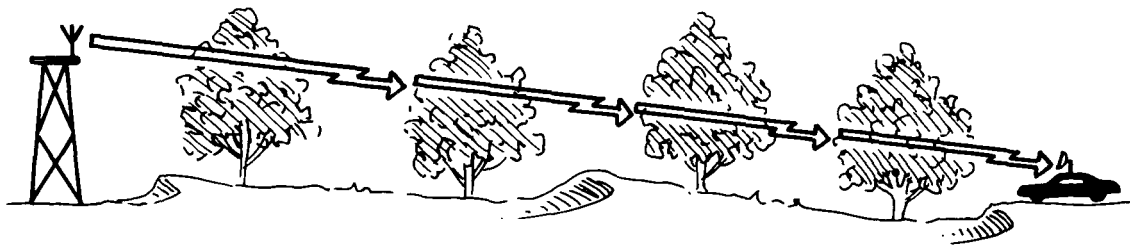


Figure 2.2: Low elevation propagation through a grove of trees giving rise to ambiguity in attenuation path length.

2.2 Attenuation and Attenuation Coefficient

For those cases in which shadowing dominates, the attenuation primarily depends on the path length through the canopy, and the density of foliage and branches in the Fresnel region along the line-of-sight path. The receiver antenna pattern may also influence the extent of fading or signal enhancements via the mechanism of multipath scattering from surrounding trees or nearby illuminated terrain. An azimuthally omni-directional antenna (such as that used for the measurements described here) is more susceptible to such multipath scattering than a directive antenna. Nevertheless, the authors found through measurements and modeling considerations for LMSS geometries, the major fading effect is a result of the extent of shadowing along the line-of-sight direction.

In Table 2.1 is given a summary of the single tree attenuation results at 870 MHz (circularly polarized transmissions) based on the measurements by the authors [Vogel and Goldhirsh, 1986; Goldhirsh and Vogel, 1987] who employed transmitter platforms such as remotely piloted aircraft and helicopters. In Table 2.2 are given the transmitter and receiver characteristics for both the static and mobile measurements. (The static measurements were

performed only at UHF.) The attenuations were calculated by comparing the power changes for a configuration in which the receiving antenna (on the roof of a van) was "in front of" and "behind" a particular tree. The former and latter cases offered non-shadowed and maximum shadowing conditions, respectively, relative to the line of sight propagation path from the transmitter on the aircraft to the stationary receiver. During each flyby, the signal levels as a function of time were expressed in terms of a series of median fades derived from 1024 samples measured over one second periods. The attenuation assigned to the particular flyby was the highest median fade level observed at the measured elevation angle. It may be deduced that the motion of the transmitter aperture and the receiver sampling rate of 1024/s resulted in more than 200 independent samples averaged each second. This sample size is normally adequate to provide a well defined average of a noisy signal. The individual samples from which the median was derived over the one second period were observed to fluctuate on the average ± 2 dB about the median due to the influence of variable shadowing and multipath.

The first column in Table 2.1 lists the trees examined where the presence of an asterisk corresponds to measurement results at Wallops Island, VA in June 1985 (remotely piloted aircraft), and the absence of the asterisk represents measurements in Central MD in October 1985 (helicopter). During both measurement periods, the trees examined were approximately in full foliage conditions. The second and third columns labeled "Largest" and "Average" represent respectively, the largest and average values of attenuation (in dB) derived for the sum total of flybys for that particular tree. The fourth and fifth columns denote the corresponding attenuation coefficients derived from the path length through the canopy. The path length was estimated from measurements of the elevation angle, the tree dimensions, and the relative geometry between the tree and the receiving antenna height. The dependence of the attenuation on elevation angle is described in Section 2.4. We note that the Pin Oak attenuation as measured at Wallops Island (with asterisk) is significantly larger than that measured in Central Maryland (without asterisk) because the former tree had a significantly greater density of foliage over approximately the same path length interval. This result demonstrates that a description of the attenuation from trees for LMSS scenarios may only be handled employing statistical processes.

Butterworth [1984b] performed single tree fade measurements at 800 MHz (circularly polarized transmissions) at seven sites in Ottawa, Canada over the path elevation interval 15° to 20° . The transmitter was located on a tower and receiver measurements were taken at a height of 0.6 m above the ground. Measurements were performed from April 28 to November 4, 1981 covering the period when leaf buds started to open until after the leaves

Table 2.1: Summary of Single Tree Attenuations at $f = 870$ MHz

Tree Type	Attenuation (dB)		Attenuation Coef. dB/m	
	Largest	Average	Largest	Average
Burr Oak*	13.9	11.1	1.0	0.8
Callery Pear	18.4	10.6	1.7	1.0
Holly*	19.9	12.1	2.3	1.2
Norway Maple	10.8	10.0	3.5	3.2
Pin Oak	8.4	6.3	0.85	0.6
Pin Oak*	18.4	13.1	1.85	1.3
Pine Grove	17.2	15.4	1.3	1.1
Sassafras	16.1	9.8	3.2	1.9
Scotch Pine	7.7	6.6	0.9	0.7
White Pine*	12.1	10.6	1.5	1.2
Overall Average	14.3	10.6	1.8	1.3

had fallen from the trees. A cumulative distribution of foliage attenuation readings covering a 19 day period in June 1981 was noted to be lognormal, where the fades exceeded 3 and 17 dB for 80% and 1% of the measured samples, respectively. The median attenuation was approximately 7 dB with an approximate median attenuation coefficient of 0.3 dB/m (24 m mean foliage depth).

The average attenuation coefficient of Butterworth is noted to be smaller than those measured by the authors in Central Maryland and Virginia. The disparity between these results is believed to be due to differences in the methods of averaging, the heights of the receiver, and the interpretation of the shadowing path length as previously described. The results in Table 2.1 may be used by the designer interested in *worst case attenuations* for individual trees.

Table 2.2: Summary of Experimental Parameters Associated with Source and Receiver System Platforms

	L-Band	UHF
Source Platform:		
Antenna Types	Spiral/Conical	Microstrip
Polarization	RHC	RHC
Antenna Beamwidths	60°	60°
Platform Type	Bell Jet Ranger Helo	Remotely Piloted Aircraft
Receiver Platform:		
Antenna Type	Crossed Drooping Dipoles	
Polarization	Right Hand Circular	
Beamwidths	60°(15°to75°)	
Bandwidth (KHz)	0.5	
Sampling Rate (KHz)	1	
Frequencies (MHz)	1502	870
Data Recorded	Quadrature Detected Outputs	Power
	Elapsed Time, Vehicle Speed	

2.3 L-Band Versus UHF Attenuation Scaling Factor: Static Case

To the authors' knowledge, systematic tree measurements at L-Band for different tree types and elevation angles have not been executed, although fade measurements due to roadside trees were noted by Yoshikawa and Kagohara [1989] who received left hand circularly polarized transmissions from the Japanese satellite ETS-V at an elevation of 47°. They reported that attenuations in the "shade" of trees at L-Band ranged between 10 and 20 dB.

Ulaby et al. [1990] measured the attenuation properties at 50° elevation associated with transmission at 1.6 GHz through a canopy of red pine foliage in Michigan at both horizontal and vertical polarizations. The path length through the canopy was approximately 5.2 m and the average attenuations measured at horizontal and vertical polarizations were 9.3 dB and 9.2 dB. Their measurements gave rise to an average attenuation coefficient of approximately 1.8 dB/m. Combining this result at L-band with the average value of 1.3 dB/m at UHF given in Table 2.1 suggests the following

$$A(f_L) \approx A(f_{\text{UHF}}) \sqrt{\frac{f_L}{f_{\text{UHF}}}} \quad (\text{dB}). \quad (2.1)$$

For the frequencies considered

$$\left\{ \begin{array}{l} f_L = 1.6 \text{ GHz} \\ f_{\text{UHF}} = 870 \text{ MHz} \end{array} \right. \quad (2.2)$$

the scaling factor relation is

$$A(f_L) \approx 1.36A(f_{\text{UHF}}) \quad (\text{dB}). \quad (2.3)$$

A comparison of the actual attenuation measurements at 1.6 GHz and 870 MHz resulted in 1.38 as the scaling factor. It is interesting to note that an identical expression as given by (2.1) was derived by the authors for the dynamic case employing simultaneous measurements at 1.5 GHz and 870 MHz (described in Section 3.5).

2.4 Effects on Attenuation Caused by Season and Path Elevation Angle

The attenuation effects caused by trees, with and without foliage, versus path elevation angle have also been explored for individual tree measurements by Goldhirsh and Vogel [1987]. The path elevation angle dictates the path length through the canopy. For the case in which the foliage and/or density of branches comprising the canopy decrease with increasing height, it should be expected that the smaller the elevation angle (relative to the horizontal), the larger the path length through the canopy, and the greater the corresponding attenuation. Figure 2.3 shows linear least square results of attenuation versus path elevation angle derived from measurements on the Callery Pear tree in October 1985 (full foliage) and March 1986 (bare branches).

The best linear fit results in Figure 2.3 may be expressed as follows:

For θ Between 15° to 40°

$$\text{Full Foliage :} \quad A(\theta) = -0.48\theta + 26.2 \quad (\text{dB}) \quad (2.4)$$

and

$$\text{Bare Tree :} \quad A(\theta) = -0.35\theta + 19.2 \quad (\text{dB}) \quad (2.5)$$

where θ is the elevation angle in degrees. The above results were obtained for a configuration in which the receiving antenna was 2.4 m from the ground (on top of a van) and at a horizontal distance of 8 m from the trunk of the tree whose height was 14 m. The diameters of the base and top of the canopy were approximately 11 and 7 m, respectively. The percentage rms deviations of the data points relative to the best fit expressions (2.4) and (2.5) were 15.3% and 11.1% (1.7 dB and 1.2 dB), respectively.

We derive from (2.4) and (2.5) the average condition

$f = 870 \text{ MHz}; \text{EI} = 15^\circ \text{ to } 40^\circ$

$$A(\text{full foliage}) \approx 1.35A(\text{bare tree}) \quad (\text{dB}) \quad (2.6)$$

which states that for the static case, the maximum attenuation contribution from the Callery Pear tree with leaves (at 870 MHz) is nominally 35% greater than the attenuation (in dB) without leaves. Hence, the predominant attenuation arises from the tree branches via the

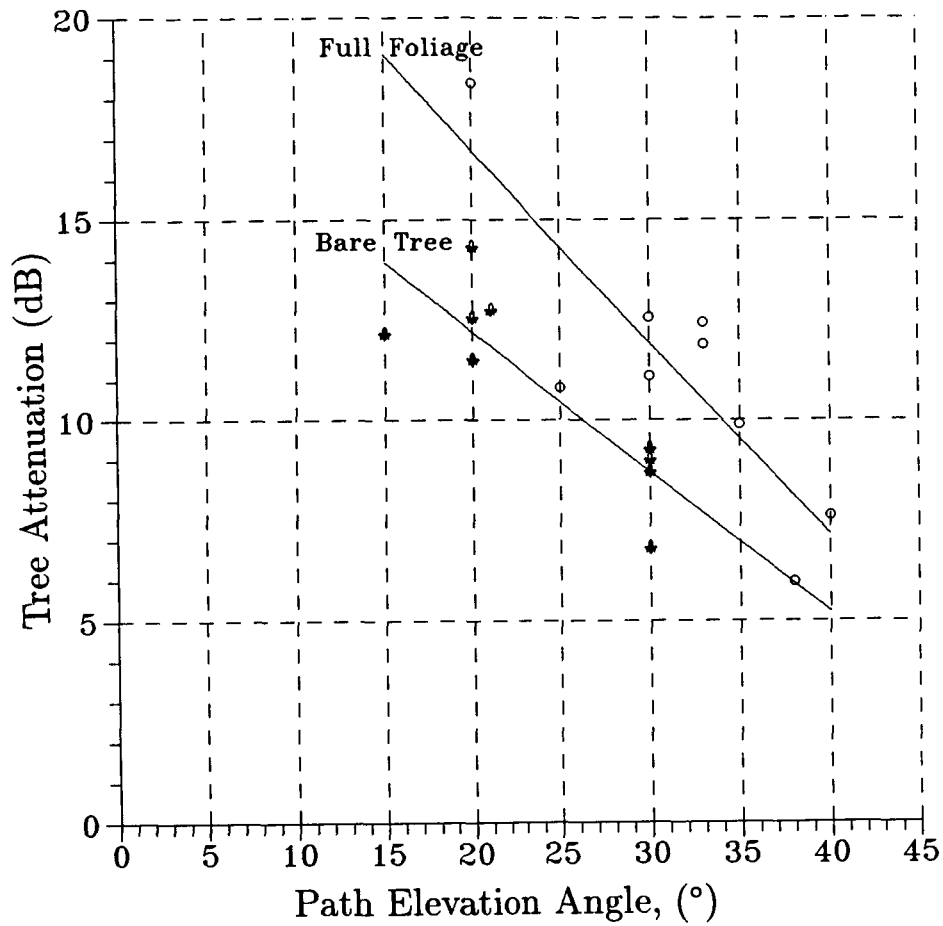


Figure 2.3: Least square linear fits of attenuation versus elevation angle for propagation through the canopy of a Callery Pear Tree at 870 MHz for a LMSS Configuration.

mechanism of absorption and the scattering of energy away from the receiver. The conclusion that the wood part of the tree is the major contributor to attenuation has also been substantiated for the mobile case (Chapter 3).

The results described in Figure 2.3 pertain to the attenuation caused by a single tree canopy in the angular range 15° to 40° . Smaller elevation angles for practical earth-satellite scenarios imply absorption and scattering from multiple tree trunks and canopies. This corresponds to the *grove case* as depicted in Figure 2.2. Hence, a description of the tree spacing, canopy dimensions, and the path length through the grove of trees are necessary to properly quantify results at elevation angles smaller than 15° .

Chapter 3

Attenuation Due to Roadside Trees: Mobile Case

3.1 Background

As of this writing, a limited number of LMSS related propagation investigations have been executed at UHF and L-Band where the transmitter platforms were located on satellites. A summary of other investigations is given in Chapter 7. LMSS propagation measurements with satellite transmitter platforms were conducted by the authors in central Maryland with MARECS-B2, [Vogel and Goldhirsh, 1990], and in Australia with the Japanese ETS-V and INMARSAT-Pacific satellites [Vogel et al., 1991; Hase et al., 1991]. Other types of transmitter platforms used for mobile measurements were also employed to derive propagation information for LMSS configurations. Vogel and Hong [1988] reported on stratospheric balloons carrying transmitters at 870 MHz and 1502 MHz where measurements were made in western Texas and New Mexico. Goldhirsh and Vogel [1989; 1987] and Vogel and Goldhirsh [1988] also describe helicopter experiments at both 870 MHz and 1.5 GHz in the central Maryland and north-central Colorado regions of the United States.

3.2 Time-Series Fade Measurements

In the analysis of times-series roadside fades for LMSS scenarios, the attenuation levels were represented by the dB ratio of the shadowed power received relative to the unshadowed levels under conditions of negligible multipath. Figures 3.1 and 3.2 are examples of measurements depicting nominal characteristics of time-series of fades (a) and phases (b) for non-shadowed and shadowed line-of-sight cases, respectively. These measurements were performed by Vogel et al. [1991] in Australia where L-Band transmissions (1.5 GHz) emanating from the Japanese ETS-V were received at an elevation angle of 50° . For the cases indicated in Figures 3.1 and 3.2, the vehicle speeds were approximately 17.4 m/s and 11 m/s for the unshadowed and shadowed cases, respectively. The receiver noise had fluctuations which were within 1 dB (rms). The unshadowed environment (Figure 3.1) may be characterized as a "flat rural region" and the shadowed case (Figure 3.2), a suburban location having roadside trees.

Fluctuations outside the one dB noise level in Figure 3.1 (a) are due to multipath. Nominally, peak-to-peak variations of less than 5 dB of power and 25° of phase were observed for non-shadowed cases. We note the shadowed case (Figure 3.2) has fades which are highly variable with fluctuations exceeding 15 dB. Some of these deep fades are also accompanied by rapid phase shifts.

Time-series of fade and phase of the above types were obtained for various LMSS geometries and environments and corresponding cumulative distributions were derived as described in the following paragraphs.

3.3 Empirical Roadside Shadowing Model

Cumulative L-Band fade distributions systematically derived from helicopter-mobile and satellite-mobile measurements in central Maryland enabled the formulation of an Empirical Roadside Shadowing (ERS) model. The measurements were obtained over approximately 600 km of driving distance comprising path elevation angles of 21° , 30° , 45° , and 60° . The 21° case was executed employing MARECS-B2 [Vogel and Goldhirsh, 1990], whereas the measurements for the other angles were obtained employing the helicopter as the transmitter platform. The configurations correspond to maximum shadowing conditions; namely, the

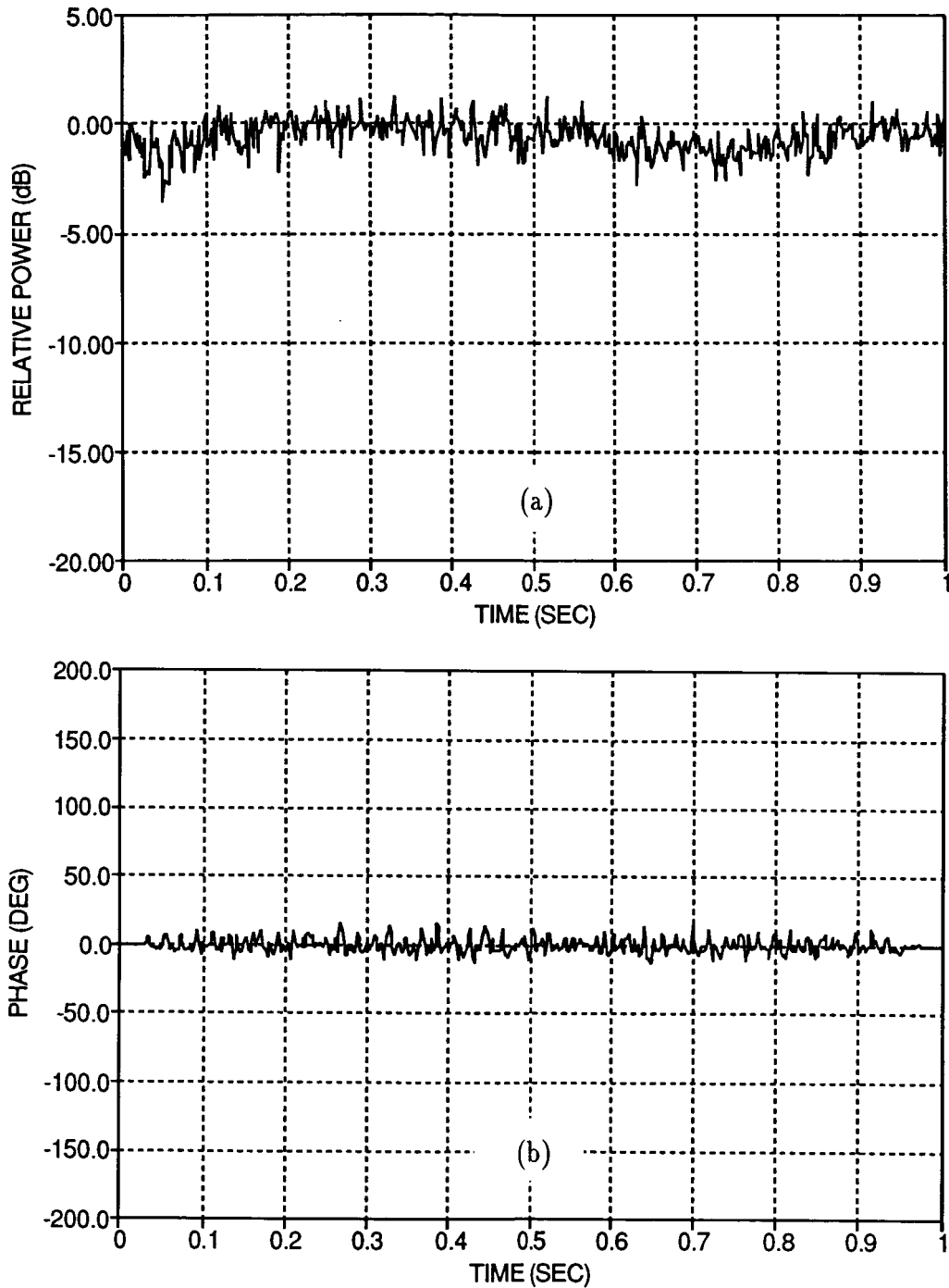


Figure 3.1: Time-series of fades (a) and phases (b) over a one second period at a sampling rate of 1 KHz in a flat rural region where the line-of-sight was unshadowed.

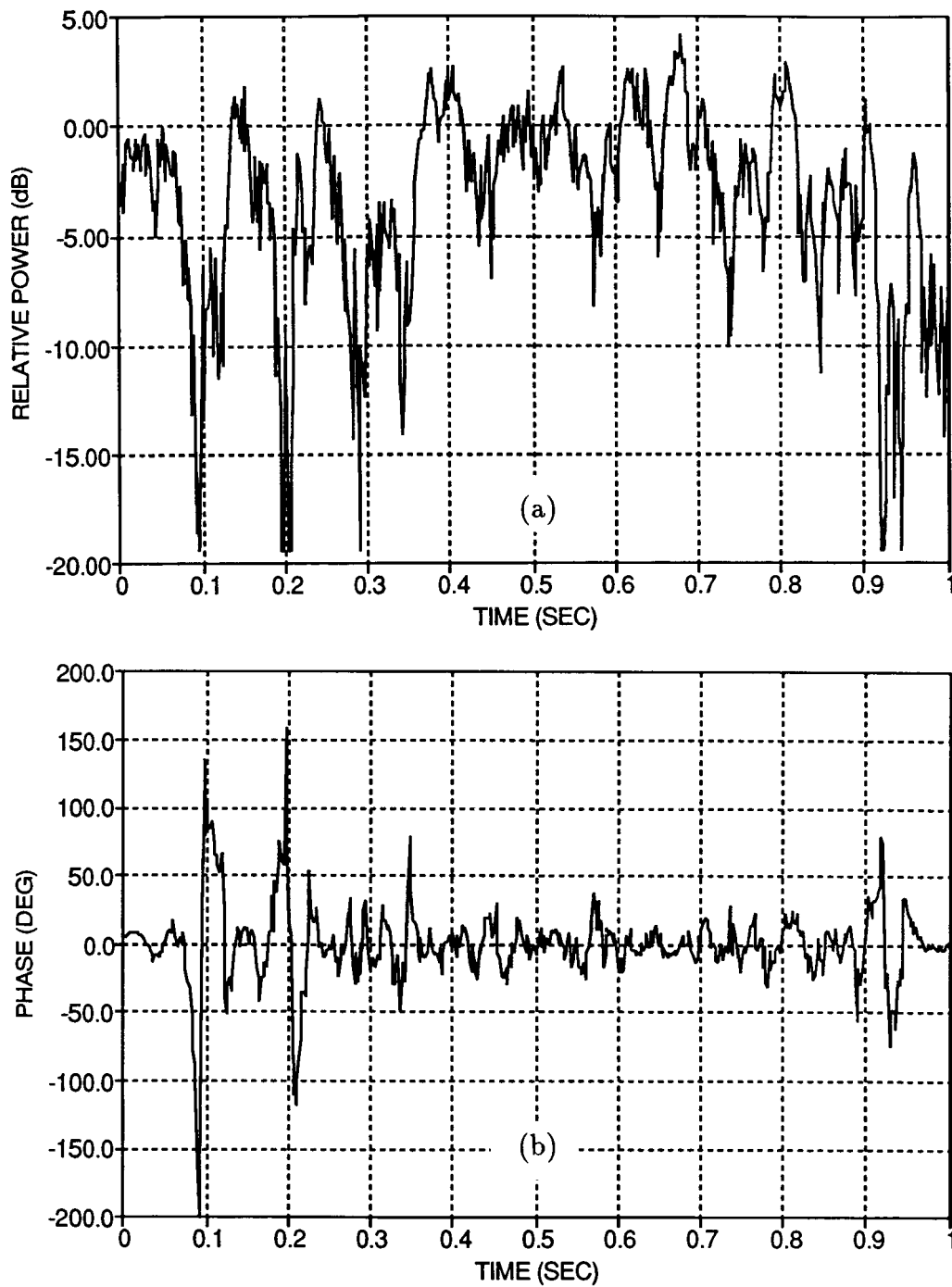


Figure 3.2: Time-series of fades (a) and phases (b) over a one second period at a sampling rate of 1 KHz in a suburban region with roadside trees where the line-of-sight was shadowed.

helicopter flew parallel to the moving vehicle and the propagation path was approximately normal to the line of roadside trees which ranged in height from approximately 5 to 30 m. The satellite path directions were such that they were also predominantly along the maximum shadowing orientation although some of the roads sampled have a number of bends in them and deviations from this aspect did arise. The measurements were performed on two lane highways (one lane each direction), and a four lane highway (two lanes each direction), where the roadside trees were primarily of the deciduous variety. In order to assess the extent by which trees populate the roadside, a quantity called percentage of optical shadowing (POS) was defined. This represents the percentage of optical shadowing caused by roadside trees at a path angle of 45° for right side of the road driving, where the path is to the right of the driver and the vehicle is in the right lane. The POS for the roads driven were predominantly between 55% and 75%.

The empirical expression, obtained by applying "best fit formulations" to the measured fade distributions at 1.5 GHz, is given by

$P = 1\% \text{ to } 20\%$

$$A(P, \theta) = -M(\theta) \ln P + N(\theta) \quad (3.1)$$

where A is the fade in dB, P is the percentage of the distance traveled over which the fade is exceeded, and θ is the path elevation angle to the satellite. Since the speed was maintained nominally constant for each run, P may also be interpreted as the percentage of the time the fade exceeds the abscissa value.

Least square fits of second and first order polynomials in elevation angle θ (deg) generated for M and N , respectively, result in

$$M(\theta) = a + b\theta + c\theta^2 \quad (3.2)$$

$$N(\theta) = d\theta + e \quad (3.3)$$

where

$$\begin{cases} a = 3.44 \\ b = .0975 \\ c = -0.002 \\ d = -0.443 \\ e = 34.76 \end{cases} \quad (3.4)$$

Table 3.1: Coefficients M and N As a function of θ for Equation (3.1)

Path Angle θ (degrees)	M	N
20	4.590	25.90
25	4.628	23.69
30	4.565	21.47
35	4.403	19.26
40	4.140	17.04
45	3.778	14.83
50	3.315	12.61
55	2.753	10.40
60	2.090	8.18

The ERS model corresponds to an overall average driving condition encompassing right and left lane driving and opposite directions of travel along highways and rural roads where, as mentioned, the overall aspect of the propagation path was for the most part orthogonal to the lines of roadside trees and utility poles. The dominant causes of LMSS signal attenuation are due to canopy shadowing, where multipath fading plays only a minimal role. The resultant fit as given by (3.1) was found to agree with the data points comprising the individual distributions at the four path elevation angles to within 1 dB.

In Table 3.1 is given a listing of M and N values for elevation angles ranging from 20° to 60° at 5° intervals which may be applied to (3.1). In Figure 3.3 are shown a family of cumulative distributions for the indicated path elevation angles.

In Figure 3.4 are plotted the fade exceeded versus the path elevation angle for a family of isopleths of constant percentages; namely, 1, 2, 5, 10, and 20%. These curves were derived from (3.1) and may be expressed by the alternate form of the ERS formulation given by

$$A(\theta, P) = \alpha(P) + \beta(P)\theta + \gamma(P)\theta^2 \quad (3.5)$$

where A is the fade exceed (in dB), θ is the path elevation angle (in degrees), and where $\alpha(P)$, $\beta(P)$, and $\gamma(P)$ are tabulated in Table 3.2 for the indicated percentage levels, P. The above formulation was found to be in agreement with the original set of median distributions

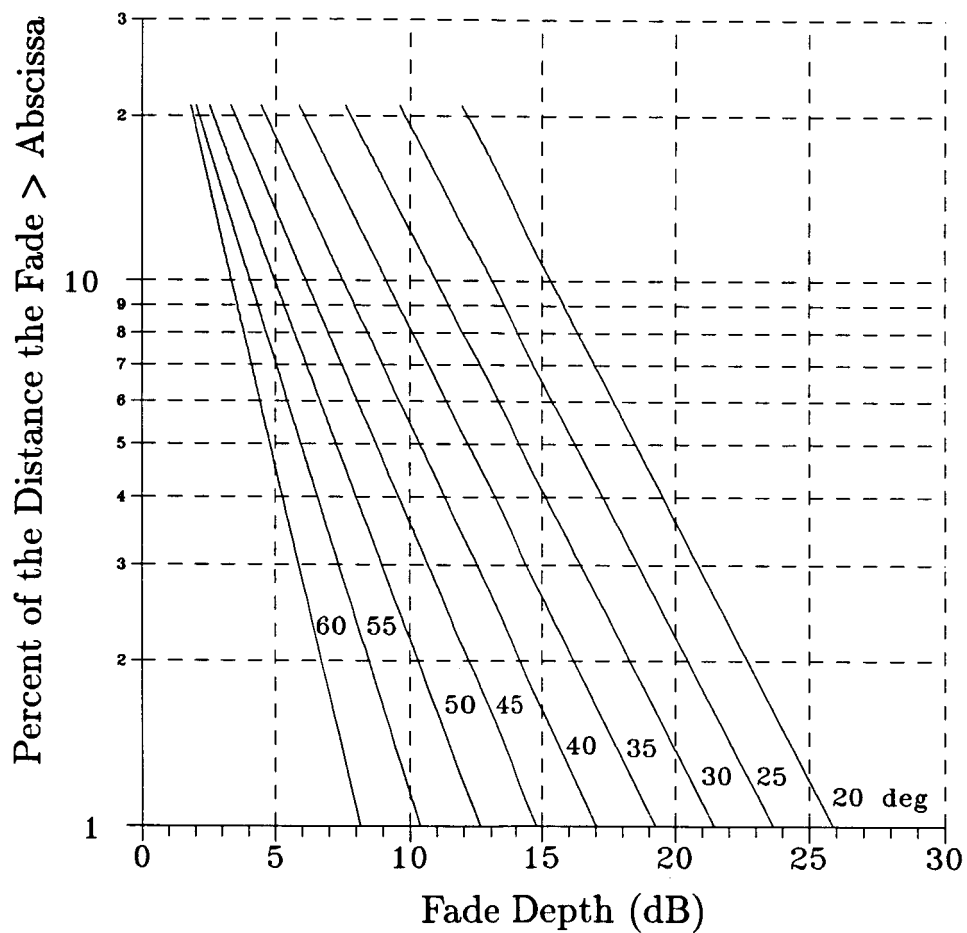


Figure 3.3: Cumulative fade distributions at 1.5 GHz for family of path elevation angles derived from the Empirical Roadside Shadowing model.

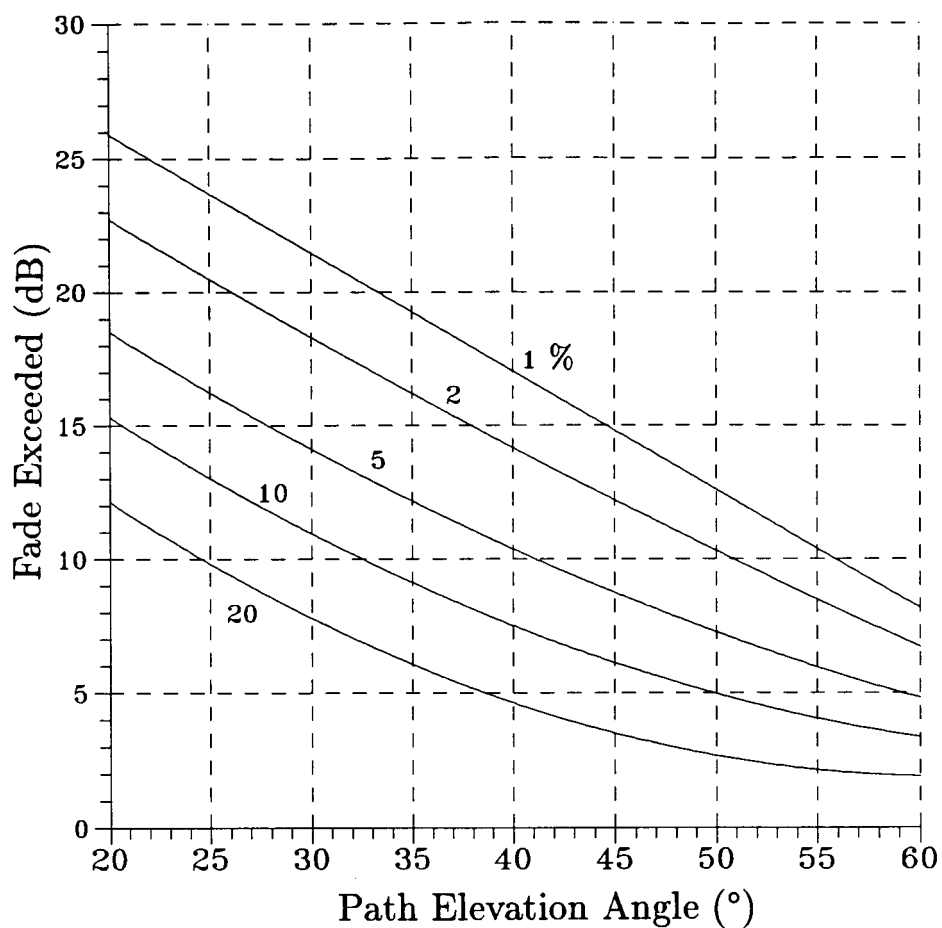


Figure 3.4: L-Band fade exceeded versus path elevation angle for family of indicated constant percentages (ERS model).

Table 3.2: Listing of parameter values $\alpha(P)$, $\beta(P)$, and $\gamma(P)$ in equation (3.5)

Percentage (P)	$\alpha(P)$	$\beta(P)$	$\gamma(P)$
20	24.45	-0.7351	5.991×10^{-3}
10	26.84	-0.6775	4.605×10^{-3}
5	29.22	-0.6000	3.219×10^{-3}
2	32.38	-0.5106	1.386×10^{-3}
1	34.76	-0.4430	0

at 21°, 30°, 45°, and 60° to within 0.3 dB.

As previously mentioned, a description of fade statistics at smaller elevation angles becomes increasingly complex as it may involve absorption and scattering due to multiple canopies and tree trunks and approach the scenario depicted in Figure 2.2. Application of the ERS model at smaller elevation angles is therefore not suggested .

3.4 Validation of the Empirical Roadside Shadowing Model

It is interesting to compare the ERS model with distributions obtained from measurements made in Australia by the authors [Vogel et al., 1989]. Two major vegetation zones were traversed in Australia; forests along the coastal roads and woodlands further inland. Forests ranged from dry sclerophyll, in which the crowns of contiguous trees do not touch each other to tropical rain-forests, in which the leafy crowns of the trees intermingle. The dominating tree genus in the forest was Eucalyptus. Other than tree types, general similarities existed between the roads traveled in Australia and those in Central Maryland (e.g., tree heights, percentage of optical shadowing, setbacks).

In Table 3.3 are given the transmitter and receiver system parameters for the Australian campaign. In Figure 3.5 are plotted the fade distribution for 403 km of road measurements comprising 15 individual runs using ETS-V. The common characteristic of each run was that at 1% of the distance traveled, 10 dB was exceeded. Also plotted for comparison is the

Table 3.3: Summary of Pertinent Transmitter-Receiver System Parameters for Australian Campaign [Vogel et al., 1991].

Transmitter Platform #1 Azimuth at Sydney Elevation at Sydney Frequency (MHz) EIRP (dBW) Polarization	ETS-V -2° 51° 1545.15 25.9 LHCP
Transmitter Platform #2 Azimuth at Sydney Elevation at Sydney Frequency (MHz) EIRP (dBW) Polarization	INMARSAT Pacific 45° 40° 1541.5 20 RHCP
Receiver Antennas (Low Gain) Gain (dB) Elevation Beamwidth Azimuth Beamwidth Polarizations: ETS-V INMARSAT Pacific	Crossed Drooping Dipole 4 15° to 75° Omnidirectional LHCP RHCP
Receiver Antennas (High Gain) Gain (dB) Beamwidths (Principal Planes) Polarizations: ETS-V INMARSAT Pacific	Helix 14 45° LHCP RHCP
Receiver Bandwidths: Quadrature Detectors (Hz) Filter (Hz)	 1000 200
Signal to Noise Ratios (dB): ETS-V (Low Gain) ETS-V (High Gain) INMARSAT Pacific (Low Gain)	 22.4 32.4 16.5
Sampling Rate (KHz) Data Recorded	1 Quadrature Detector Outputs 200 Hz Filter Output Vehicle Speed Time

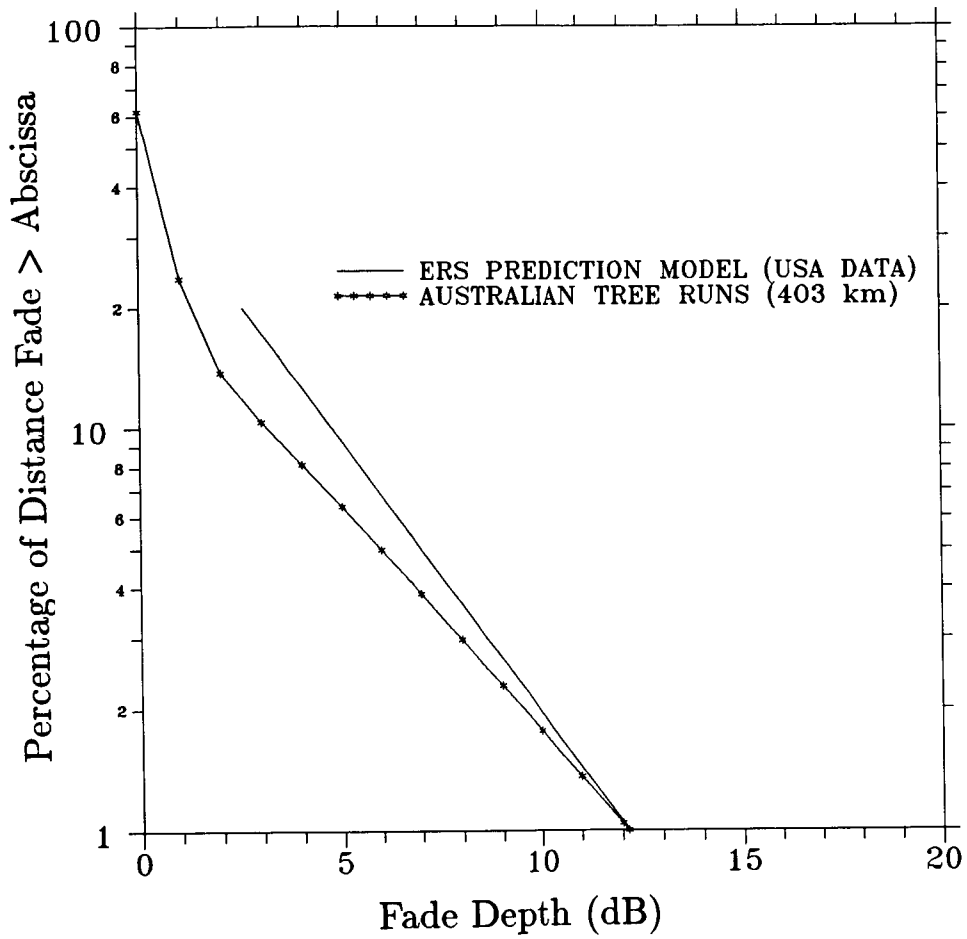


Figure 3.5: Comparison of Australian fade distribution comprising 15 runs with ERS model.

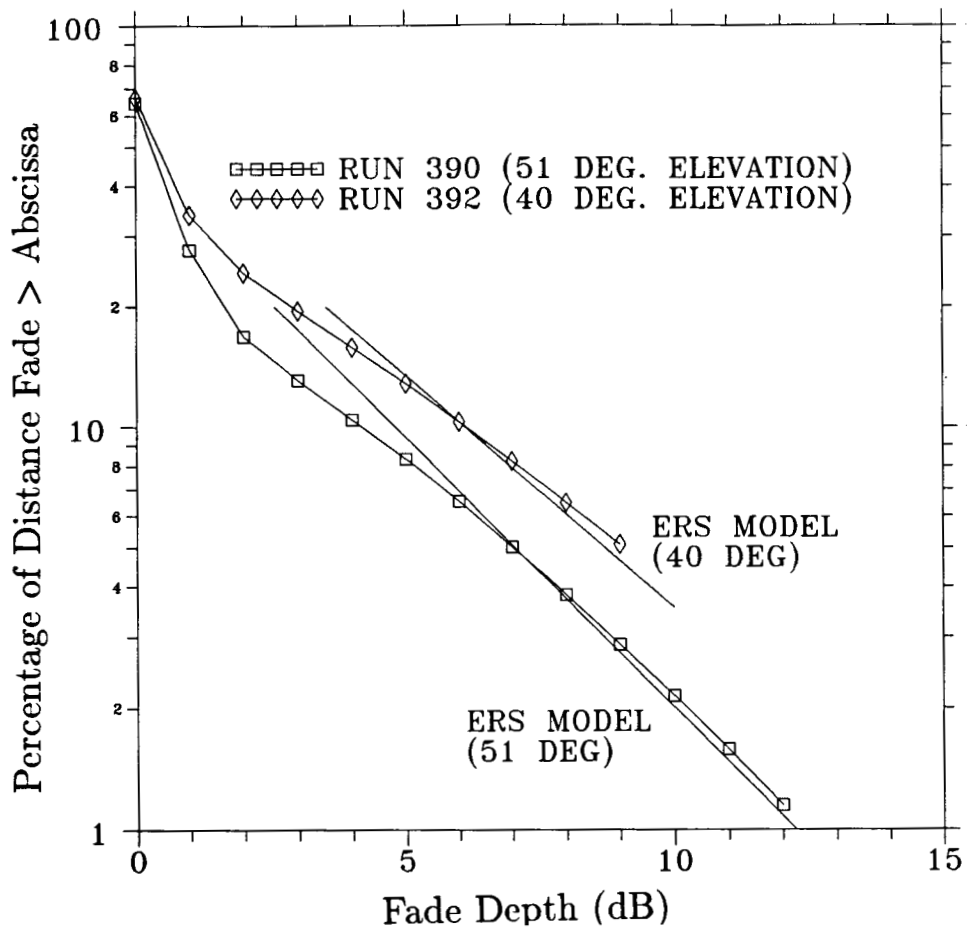


Figure 3.6: ERS and Australian fade distributions for different elevation angles from measurements obtained with INMARSAT Pacific (40°) and ETS-V (51°).

fade distribution as predicted by the ERS model (at 51°). We note the maximum difference between the two distributions is less than 2 dB at the 14% probability level, and thereafter this difference monotonically reduces.

In Figure 3.6 are distributions applied to separate runs along a tree lined road (≈ 55 km) in which different satellites were accessed sequentially; INMARSAT-Pacific (elevation angle = 40°) and ETS-V (elevation angle = 51°). For both distributions, the fade differences (relative to the model) are less than 1 dB over the percentage range of validity.

3.5 L-Band Versus UHF Attenuation Scaling Factor: Dynamic Case

Simultaneous mobile fade measurements by the authors [Goldhirsh and Vogel, 1989; Vogel and Hong, 1988] at L-Band (1.5 GHz) and UHF (870 MHz) have demonstrated that the ratio of fades (fades are in dB) are approximately consistent with the ratio of the square root of frequencies. Hence,

For P = 1% to 30%

$$A(f_L) = A(f_{UHF}) \sqrt{\frac{f_L}{f_{UHF}}} \quad (\text{dB}) \quad (3.6)$$

For $f_L = 1.5$ GHz, $f_{UHF} = 870$ MHz

$$A(f_L) \approx 1.31 A(f_{UHF}) \quad (\text{dB}) \quad (3.7)$$

The above result represents an overall average condition derived from 24 measurement runs along tree-lined roads in Central Maryland [Goldhirsh and Vogel, 1989]. The runs comprise path elevation angles of 30°, 45°, and 60° and a driving distance of 480 km. The multiplying coefficient 1.31 in (3.7) was shown to have an rms deviation of ± 0.1 over a fade exceedance range from 1% to 30%. As mentioned in Section 2.3, the result (3.6) for the dynamic case is consistent with (2.1) for the static case.

The multifrequency measurements of Bundrock and Harvey [1988] represent an independent validation of (3.6). In Table 3.4 are the 1% and 10% fade levels derived from simultane-

Table 3.4: Fades at the 1% and 10% levels derived from the multifrequency measurements of Bundrock and Harvey [1988]. Also shown in parentheses are the predicted levels employing frequency scaling and the UHF values.

Percentage	893 MHz	1550 MHz	2660 MHz
1	8.8	11.4 (11.6)	16.1 (15.2)
10	4.6	5.5 (6.1)	8.3 (7.9)

ous measurements made by them in Australia at 893 MHz, 1550 MHz, and 2660 MHz. Also shown in parentheses are the fade levels derived employing the UHF fades and expression (3.6). We note that overall agreement is quite good with an overall average percent error of less than 6% and a peak error smaller than 1 dB. Predictability even exists at the S-Band frequency, giving smaller than a 6% peak error.

3.6 Seasonal Effects on Attenuation – Dynamic Case

It may be recalled from Section 2.4, that a 35% increase in the attenuation was experienced at 870 MHz when comparing attenuation from trees having no foliage and those having foliage (winter versus summer). This case corresponded to a configuration in which the vehicle was stationary and the propagation path intersected the canopy. Seasonal measurements were also performed by the authors for the dynamic case in which the vehicle was traveling along a tree-lined highway in Central Maryland (Route 295) along which the propagation path was shadowed over approximately 75% of the road distance [Goldhirsh and Vogel, 1987; 1989]. Cumulative fade distributions were performed in March 1986 during which the deciduous trees were totally without foliage. These were compared with similar distributions acquired on October 1985 and June 1987, during which the trees were approximately in 80% and full blossom stages, respectively. The results may be expressed by

$f = 870 \text{ MHz}, P = 1\% \text{ to } 30\%$

$$A(\text{full foliage}) = 1.24A(\text{no foliage}) \quad (\text{dB}) \quad (3.8)$$

Equation (3.8) states that over the exceedance range 1% to 30% of the seasonal cumulative distributions, there is an average increase in the dB fade of $24\% \pm 2\%$ rms relative to fades from trees with no leaves.

The percentage fade increase (seasonal) for the dynamic case (24%) is less than that for the static case (35%) because the dynamic case has associated with it measurements which include evergreens (minimal seasonal change) and some stretches of road over which there were no trees. The static case also represents a maximum attenuation condition, whereas the dynamic case is expressed in terms of cumulative distributions. Although the above measurements have been made at 870 MHz, the result should not be significantly different at 1.5 GHz.

3.7 Fade Reduction Due to Lane Diversity

We examine the extent by which the fade reduces (or increases) by switching lanes for LMSS configurations. Figures 3.7 (a) and (b) show vehicles driving on the right and left lanes, respectively, where the satellite is to the right and the propagation path passes through the tree canopy on the right side of the road. We note that the path length through the canopy is greater when the vehicle is closest to the tree line (right side of road for examples given). A fade reduction should therefore be experienced by switching lanes from the right to the left side. The authors measured this effect at UHF (870 MHz) [Goldhirsh and Vogel, 1987], and L-Band (1.5 GHz) [Goldhirsh and Vogel, 1989]. Repeated distributions from helicopter measurements were derived for left and right lane driving at fixed path elevation angles of 30° , 45° , and 60° . A quantity defined as the "fade reduction, FR" is used to characterize the increase in signal power gained by switching lanes. This quantity is obtained by differencing equi-probability fade values from distributions pertaining to right and left side driving. The fade reductions at L-Band and UHF are plotted in Figures 3.8 and 3.9 as a function of the equal probability maximum fades. The maximum fades were derived from the distribution for the right lane driving case as shown in Figure 3.7 (a).

At each of the elevation angles, the individual data points have been replaced by the "best third order polynomial fit" which may be expressed by

f = 1.5 GHz and 870 MHz

$$FR = a_0 + a_1A + a_2A^2 + a_3A^3 \quad (3.9)$$

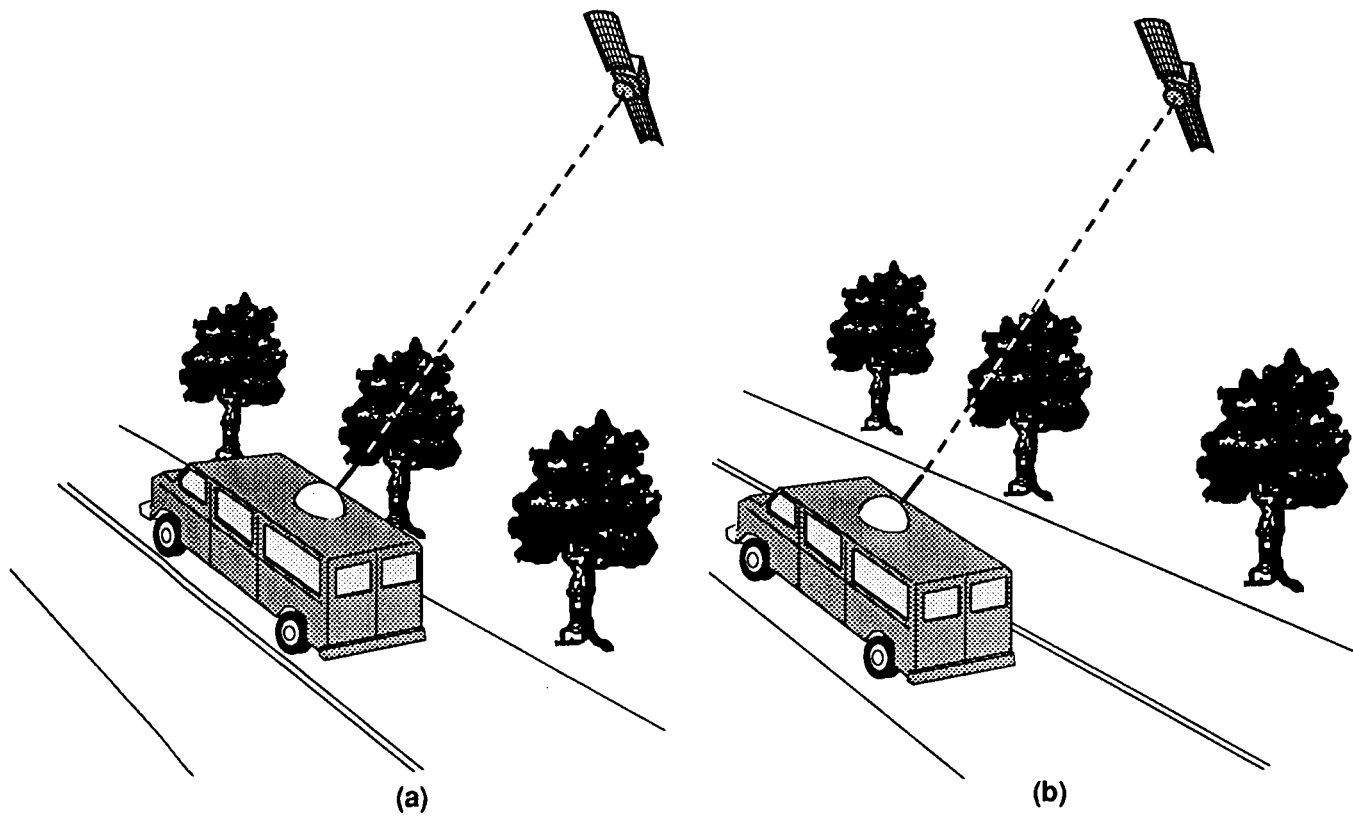


Figure 3.7: Mobile-satellite configurations depicting (a) larger intersecting path length with tree canopy when vehicle is driven in the right lane, and (b) smaller intersecting path length when vehicle is driven in the left lane.

where FR (in dB) represents the fade reduction obtained in switching lanes from the greater shadowing configuration (Figure 3.7 (a)) to the lesser one (Figure 3.7 (b)). Also, a_0 , a_1 , a_2 , and a_3 are tabulated in Tables 3.5 and 3.6 for L-band and UHF, respectively. The parameter A (in dB) represents the maximum fade level value (derived for the configuration in Figure 3.7 (a)). The "best fit polynomials" were observed to agree with FR as derived from the measured distributions to within 0.1 dB rms.

It is interesting to note that larger fade reductions occur the greater the elevation angle. This arises because at the larger angles a change of lanes may radically alter the earth-satellite path from a shadowed to a non-shadowed condition (Figure 3.7). At the lower elevation angles, this change of conditions becomes less likely.

Table 3.5: Coefficients of fade reduction formulation (3.9) for lane diversity at $f = 1.5$ GHz.

El. Angle θ (deg)	a_0	a_1	a_2	a_3	dB Range
30	0.2818	0.2840	-1.876×10^{-2}	4.811×10^{-4}	3-25
45	-1.073	0.8816	-4.651×10^{-2}	7.942×10^{-4}	3-17
60	-4.206×10^{-2}	0.1671	6.602×10^{-2}	-2.720×10^{-3}	3-15

Table 3.6: Coefficients of fade reduction formulation (3.9) for lane diversity at $f = 870$ MHz.

El. Angle θ (deg)	a_0	a_1	a_2	a_3	dB Range
30	5.020×10^{-3}	.3354	-2.439×10^{-2}	7.764×10^{-4}	2-20
45	-0.8193	0.8430	-5.758×10^{-2}	1.222×10^{-3}	2-12
60	-0.2004	0.2112	7.076×10^{-2}	-3.764×10^{-3}	2-11

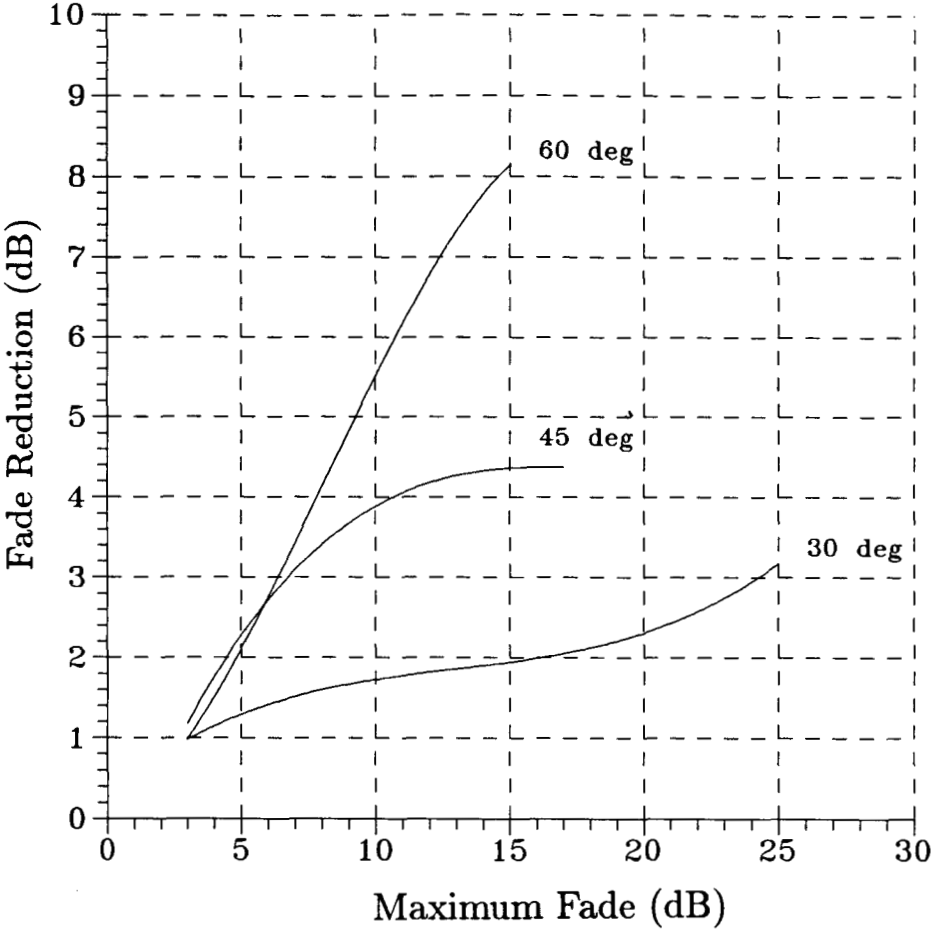


Figure 3.8: Best fit fade reduction at 1.5 GHz versus equi-probability attenuation at path elevation angles of 30°, 45°, and 60°.

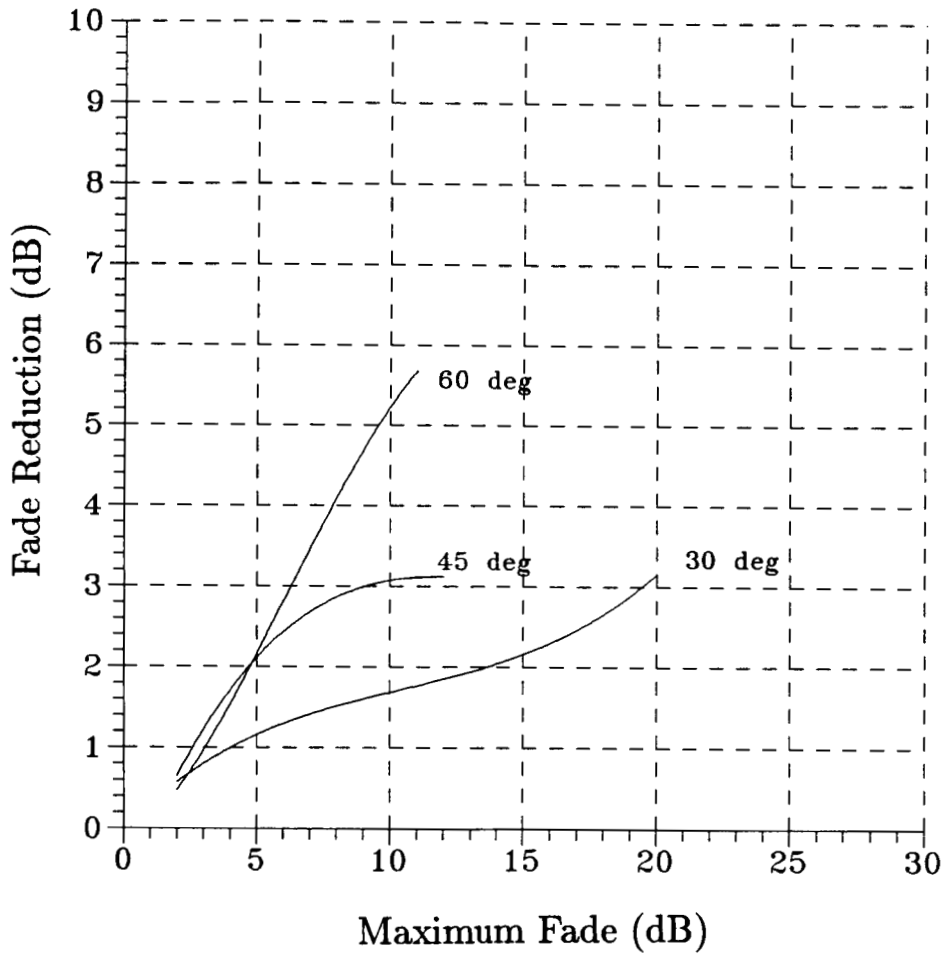


Figure 3.9: Best fit fade reduction at 870 MHz versus equi-probability attenuation at path elevation angles of 30°, 45°, and 60°.

Chapter 4

Signal Degradation for Line-of-Sight Communications

4.1 Background

This chapter broaches the question, "What is the LMSS signal degradation for a configuration in which line-of-sight communications are maintained in an environment where multipath is prevalent?" The multipath environment may consist of roadside trees, utility poles, hills, and mountains. This question was addressed through the implementation of a series of experiments by the authors in central Maryland [Goldhirsh and Vogel, 1989], and north-central Colorado [Vogel and Goldhirsh, 1988].

A typical multipath scenario is one in which direct signals are received at the same time as indirect ones which arrive at the antenna via scattering from nearby trees, utility poles, other structures, and/or the side of a mountain. The sum total of received signals may add constructively or destructively resulting in signal enhancement or fade. The received power is a manifestation of the phasor sum of the direct transmission and the resultant indirect voltage levels which depend upon the scattering cross sections of the multipath reflectors, their number, their relative distances to the antenna, the received field polarizations, and the receiving antenna gain pattern function.

Simultaneous LMSS measurements were made at L-Band and UHF where the experimental parameters are described in Table 2.2. The receiving antennas were located on the roof of a van (2.4 m above the ground) where the pattern functions were nominally azimuthally omni-directional with a 3 dB beamwidth in elevation between 15° and 75°. Below 15°, the antenna gain function dropped off rapidly and any multipath arriving via scattering from surfaces near or below the horizontal were diminished by the pattern by at least 10 dB.

4.2 Multipath for A Mountain Environment

The results described here were obtained from LMSS line-of-sight measurements in canyon passes in north-central Colorado. The transmitter was on a helicopter which, for each run, flew behind a receiving mobile van and maintained a relatively fixed distance and path depression angle relative to the receiving antenna. The radiating antennas on the helicopter transmitted simultaneous L-Band (1.5 GHz) and UHF (870 MHz) cw signals. For each of the canyon roads driven, the wall facets were highly variable in height, orientation, foliage overlay, and distance from the roads. The mountain walls consisted of randomly oriented facets of rocks with protruding patches of trees. The roads through the canyons made many twists and turns, offering highly variable aspects to the multipath illumination scene. Such a scenario was considered as a worst case for multipath.

Figure 4.1 shows four cumulative fade distributions depicting “least square power curve fits” for the above described multipath scenario at frequencies of 870 MHz and 1.5 GHz and path elevation angle 30° and 45°. Each curve was derived from a subset of four runs taken in two canyon passes (Boulder and Big Thompson Canyons); a run representing measurements where the vehicle traveled up or down a canyon pass at a particular path elevation angle to the transmitter. The resultant curves define the combined distribution corresponding to a driving distance of 87 km through canyon passes. Each of the best fit power curves agree with the measured cumulative distribution data points to within 0.1 dB rms. As mentioned, simultaneous measurements at L-Band and UHF were made for each run. The distributions may be expressed by

$P = 1\% \text{ to } 10\%$

$$P = aA^{-b} \quad (4.1)$$

where P is in %, A in dB, and a and b are tabulated in Table 4.1 at the two frequencies and

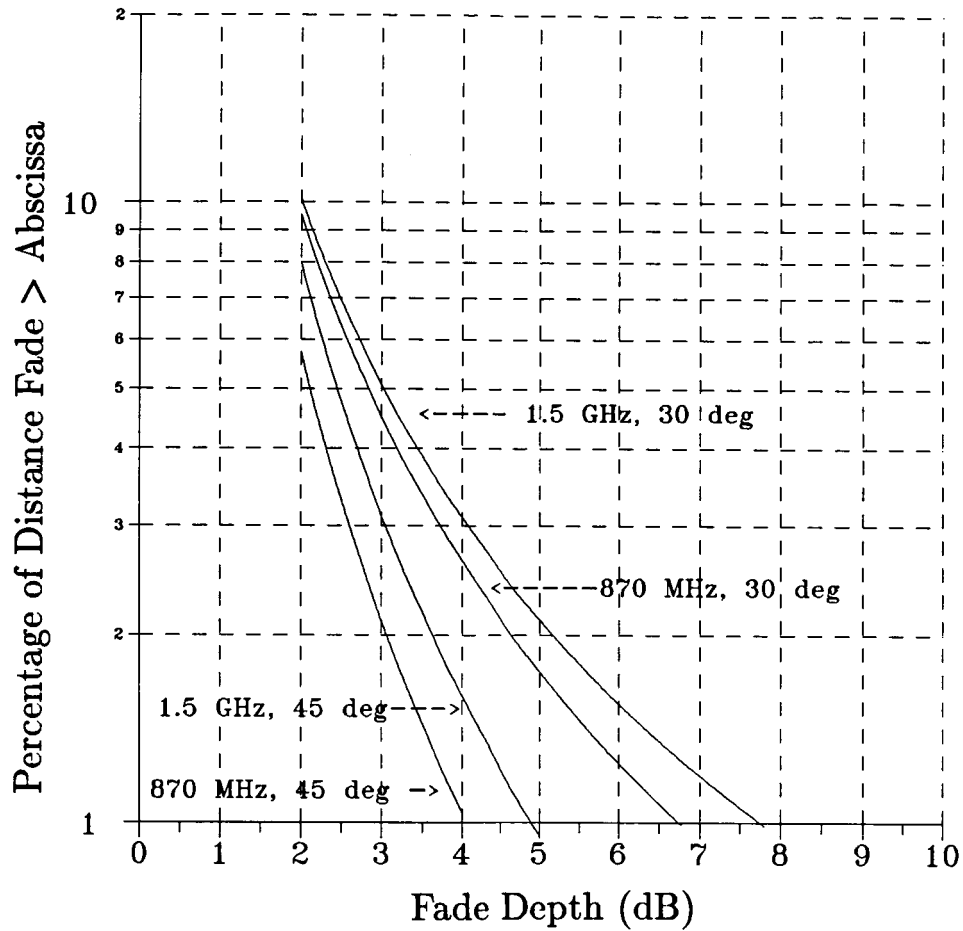


Figure 4.1: Best fits power curve cumulative fade distributions of form (4.1) for line of sight distributions in which multipath fading dominates for mountainous terrain.

Table 4.1: Coefficients a and b in formulation (4.1) describing best fit cumulative fade distribution for multipath in mountainous terrain

Frequency (GHz)	El = 30°			El = 45°		
	a	b	dB Range	a	b	dB Range
0.870	34.52	1.855	2-7	31.64	2.464	2-4
1.5	33.19	1.710	2-8	39.95	2.321	2-5

elevation angles.

We note from Figure 4.1 that over the percentage range of 1% to 10%, the fades due to multipath vary between 2 and 5 dB at 45°, and 2 and 8 dB at 30° elevation. The higher frequency (L-Band) exhibits slightly larger fades which are generally within 1 dB or less relative to UHF. The slightly larger fades at L-Band can be attributed to the small amount of tree fading which may have been present. There may also have been a presence of more reflecting facets on the canyon walls with sizes comparable to 20 cm (L-Band) or larger than does exist for the UHF case (34 cm). Such facets (L-Band case) would offer larger cross sections (Mie scattering) than facets whose dimensions were small relative to a wavelength (UHF case) where Rayleigh scattering is applicable.

Larger fades at the 30° elevation relative to 45° can be attributed to some tree shadowing where the smaller elevation angle offers more propagation path through the foliage and hence greater attenuation. It can also be attributed to the fact that multipath is dominated by illuminated surfaces closer to the vehicle; which implies lower reflecting heights and more shallow elevation angles.

4.3 Multipath Due to Roadside Trees

Similar types of line-of-sight measurements were performed by the authors in central Maryland along tree lined roads [Goldhirsh and Vogel, 1989] as were described for the mountainous terrain case in Section 4.2. That is, repeated measurement runs at 30°, 45°, and 60° were implemented with the helicopter following the vehicle and cumulative distributions were derived at both UHF and L-Band. The distributions were observed to be relatively insensitive

Table 4.2: Coefficients u and v in formulation (4.2) describing best exponential fit cumulative fade distributions for multipath for tree-lined roads.

Frequency (GHz)	u	v	Fade Range (dB)
0.870	127.7	0.8573	1-4.5
1.5	125.6	1.116	1-6

to path elevation. The three runs were combined into one distribution at each frequency comprising 75 km of driving. The resultant distributions were found to follow an exponential form given by,

$P = 1\% \text{ to } 50\%$

$$P = u \exp(-vA) \quad (4.2)$$

where u and v are tabulated in Table 4.2 and the corresponding distributions are plotted in Figure 4.2.

The fades at the two frequencies fit very well an exponential function from 1 dB (at an exceedance of 40% to 50%) to approximately 4.5 to 5.5 dB (at an exceedance of 1%). We note a slight dependence exhibited due to frequency with L-Band giving approximately 1.5 dB greater fades at 1%. The indicated best fit exponentials were found to agree with each of the original measured cumulative distributions to within 0.2 dB. Fading due to multipath is presumed to emanate from scattering off of tree canopies which reradiate, more or less, isotropically in elevation angle. Such an explanation is consistent with the fact that the distributions were relatively insensitive to path elevation angle in the angular interval between 30° and 60° .

Enhanced fading due to multipath effects are expected for antennas pointed at lower angles (e.g., 5° to 20°) where scattering from tree canopies and trunks, other vehicles, and the road itself may be received with smaller antenna gain filtering. Also, a greater likelihood exists for shadowing to occur at the lower elevation angles.

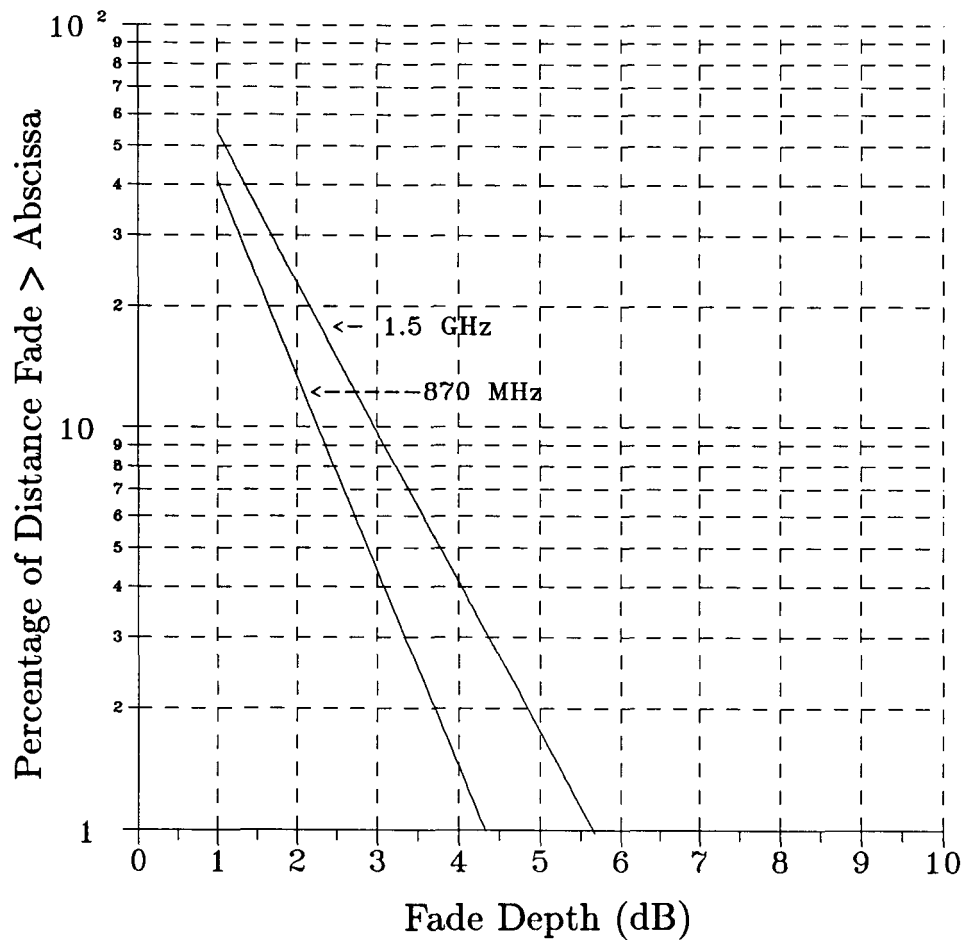


Figure 4.2: Best exponential fit cumulative fade distributions of the form (4.2) for line of sight distributions in which multipath fading dominates for tree-lined roads.

Chapter 5

Fade and Non-Fade Durations and Phase Spreads

5.1 Background

It is important to know the length of time an LMSS channel is available and unavailable without interruption for optimally designing communication systems which handle coded messages over defined bandwidths. Receivers designed by communication engineers may, for example, be equipped with a digital soft-decision modem and a powerful forward error correcting code implemented with a convolution coder and Viterbi decoder. To optimally design such receivers, which have only two states, good or bad, a knowledge is required of the statistics associated with durations of fades which fall below and above defined attenuation thresholds. In order to implement proper designs of demodulators for coded data, it is also important to have knowledge of the phase fluctuations during conditions of fading arising from multipath and shadowing.

Fade duration results at L-Band were derived by the authors from measurements in central Maryland [Goldhirsh and Vogel, 1989] and South-Eastern Australia [Hase et al., 1991]. The former measurement campaign was implemented employing a helicopter as the transmitter platform, and the latter, the Japanese ETS-V [Vogel et al., 1991]. During the latter campaign, phase fluctuations were also measured and associated statistics described

[Hase et al., 1991].

5.2 Experimental Aspects

Measurements performed in south-eastern Australia employed left-hand circularly polarized cw transmissions radiated from the Japanese ETS-V satellite at a frequency of 1545.15 MHz. The in- and quadrature-phase detector voltages (noise bandwidth = 1 kHz) as well as the output from a power detector with pre-detection bandwidth of 200 Hz were recorded at a 1 kHz rate. The receiver antenna consisted of a crossed drooping dipole antenna having a 4 dB gain, an azimuthally omni-directional radiation pattern, and a relatively flat elevation pattern over the beamwidth 15° to 75° (Table 3.3).

Fade duration results were derived by analyzing the average of two consecutive 1 millisecond samples. All fade and non-fade durations were expressed in units of traveled distance (m) for which the fades were continuously exceeded or were less than thresholds ranging from 1 to 8 dB. The “distance durations” may be converted to “time durations” by dividing the former by the speed (which was nominally 25 m/s).

The phase data were extracted from the quadrature detected signals where the low frequency components, due primarily to oscillator drift and Doppler shift changes, were rejected by digital filtering. The phase shifts measured were therefore caused by roadside obstacles.

The following emphasizes the Australian data base (elevation to satellite = 51°). Fade durations have also been examined for the central Maryland region [Goldhirsh and Vogel, 1989] and these results show a slight dependence on elevation angle.

5.3 Cumulative Distributions of Fade Durations

The fade durations were with good accuracy observed to follow the lognormal distribution

dd ≥ .02 m

$$P(\text{FD} > dd \mid A > A_q) = \frac{1}{2} \left\{ 1 - \operatorname{erf} \left[\frac{(\ln dd - \ln \alpha)}{\sqrt{2} \sigma} \right] \right\} \quad (5.1)$$

Table 5.1: Best fit exponential cumulative fade distributions parameters u and v from form (5.3) derived from measurements on roads exhibiting “extreme” and “moderate” shadowing for a path elevation angle of 51° .

Road Type	u	v	rms (dB)	Fade Range (dB)
Moderate	17.57	0.2184	0.1	2 – 13
Extreme	95.78	0.1951	0.3	2 – 15

where $P(\text{FD} > dd \mid A > A_q)$ represents the probability that the distance fade duration FD exceeds the duration distance dd under the condition that the attenuation A exceeds A_q . Also, erf is the error function, σ is the standard deviation of $\ln dd$, and $\ln \alpha$ represents the mean value of $\ln dd$. The left hand expression (5.1) was estimated by computing the percentage number of “duration events” which exceed dd relative to the total number of events for which $A > A_q$. An event of duration distance dd occurs whenever the fade crosses a threshold level A_q and persists “above that level” for the driving distance dd . A desired expression is the joint probability that FD exceeds dd and A exceeds A_q . This is given by

$$P(\text{FD} > dd, A > A_q) = P(\text{FD} > dd \mid A > A_q) P(A > A_q) \quad (5.2)$$

where $P(A > A_q)$ is the absolute probability that the fade exceeds the threshold A_q and is given by cumulative fade distributions described in Figure 5.1 for road-types whose degrees of shadowing are classified as “extreme” and “moderate”. The “extreme” condition corresponds to measurements along a road having a continuum of overhanging tree canopies where almost persistent shadowing occurred. This condition is generally not encountered and is presented here as a “worst case” scenario. The “moderate” condition corresponds to measurements in which there were 50% to 75% of optical shadowing. This distribution was used as part of the overall data base employed to validate the ERS model (Section 3.4). These distributions are described by the “best fit” exponential

$$P(A > A_q) = u \exp(-vA_q) \quad (5.3)$$

where P is the percentage of the distance driven over which the fade A_q (in dB) is exceeded. The parameters u and v are tabulated in Table 5.1 along with the rms deviations of the measured distributions relative to the best fit curves.

For the case in which there was a 5 dB fade threshold, fade duration measurements executed on three roads (2 moderate and 1 extreme) exhibited values of α and σ which were

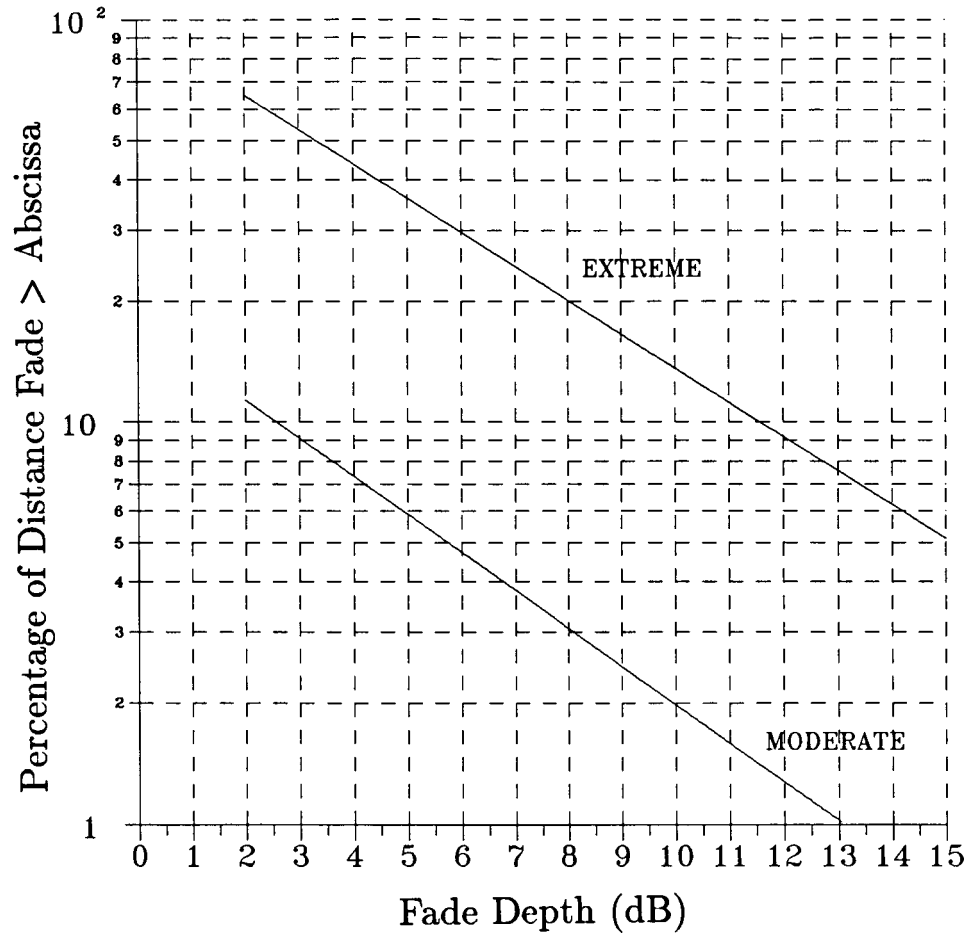


Figure 5.1: Best fit exponential fade distributions of the form (5.3) derived from measurements in South-Eastern Australia along road-types classified as “moderate” and “extreme”. Measurements were made at a path elevation of 51°.

Table 5.2: RMS deviations relative to log-normal fit ($\alpha = 0.22$, $\sigma = 1.215$) of cumulative distributions of fade durations (threshold of 5 dB) for various runs exhibiting moderate and extreme shadowing [Equation (5.1)].

Shadowing Level	% RMS Deviation	Distance (km)
Moderate (Run 1)	16.4	33.0
Moderate (Run 2)	18.0	8.1
Extreme	13.6	2.4

nearly coincident for the individual runs. The resultant “best fit” regression values are given by

$$\alpha = 0.22 \quad (5.4)$$

$$\sigma = 1.215 \quad (5.5)$$

As may be noted from Table 5.2, the measured fade durations for the various runs showed an overall rms deviation of less than 20% relative to the those derived employing the best-fit log normal distribution shown plotted in Figure 5.2. For engineering convenience, the lognormal distribution is plotted on logarithmic scales since the percentage values are easier to read.

The fact that a single set of values of α and σ may be applied to the “moderate” and “extreme” road-types suggests that whenever a fade is encountered which exceeds 5 dB, the physical characteristics of the trees which create the fades are the same. In other words, the different roads are distinguished by the frequency with which tree shadowing is encountered. Once encountered, the shadowing duration characteristics are similar.

Fade duration statistics have also been compiled by Goldhirsh and Vogel [1989] in central Maryland for angles of 30°, 45°, and 60° for 5 dB and 10 dB thresholds. A slight elevation angle dependence was discernible for the three cases; the smaller the elevation angle, the larger the fade duration for any fixed percentage. For example, the 30° fade duration showed approximately twice that for the 60° case. This is consistent with the fact that at the lower elevation angles there is generally more persistent shadowing.

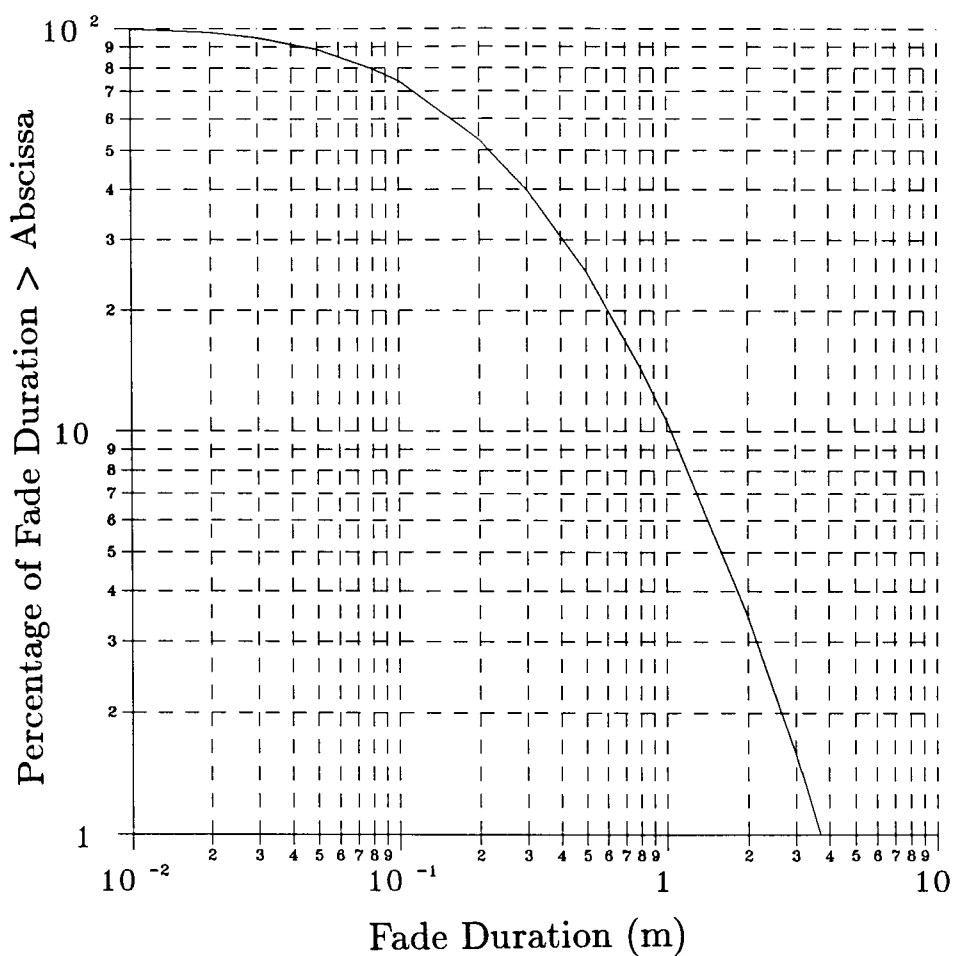


Figure 5.2: Best fit log-normal distribution (5.1) depicting fade durations for a 5 dB threshold. The distribution encompasses road types which exhibit “moderate” and “extreme” shadowing. The distribution is plotted on logarithmic scales for convenience.

Table 5.3: Non-fade duration regression values of β and γ satisfying the power expression (5.6) at a 5 dB threshold for road-types exhibiting “moderate” and “extreme” shadowing at a path elevation angle of 51° .

Shadowing Level	β	γ	% rms Deviation	Distance (km)
Moderate (Run 1)	20.54	0.58	33.3	33.0
Moderate (Run 2)	20.54	0.58	20.5	8.1
Extreme	11.71	0.8371	9.3	2.4

5.4 Cumulative Distributions of Non-Fade Durations

A “non-fade duration” event of distance duration dd is defined as the distance over which the fade levels are persistently smaller than a prescribed fade threshold. A non-fade duration analysis was performed by the authors employing the same data set as described above for the “fade duration” case. The measured data were noted to fit the power expression

$$P(\text{NFD} > dd \mid A < A_q) = \beta(dd)^{-\gamma} \quad (5.6)$$

where $P(\text{NFD} > dd \mid A < A_q)$ is the percentage probability that a continuous non-fade distance NFD exceeds the duration distance dd (m) given the condition that the fade is smaller than the threshold A_q . The values of the parameters β and γ in the formulation (5.6) are listed in Table 5.3 for road types exhibiting “moderate” and “extreme” shadowing assuming a 5 dB fade threshold. As noted, a single best fit power curve has been derived for the two “moderate” runs. In Figure 5.3 are plotted the best fit curves (5.6) for the indicated parameter values given in Table 5.3.

Employing an analogous expression to (5.2), the joint absolute probability of exceeding a non-fade duration distance dd for which the fade is smaller than A_q is given by,

$$P(\text{NFD} > dd, A < A_q) = P(\text{NFD} > dd \mid A < A_q) P(A < A_q) \quad (5.7)$$

where the first right hand factor is given by (5.6) and the second is obtained from $1 - P(A > A_q)$ from (5.3).

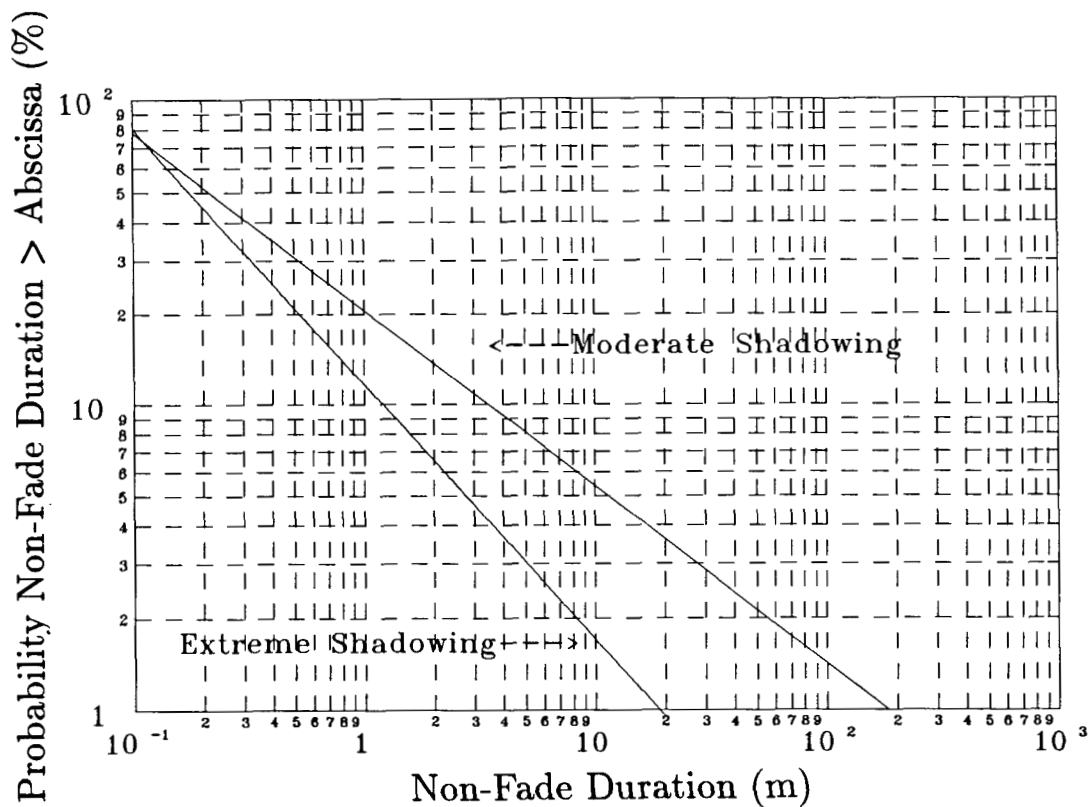


Figure 5.3: Best fit power curves (5.6) depicting non-fade durations for a 5 dB threshold for road types which exhibit “moderate” and “extreme” shadowing.

5.5 Cumulative Distributions of Phase Fluctuations

Phases were obtained from measured I and Q components after variations due to Doppler and oscillator drifts were eliminated using a high pass filter [Hase et al., 1991]. Conditional cumulative phase distributions were derived for each of the road-types described above. The conditions for these distributions were that the fades exceed attenuation thresholds levels ranging between 2-8 dB.

The “best fit” phase fluctuation distributions were found with good accuracy to follow a fifth order polynomial over a percentage exceedance range of 1% to 90% having the form

$$P(\phi > \phi_u | A > A_q) = \sum_{i=1}^6 a_{i-1} \phi^{i-1} \quad (5.8)$$

where (5.8) may be read as the probability that the phase ϕ (degrees) exceeds the threshold level ϕ_u given a fade A (dB) exceeds the threshold level A_q . In Table 5.4 is given a listing of the values of the polynomial coefficients a_i at the threshold fade level of 5 dB for the “extreme” and “moderate” road types (Figure 5.1). The corresponding phase fluctuation distributions are given in Figure 5.4.

We note that over the range 5% to 95% in Figure 5.4, the phases are within $\pm 15^\circ$ relative to the average for both the “moderate” and “extreme” cases. The indicated “best fit” polynomials agreed (in phase) with the individual measured distributions to within 15% rms.

For the “moderate” runs, cumulative distributions of phases over the probability range 1% to 90% were found to be minimally dependent on fade thresholds of 2 to 8 dB. We define the “phase spread” as the maximum phase difference (at equal probability) between the individual distributions for the different fade thresholds. A phase spread of less than 5° was noted for the “moderate” case over the range of distributions having fade thresholds 2 to 8 dB. For the “extreme” case, an approximate 20° phase spread (or less) was noted within the 1% and 99% levels over the fade threshold level of 2 to 8 dB.

Based on the above results, it would appear the influence of phase fluctuations on demodulation techniques at the elevation angle considered (e.g., 51°) is minimal and that LMSS channel characteristics can be estimated without considering phase. At lower elevation angles, greater multipath may be prevalent increasing the phase fluctuation spread. Loo

Table 5.4: Listing of polynomial coefficients characterizing phase fluctuation distributions of the form (5.8) for road types exhibiting “moderate” and “extreme” shadowing and a 5 dB fade threshold

Road Type	Polynomial Coefficients					
	a_0	a_1	a_2	a_3	a_4	a_5
Moderate	56.51	-6.516	-7.325×10^{-2}	2.380×10^{-2}	2.059×10^{-4}	-3.985×10^{-5}
Extreme	54.23	-4.242	-1.0897×10^{-2}	6.425×10^{-3}	2.082×10^{-5}	-4.258×10^{-6}

(private communication) reported large phase fluctuations for elevation angles between 5° and 20° which have a significant impact on digital communications.

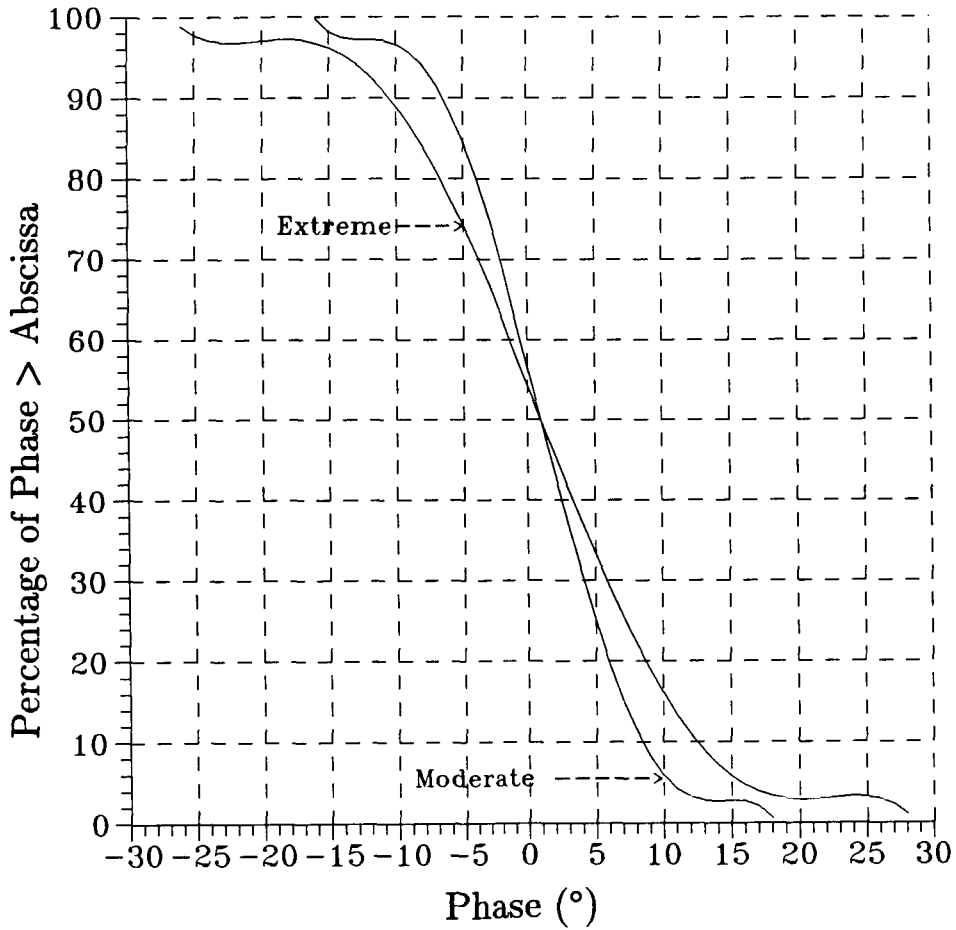


Figure 5.4: “Best polynomial fit” (5.8) cumulative phase distributions for road types which exhibit “moderate” and “extreme” shadowing for a 5 dB fade threshold.

Chapter 6

Propagation Effects Due to Cross Polarization, Gain, and Space Diversity

6.1 Background

Three questions are broached in this chapter, namely:

1. During conditions under which fading occurs, are LMSS systems employing simultaneous transmissions at two polarizations (right hand circular and left hand circular) viable?
2. What are the relative fading effects for low and high gain antennas?
3. Do space diversity systems employing spaced dual antennas on a vehicle provide an advantage in reducing the likelihood of fading?

The above questions have been addressed by the authors through the analysis LMSS measurements at 1.5 GHz in Australia [Vogel et al., 1991].

6.2 Frequency Re-Use

By making repeated measurements at co- and cross-polarizations for selected runs during the Australian campaign, equi-probability “cross-polar isolation levels, CPI” were determined. These are given by

$$\text{CPI}(P) = \frac{\text{COPS}(P)}{\text{CRPS}(P)} \quad (6.1)$$

where COPS and CRPS represent the co-polarization and cross-polarization signal levels at the equi-probability level of fade exceedance, P. The CPI (in dB) was found to follow the linear relation,

$$\text{CPI} = -1.605A + 18.94 \quad (6.2)$$

where A is the co-polarization fade (in dB).

The rms deviation between the “best fit linear” relation (6.2) and the data points for the corresponding runs was 0.4 dB. We note from the plot in Figure 6.1 that the isolation severely degrades as a function of fade level. For example, an approximate 11 dB isolation at a 5 dB fade is observed. This result suggests that the simultaneous employment of co- and cross-polarized transmissions in a “frequency re-use” system is implausible because of the poor isolation due to multipath scattering into the cross-polarized channel.

6.3 Distributions from Low and High Gain Receiving Antennas

During the Australian campaign, a number of repeated runs were executed in which high and low gain antennas were employed. The characteristics of these antennas are given in Table 6.1. Figure 6.2 shows a plot of the high gain receiver fade versus the low gain fade over the low gain fade interval of 0 to 15 dB. The data points were found to follow the linear relation

$$A(\text{HG}) = 1.133 A(\text{LG}) + 0.51 \quad (6.3)$$

where A(HG) and A(LG) represent the high and low gain fades (in dB), respectively. Agreement between the relation (6.3) and the data points for A(HG) were within 0.2 dB rms.

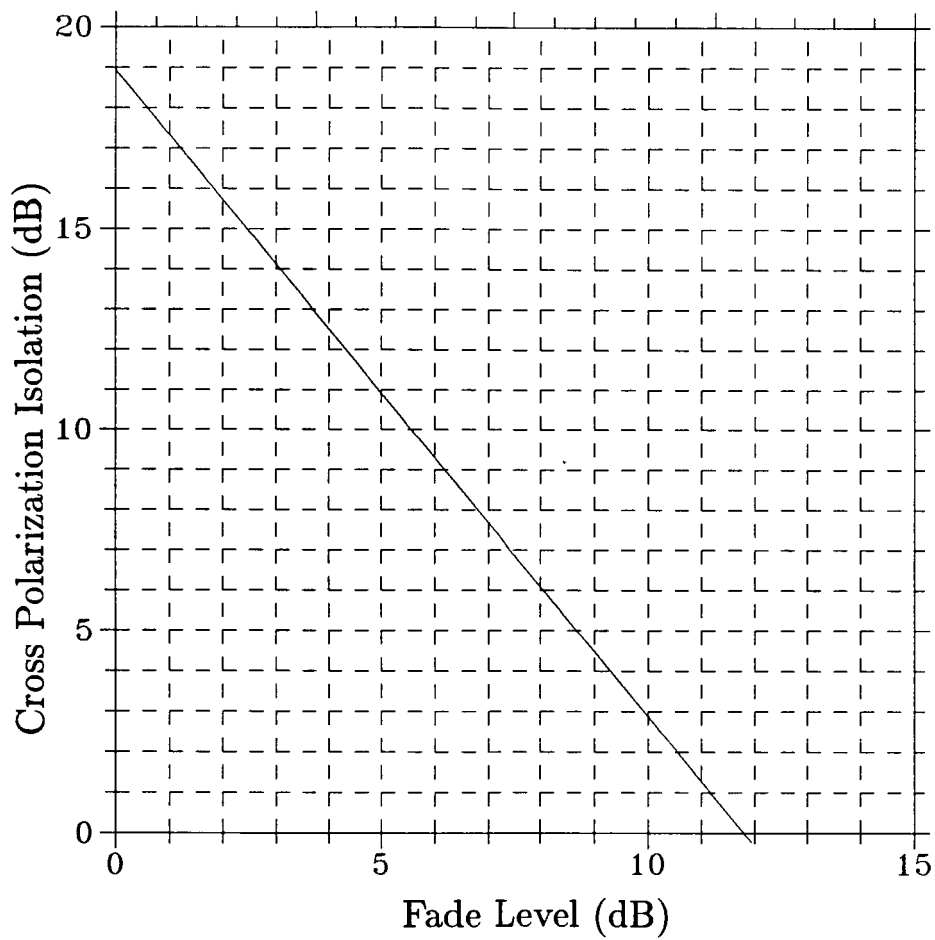


Figure 6.1: Cross-polarization isolation (CPI) as a function of co-polarization fade at equi-probability levels.

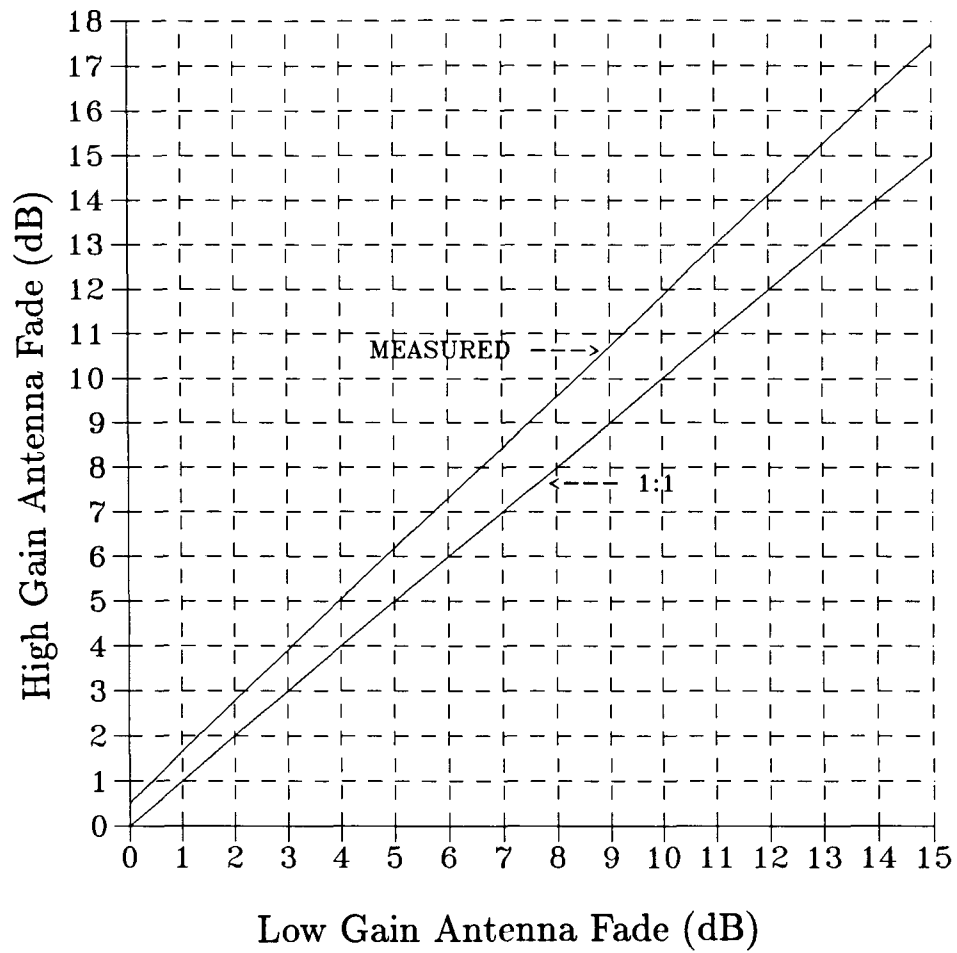


Figure 6.2: Fade for measured by high gain receiver system versus fade measured by low gain system at equi-probability levels.

Table 6.1: Summary of pertinent characteristics for high and low gain receiver antennas used during the Australian campaign [Vogel et al., 1991]

Characteristic	Low Gain	High Gain
Type	Crossed Drooping Dipoles	Helix
Gain (dB)	4	14
Nominal Pattern (El)	15° - 70° (Fixed)	45° (Principal Planes)
Nominal Pattern (Az)	omni-directional	45°
Polarization	LHCP or RHCP	RHCP or LHCP

We note that the high gain system experiences consistently more fading than the low gain case. For example at 3 and 14.5 dB (of low gain fades), the high gain fades are 4 and 17 dB, respectively, which represent 33% and 17% increases. This slight increase in attenuation for the high gain case occurs because less average power is received via multipath since the associated antenna beam is narrower. On the other hand, the azimuthally omni-directional low gain antenna receives more scattered multipath contributions resulting in an enhanced averaged received power. It is important to note that because the high gain antenna has 10 dB more gain associated with it, the net power received by it is still significantly higher than that received for the low gain case. Even at the 15 dB fade level (low gain receiver system), the net received power for the high gain mode is larger by 7.5 dB.

6.4 Diversity Operation

A space diversity simulation has been carried out employing the data base corresponding to 400 km of roadside tree shadowing measurements taken during the Australian campaign. Space diversity operation for LMSS configurations may be envisaged by the scenario of two spaced antennas mounted atop a vehicle where each antenna is fed to a separate receiver system. Because the signal levels at the two antennas are expected to be different at any instant of time, rapid switching between the two receiver outputs followed by subsequent processing should enable the larger signal to be accessed. Such a system should therefore require smaller fade margins for the same "signal access distance" than single terminal systems. The signal access distance represents that distance over which the received signal level operates within the designed fade margin.

Questions which have been broached are:

- What is the increase in “signal access distance” as a function of antenna spacing along the driving direction?
- What is the improvement in terms of reduced fading (enhanced signal) for a given “signal access distance” as a function of antenna spacing?

The first question is addressed employing the concept of “diversity improvement factor, DIF” and the second “diversity gain, DG,” both of which are characterized in the following paragraphs.

6.4.1 Joint Probabilities

In Figure 6.3 are shown a family of cumulative fade distribution functions derived from the above mentioned simulation. The curve labeled $d = 0$ represents the single terminal cumulative fade distribution corresponding to data acquired from over 400 km of driving in Australia. The curves labeled $d = 1$ to 10 m represent the individual joint probability cumulative fade distribution for the indicated antenna separations (in the direction of vehicle motion). Such a distribution represents “the joint probability that two antennas spaced a distance d mutually exceed the abscissa value of fade.” We note that the joint probabilities tend to coalesce with increasing antenna separation. That is, the fade distributions for 8 m and 10 m separations show insignificant differences.

6.4.2 Diversity Improvement Factor, DIF

The DIF is defined as

$$\text{DIF}(A, d) = \frac{P_o(A)}{P_d(A)} \quad (6.4)$$

where $P_o(A)$ represents the single terminal probability distribution at the fade depth A , and $P_d(A)$ represents the joint probability distribution for an antenna spacing d assuming the same attenuation A is exceeded. These probabilities may be obtained from Figure 6.3. We note, for example, that $\text{DIF}(8,1) \approx 3$ implies that when the antennas are separated 1 m,

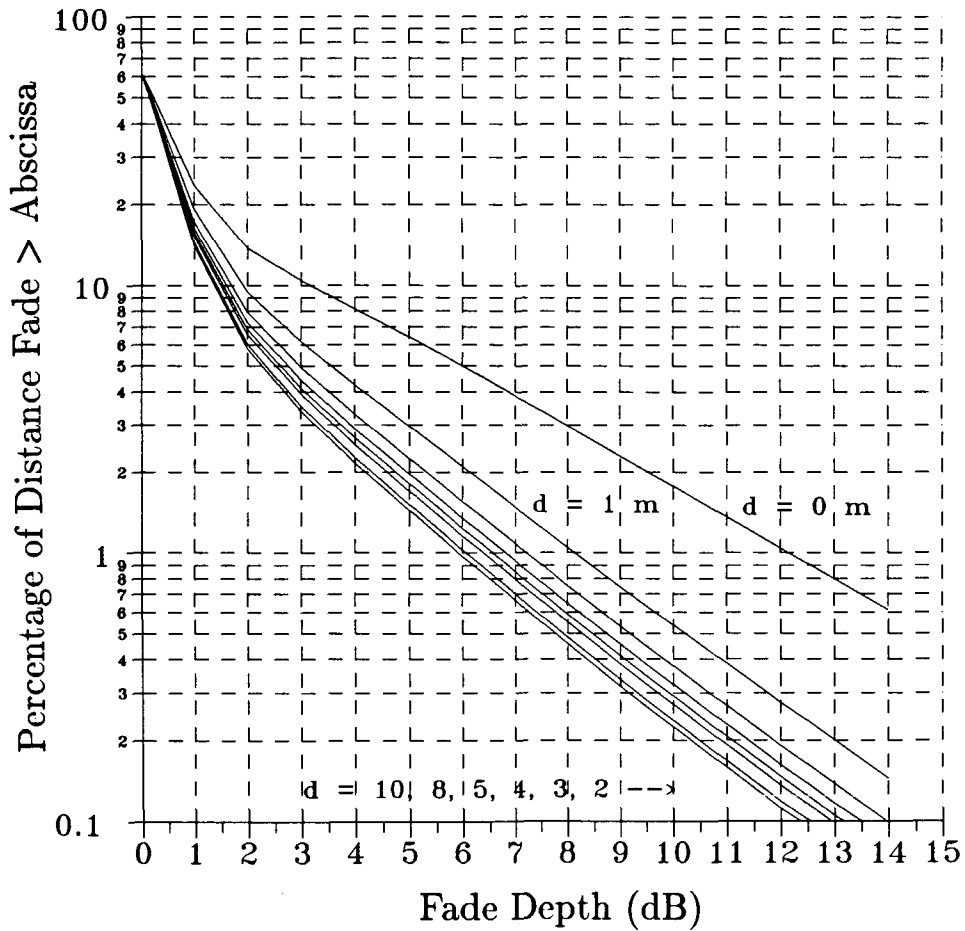


Figure 6.3: Single and joint probability fade distributions for mobile communications operating in a space diversity mode with antennas separated by the distance, d .

the distance over which the signal is received above noise is three times greater for diversity operation relative to the single terminal case assuming an 8 dB fade margin.

Employing the above results, a least square estimate of DIF was derived given by,

$$\text{DIF}(A, d) = 1 + [0.2 \times \ln(d) + 0.23] \times A \quad (6.5)$$

where d is the antenna separation expressed in m and A is the fade depth in dB.

In Figure 6.4 are plotted a family of curves of DIF as a function of fade depth for antenna separations between 1 and 10 m. We note that at the larger separations for any given fade depth, the rate at which DIF increases diminishes rapidly.

6.4.3 Diversity Gain

The diversity gain is a concept defined by Hodge [1978] for an earth-satellite communications system involving two spaced antennas operating in a diversity mode in the presence of precipitation. This concept may also be applied to separated antennas atop a vehicle for LMSS scenarios. The diversity gain is defined as the fade reduction experienced while operating in the diversity mode at a given probability. It is equal to the difference in fades between the single terminal and joint probability distributions at a fixed probability level. For example, for 1% of the time (Figure 6.3) a fade depth of 12 dB will be encountered with no diversity ($d = 0$) and 8 dB with diversity assuming a 1 m separation ($d = 1$). Hence, operation in the diversity mode with a 1 m separation yields a diversity gain of 4 dB.

In Figure 6.5 are plotted the diversity gains versus antenna separations for a family of single terminal fade levels. Each single terminal fade uniquely defines a probability level. For example, an 8 dB fade occurs at a probability level of 3% as is noted from Figure 6.3 (for $d = 0$). Figure 6.5 shows that the effect of the antenna separation is dramatic the first 2 meters, whereas at larger spacings, relatively little additional fade reduction ensues. It might be suggested that at antenna spacings greater than the canopy width (e.g., 8 to 10 m), the diversity gain would show a noticeable improvement since one antenna would have an associated unshadowed line-of-sight during the time the line-of-sight for the other antenna is shadowed. This would be the case for a single tree scenario. However, the results depicted in Figure 6.5 correspond to cases where multiple trees exist along roads such that the canopies form a continuum of shadowing. Hence, the single tree model no longer holds.

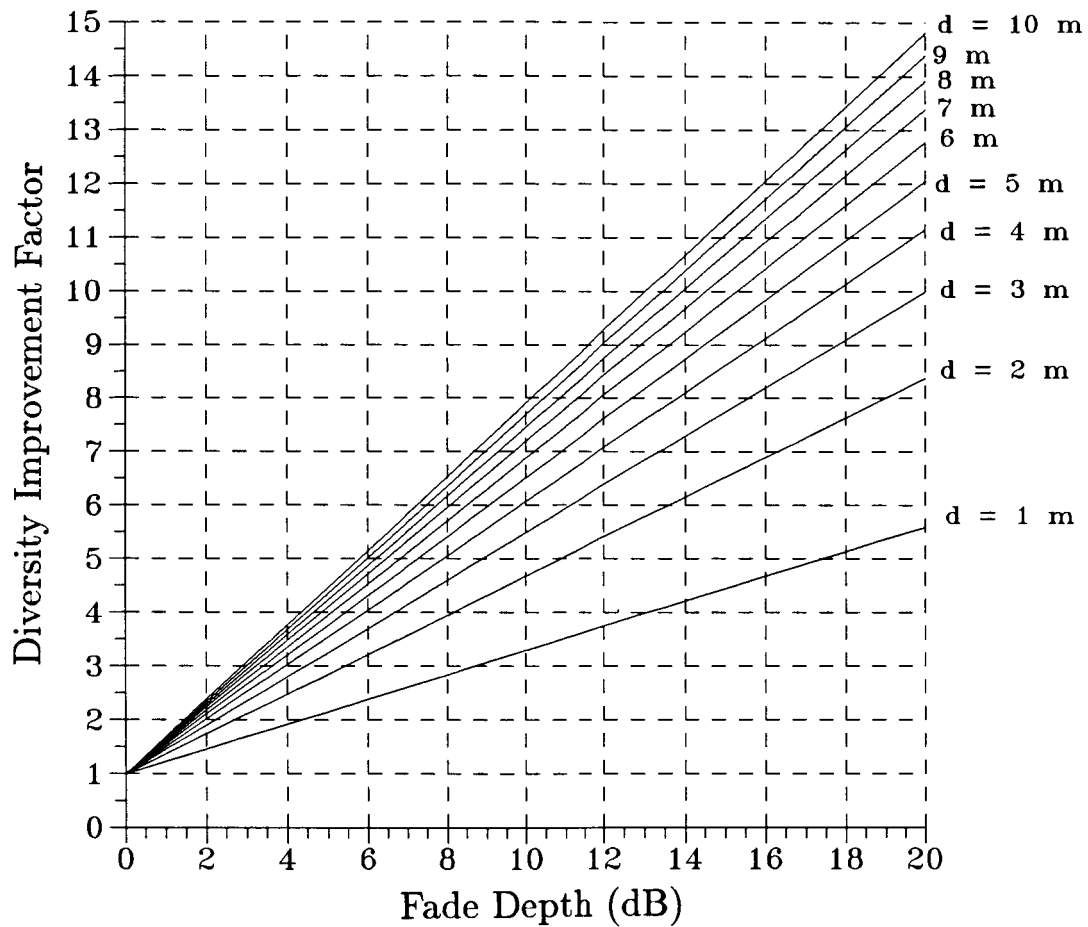


Figure 6.4: Diversity Improvement Factors (DIF) as a function of fade depth for a family of antenna separation distances.

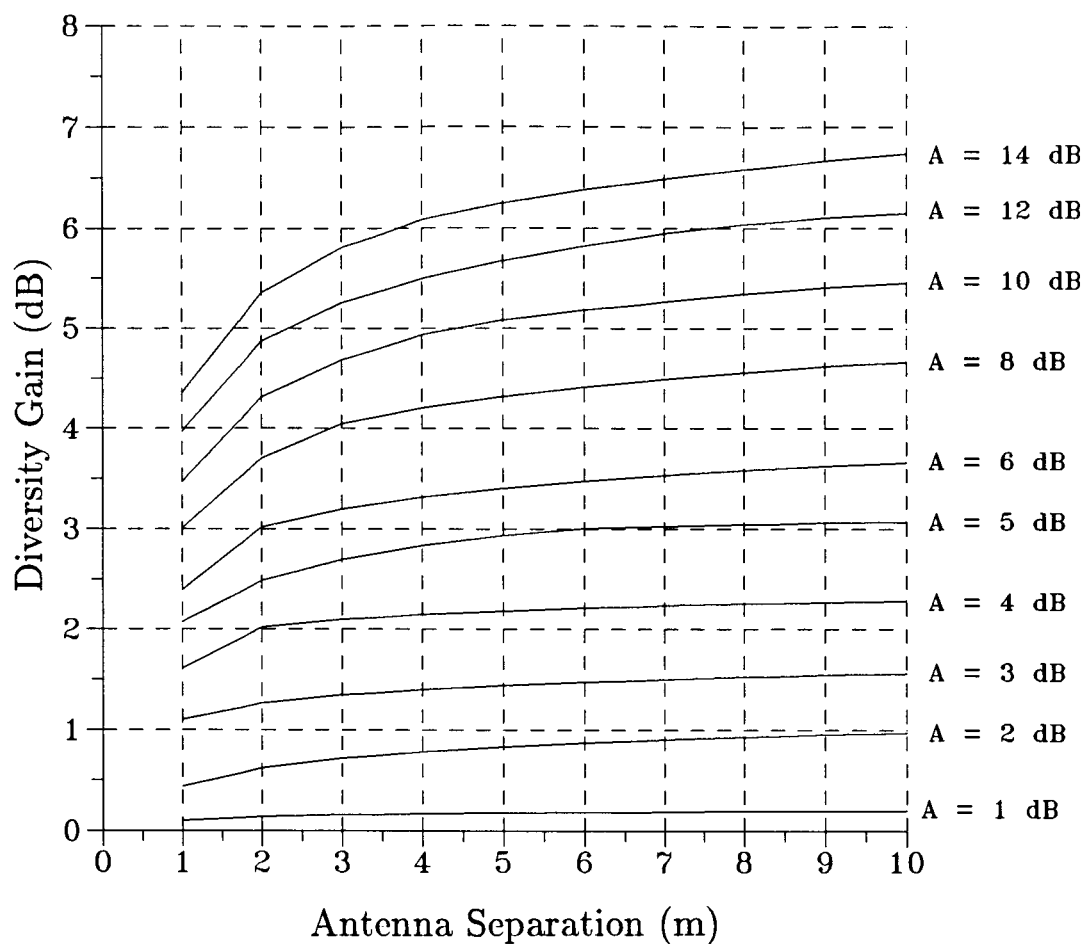


Figure 6.5: Diversity gain versus antenna separation distance for a family of single terminal fade levels.

Chapter 7

Investigations from Different Countries

The results described here provide a sampling of measured cumulative fade distributions for LMSS geometries pertaining to significant experiments in various countries. We emphasize distributions associated with rural and suburban regions as opposed to measurements in urban environments.

In comparing the results of the different investigations, the reader should be cognizant of the fact that the various experiments were conducted at a variety of elevations angles and bearings to the source. The diverse geographic regions (e.g., wooded, forest, rural, mountainous, highways) also have associated with them dissimilar conditions of foliage density along the propagation path, and variable distances between vehicle and foliage line. The distributions shown have been replotted consistent with the scales considered previously; namely, the fade (in dB) along the abscissa and the percentage of distance along the ordinate. Table 7.1 represents a summary of nominal fade values at the 1% and 10% levels for the various investigations. It is apparent from the wide variance of fades in this table that elevation angle and geographic region play important roles in the determination of LMSS attenuation.

Table 7.1: Comparison of L-Band fade levels at 1% and 10% probabilities derived from cumulative distributions in different countries.

Country	Elev. (deg)	Fade (dB)		Reference
		1%	10%	
Australia:				Bundrock [1988]
Case 1	30	16.7	10.8	
Case 2	45	13.5	8.8	
Case 3	60	11.3	7.1	
Australia:				Vogel et al. [1991] (Fig. 3.6)
Case 1	51	12.2	4.0	
Case 2	40	—	6.1	
Belgium	26	20.3	7.3	Jongejans et al. [1986]
Canada:				Butterworth [1984a]
Suburban	19	11	3.5	
Rural/Forest	19	20	8	
Rural/Farmland	19	21	10.5	
England	40	9	5.6	Renduchintala et al. [1990]
Japan	46	6.3	2.0	Saruwatari et al. [1989]
United States:				Vogel and Goldhirsh [1990]
Case 1	20	25.9	15.3	
Case 2	30	21.5	11.0	
Case 3	45	14.8	6.1	
Case 4	60	8.2	3.4	

7.1 Measurements in Australia

Bundrock and Harvey [1988] reported on cumulative fade distributions obtained on typical double lane roads in Melbourne, Australia. Messmate (stringybark) Eucalyptus trees approximately 15 m high lined the road and measurements were made over sections of the road corresponding to tree densities of 35% and 85%. Systematic measurements were made at varying elevation angles at simultaneous frequencies of 897 MHz, 1550 MHz, and 2660 MHz employing a helicopter as the transmitter platform and a receiver system in a mobile van. Figure 7.1 represents a set of cumulative fade distributions for the 85% tree density case at a frequency of 1550 MHz for elevation angles of 30°, 45°, and 60°. Figure 7.2 shows the distributions for the 85% tree density case and the three frequencies considered at a 45° elevation angle.

Vogel et al. [1991] also measured cumulative fade distributions in Australia employing the ETS-V and INMARSAT-Pacific geostationary satellites as transmitter platforms where the nominal elevation angles were 51° and 40°, respectively. These results were consistent with the ERS model described in Chapter 3. To provide a basis of comparison, fades at the 1% and 10% percentage levels pertaining to the ERS model are also given in Table 7.1 for a series of elevation angles denoted by the different cases. As previously mentioned, the model represents an overall driving condition and is generally representative of a maximum shadowing geometry; namely, the case for which the line-of-sight is orthogonal to the line of roadside trees.

7.2 Measurements In Canada

Canadians were early pioneers in the implementation of fade measurements for mobile-satellite system geometries [Butterworth and Matt, 1983; Huck et al., 1983; Butterworth 1984a, 1984b]. Butterworth [1984a, 1984b] describes roadside fade statistics measured at UHF (870 MHz) and L-Band (1.5 GHz) in Ottawa, Ontario, Canada. Various transmitter platforms were employed. These included a tower, a tethered balloon, a helicopter, and the MARECS A satellite.

Figure 7.3 shows UHF fade distributions at various elevation angles as derived from helicopter measurements in June 1983 for a rural region in which woodlands constituted

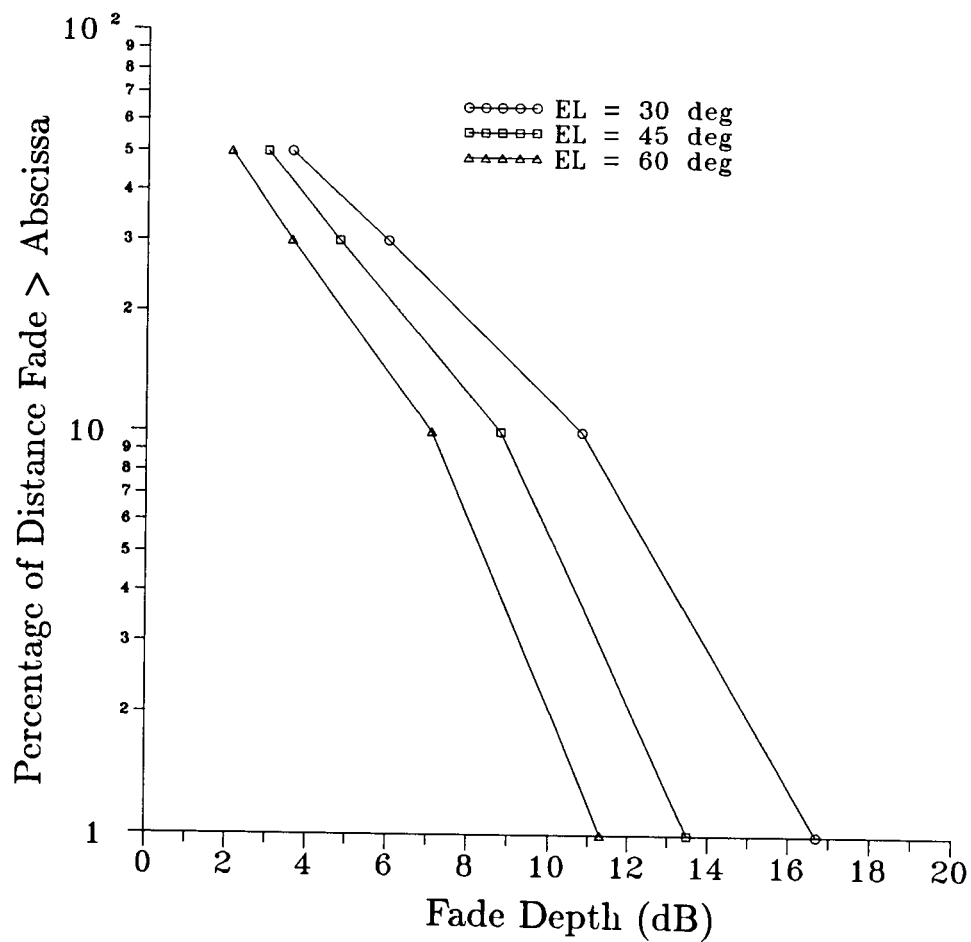


Figure 7.1: Cumulative fade distributions at various elevation angles derived by Bundrock and Harvey [1988] for Melbourne Australia at 1.55 GHz for a tree lined road having a 85% tree incidence.

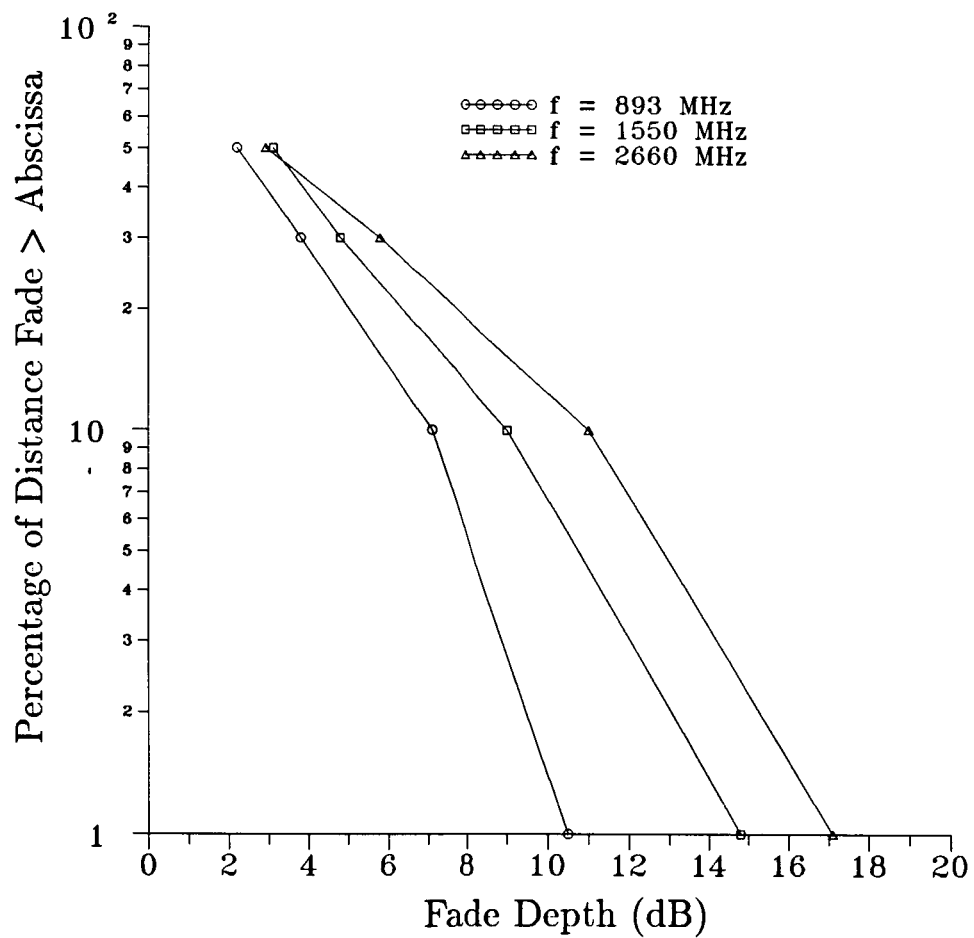


Figure 7.2: Cumulative fade distributions at UHF, L-Band, and S-Band derived by Bundrock and Harvey [1988] for Melbourne Australia at an elevation angle of 45°.

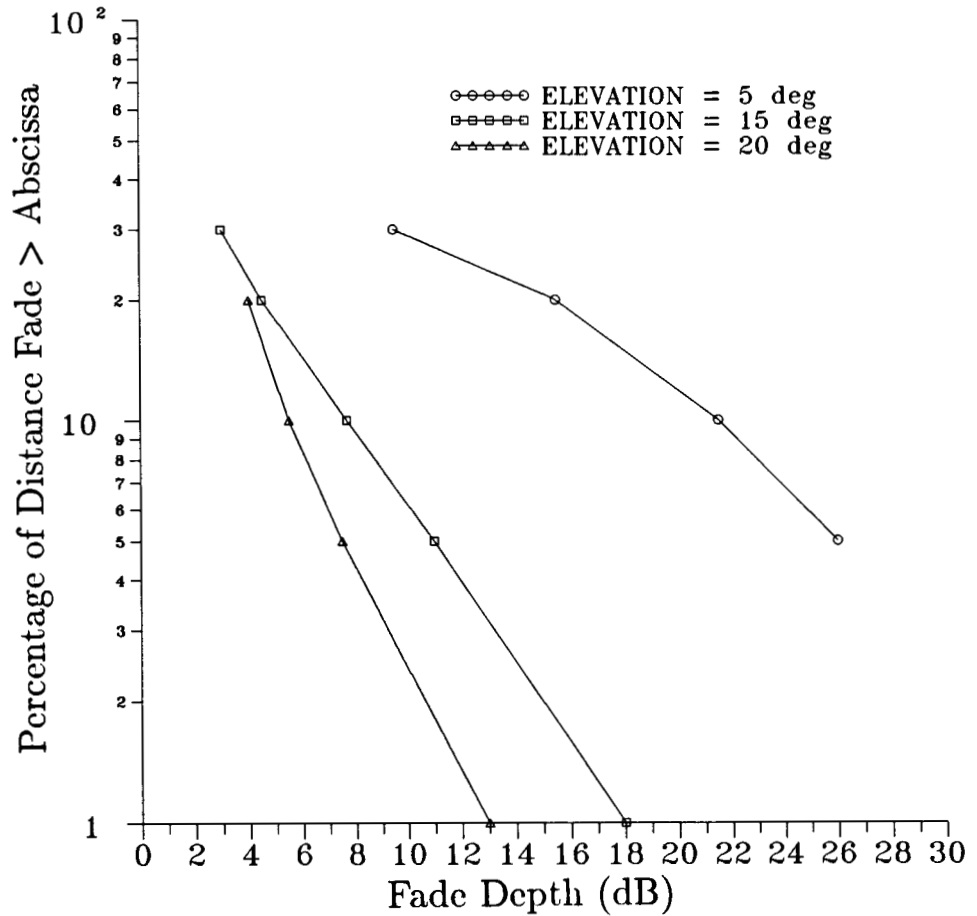


Figure 7.3: Cumulative fade distribution at UHF (870 MHz) in Ottawa, Ontario, Canada derived from helicopter measurements in a rural region (35% woodland) [Butterworth, 1984b].

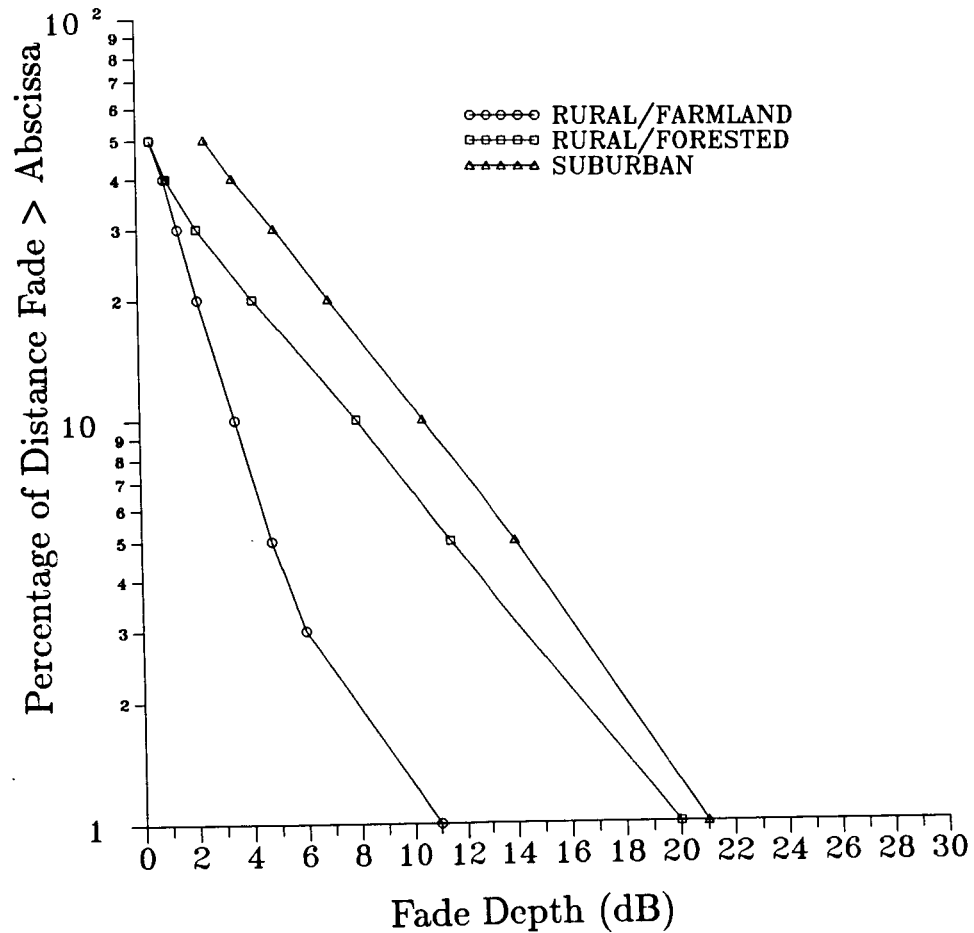


Figure 7.4: Cumulative fade distribution at L-Band (1.5 GHz) in Ottawa, Ontario, Canada derived from MARECS A satellite measurements in rural and suburban regions at 19° elevation [Butterworth, 1984a].

35% of the land area.

In Figure 7.4 are shown three distributions obtained from the MARECS A satellite transmissions at 1.5 GHz for a 19° elevation for suburban, rural/forested, and rural/farmland. Butterworth characterized these regions as follows:

Suburban - "an older suburban residential area consisting mainly of one and two-storey single-family dwellings."

Rural/Forested - "consisting of hilly terrain covered with immature timber of mixed species, interspersed with occasional cleared areas. The route followed a series of paved provincial highways with one lane for each traffic direction and with gravel shoulders."

Rural/Farmland - "area consisting of almost entirely of flat, open fields. About 5% of this route ran through occasional wooded areas. The roads were paved county roads with one lane for each traffic direction and with gravel shoulders."

7.3 PROSAT Experiment-Belgium

The PROSAT Experiment was instituted by the European Space Agency (ESA) with the objective to accelerate the development of LMSS in Europe [Jongejans et al., 1986]. This experiment involved seven ESA member states; namely Belgium, Federal Republic of Germany, France, Italy, Spain, United Kingdom and Norway. The MARECS B-2 satellite was used as the transmitter platform where transmissions were executed at L-Band (1.5 GHz).

In Figure 7.5 is shown the cumulative distribution for Belgium obtained in January 1984 in a rural area. The area (Ardennes) was hilly and the roadside was lined with bare trees [Jongejan et al., 1986].

7.4 Measurements Performed in England

In Figure 7.6 are cumulative fade distributions obtained in England in typical, rural, tree shadowed environments where all the trees had full leaf cover [Renduchintala et al., 1990;

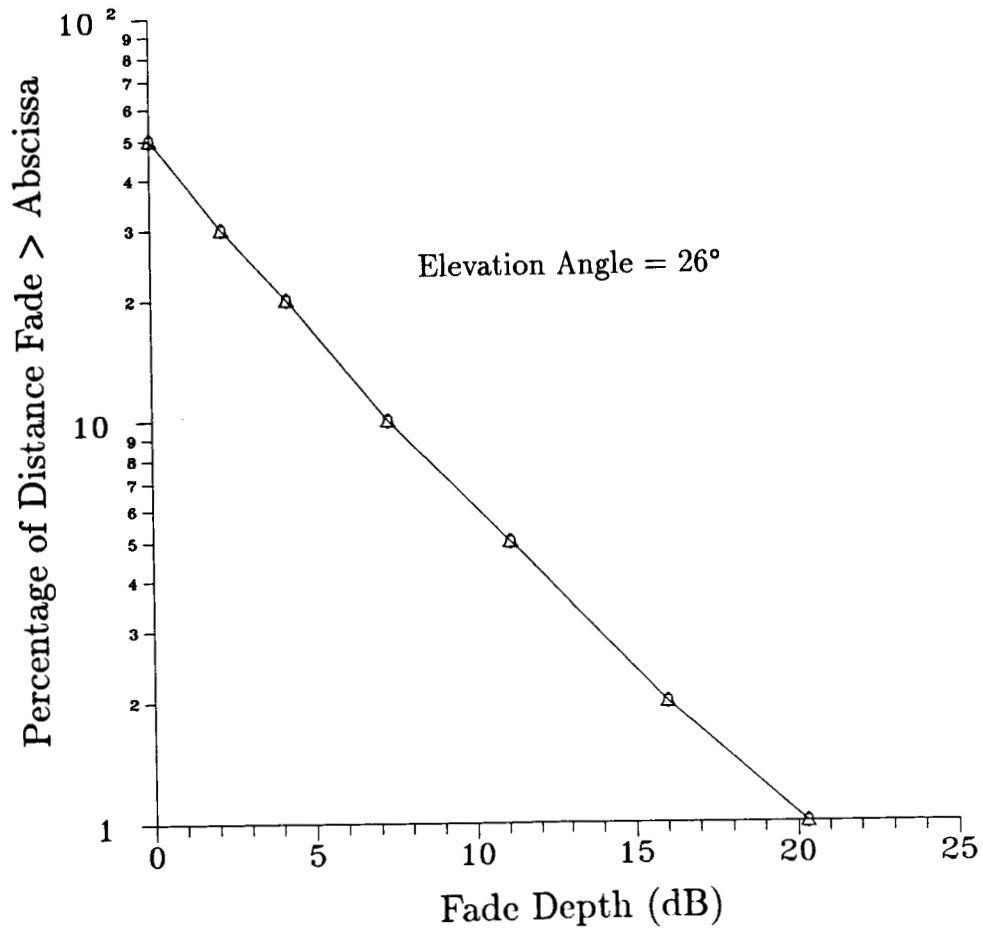


Figure 7.5: Fade distribution for a rural region at 1.5 GHz derived from measurements in Belgium in January 1984 [Jongejan et al., 1986].

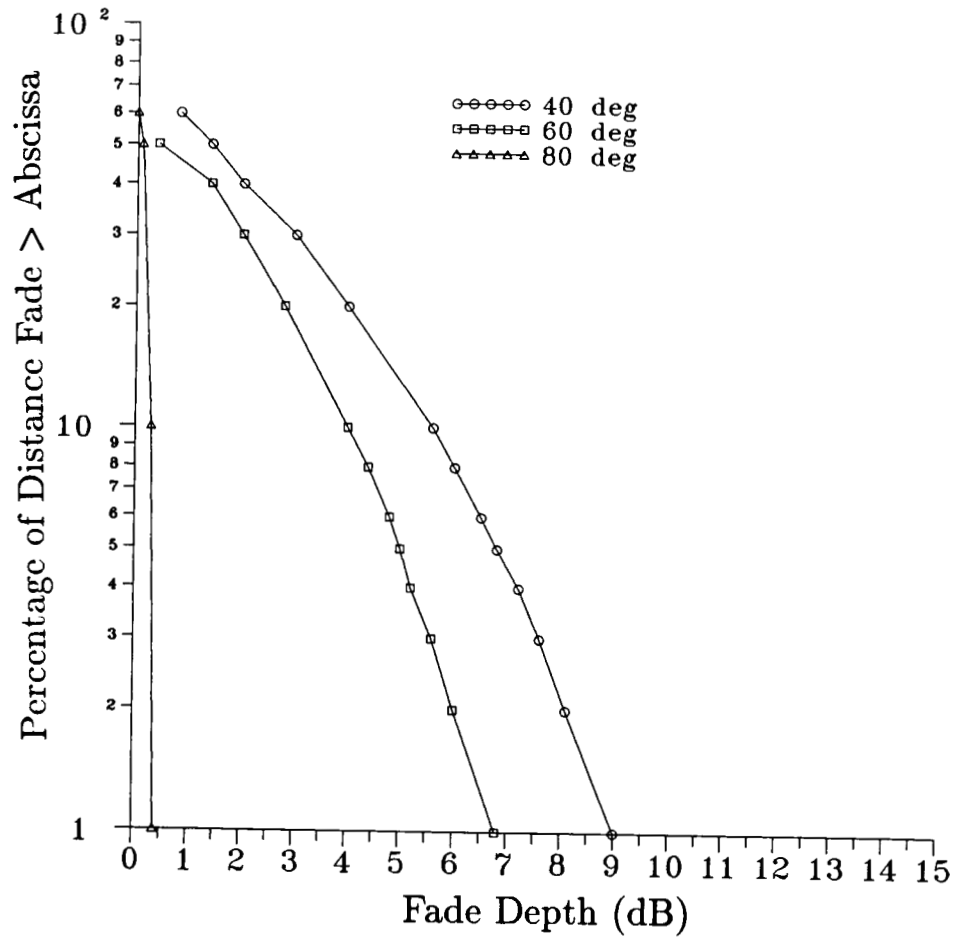


Figure 7.6: Fade distributions (L-Band) for tree shadowed environments in England for different elevation angles [Renduchintala et al., 1990; Smith et al., 1990].

Smith et al., 1990]. These results were derived from L-Band transmissions from an antenna mounted on an aircraft and received by a mobile van. Figure 7.6 depicts the distributions for a sequence of runs executed at the elevation angles of 40°, 60° and 80°. As in the case of other investigations, the results demonstrate the strong dependence of fades on elevation angle.

7.5 Measurements Performed in the United States

Early LMSS measurements were reported by Hess [1980] who received the vertically polarized components of right hand circular transmissions at 860 MHz and 1550 MHz from the ATS-6 geostationary satellite. Systematic fade measurements were obtained with the receiver system on a moving van as a function of local environment, vehicle heading, frequency, elevation angle, and street side. Since the circularly polarized transmissions were received with a vertical dipole, the measured signal levels were susceptible to low elevation multipath scattering. Because the distributions described by Hess mainly correspond to urban environments in Denver, his results will not be covered here other than to point out that 25 dB fades were typical for the urban areas. Hess does report, however, that of the measurements made in suburban and rural areas, typical fade levels of 10 dB were measured. An empirical propagation model derived by Hess from his measurements is described in Chapter 8.

As mentioned previously, systematic propagation measurements were made in the United States by the authors over the period 1983 - 1988. For example, measurements were made in southwest United States for suburban and rural regions by the University of Texas in 1983, 1984, and 1986 at both UHF and L-Band employing stratospheric balloons as the transmitter platform [Vogel and Hong; 1988]. In 1985-88, LMSS measurements were performed by the authors employing helicopters and satellites as transmitter platforms [Table 1.1]. The different cases in Table 7.1 pertain to the indicated elevation angles where the associated fades were derived from the ERS model described in Section 3.3. Since the dominant part of this text deals with the results of these measurements, no additional comments relating to these investigations are presented here.

7.6 Measurements Performed in Japan

Saruwatari and Ryuko [1989] performed a series of LMSS measurements employing L-Band transmissions from the Japanese ETS-V satellite which were received by a moving van. Figure 7.7 shows three distributions corresponding to elevation angle of approximately 46° . The distributions were derived from measurements executed on two expressways and one "old road" which runs alongside one of the expressways (Kan-etsu). Both expressways traverse flat areas, mountainous terrain, and have many two-level crossing with local roads. The "old road" runs through local urban areas, suburbs, farms, with a number of bridge crossings for pedestrians.

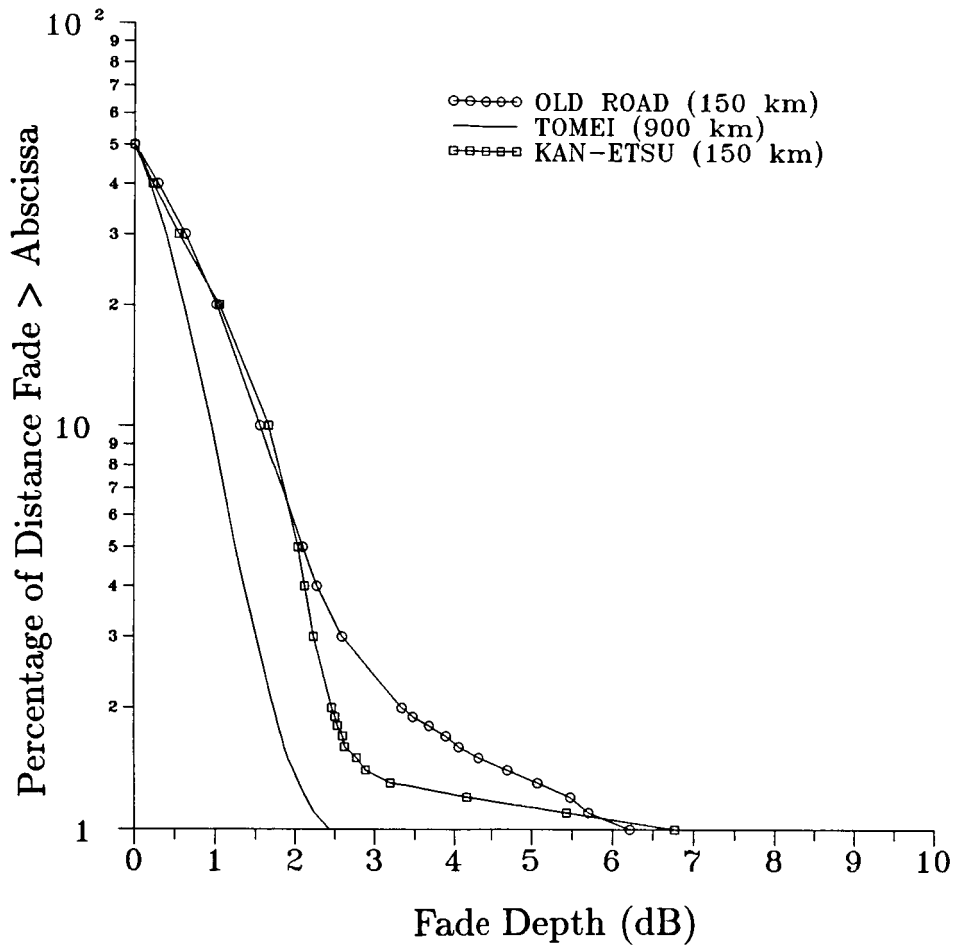


Figure 7.7: Fade distributions at L-Band for two expressways and an “old road” in Japan [Saruwatari and Ryuko, 1989].

Chapter 8

Modeling for LMSS Scenarios

8.1 Background

Modeling serves a variety of purposes for characterizing land mobile satellite propagation. Without the availability of data, a qualitative propagation model is desirable in order to design propagation experiments which measure important signal characteristics without imposing instrumentation limitations. Once data are available, quantitative models can be developed to explain the observed signal variations and their dependence on a wide range of experimental parameters, such as the environment topography, link elevation angle, vehicle speed, or receiver antenna pattern. As models reach maturity, they can be employed to predict system performance under specified conditions or to simulate the actual operation for LMSS scenarios with a particular choice of modulation and coding. Good models based on a thorough understanding of the causes of signal degradation can then be used as aids in optimizing system design and to explore fade mitigation strategies.

Much work has been done to characterize the signal variations observed in terrestrial land mobile propagation at UHF [Jakes, 1974; Lee, 1986]. While some of the same basic concepts of signal statistics apply also to LMSS, significant differences exist and require the development of LMSS specific models. Satellite systems are usually power limited because it is expensive and/or impractical to operate high-power transmitters and high-gain antennas in space. Such systems therefore function with relatively low fade margins at or near the

line-of-sight signal level. On the other hand, terrestrial systems can apply higher power levels and do not need to establish a line-of-sight signal path. They normally operate by utilizing the scattered multipath signals. In contrast, satellite systems must utilize the line-of-sight component for communications, and multipath scattering represents interference.

In response to the needs of experimenters and system designers, several distinct types of LMSS models have been developed. Three classes of models are described in the following paragraphs. They are classified here as: (1) empirical regression fits to data, (2) probability distribution models, and (3) geometric-analytic models. The empirical regression fits to data models describe probability distributions of fades based on experimental measurements. The second class, statistical probability distributions models, are based on the utilization of a composite of several probability density functions customarily used in radio wave propagation; namely, Rayleigh, Rician, and lognormal statistics. Among these, some combine densities based on physical reasoning about the propagation process, while others add the use of fade state or fade state transition probabilities. The third class of models employ geometrical analytical procedures for predicting the effects of single and multiple scatterers.

The choice as to which model is most appropriate depends very much on the intended application and which propagation phenomenon one wants to predict. Of the different types, empirical models do not provide insight into the physics of propagation processes, but they characterize the sensitivity of the results to important parameters. Statistical models build upon an understanding of the processes which cause signal variations, but with simplifying assumptions. Analytical models attempt to describe a particular propagation scenario deterministically, but then have to use statistics to extend the results to realistic situations.

In this chapter are described background information associated with the important elements of model development. Also described are the dominant LMSS propagation models of the above types, their input and output parameters, as well as their advantages and limitations.

8.2 Background Information Associated with Model Development

8.2.1 Diffusely Scattered Waves

To explain signal variations specific to LMSS transmissions between a satellite and a moving vehicle, the interactions of two important signal components have to be considered: line-of-sight and diffusely scattered waves. We ignore the ground reflected waves since it is presumed that for LMSS scenarios, any energy directed towards the antenna near the horizontal will be outside its beamwidth and be filtered out by the low gain pattern function values.

The direct wave may be approximated by a plane wave propagated along the line-of-sight path, with most of the power transmitted through the central few Fresnel zones. It may be completely obscured by obstacles such as mountains, buildings, or overpasses, or it may be partially shadowed by roadside trees or utility poles. The shadowing process may be explained by absorption, diffraction, scattering, or a combination thereof. The frequency of the direct wave is shifted by an amount proportional to the relative speed between the satellite and the vehicle.

A scenario for diffuse scattering for mobile reception may be described as follows. Transmissions from a satellite illuminate obstacles in the vicinity of the vehicle resulting in reflected energy emanating from multiple scatterers. Waves from these scatterers arrive at the receiving antenna with random, polarizations, amplitudes, and phase, where the individual contributions have been delayed by the amount of time corresponding to the extra path traveled. In addition, the individual contributions undergo a Doppler shift proportional to the relative speed between any particular scatterer and the vehicle. It is limited to a band of frequencies relative to the zero speed center frequency given by,

$$\Delta f_D = \pm \frac{v}{\lambda} \quad (8.1)$$

where v is the vehicle speed in m/s and λ is the wavelength in m. The + and - signs denote an increase and decrease of frequency assuming the illuminated obstacles are directly in front of and behind the vehicle, respectively. This, of course, represents a worst case scenario which may occur at locations where there are sharp bends in the road. As an example, a vehicle traveling at 25 m/s (≈ 55 mi/h) receiving L-Band (1.5 GHz or $\lambda = 0.2$ m), will experience Doppler shifts limited to ± 125 Hz.

8.2.2 Faraday Rotation

Faraday rotation effects [Davies, 1990; Flock, 1987] are potential contributors to signal strength variations which can be neglected for LMSS systems which employ circular polarization. The ionosphere contains free electrons in a relatively static magnetic field. This combination causes polarization rotation of linearly polarized waves as given by (for $f > 100$ MHz)

$$\phi = 1.35 \times 10^6 \frac{B_e \text{ TEC}}{f^2} \quad (\text{deg}) \quad (8.2)$$

where where f is the frequency in Hz and B_e is the effective earth's magnetic field in Webers/m² defined by

$$B_e = \frac{\int N B \cos \theta_B d\ell}{\text{TEC}} \quad (8.3)$$

and where θ_B is the angle between the direction of propagation and the earth's magnetic flux density vector. TEC is the total electron content (#/m²) given by

$$\text{TEC} = \int N d\ell \quad (\# \text{ of electrons/m}^2) \quad (8.4)$$

where ℓ is the path length through the ionosphere and N (#/m³) is the electron density along the path. Assuming, extreme values of TEC and B_e given by [CCIR, 1986b (Report 263-6)],

$$\text{TEC} = 1.86 \times 10^{18} \quad (\#/\text{m}^2) \quad (8.5)$$

$$B_e = 0.43 \times 10^{-4} \quad (\text{Webers/m}^2) \quad (8.6)$$

polarization rotations of 142.7° and 48.0° occur at $f = 870$ MHz and $f = 1.5$ GHz, respectively. It is apparent that at UHF frequencies, significant signal loss due to polarization mismatch may occur. As mentioned, this is normally avoided by transmitting and receiving circular polarized signals since the receiving antenna is insensitive to the same polarization shifts of the orthogonal linear components comprising the circular polarized wave.

8.2.3 Ground Specular Reflection

This type of specular reflection is generated on the ground near the vehicle, where the ray from the reflection point to the antenna is below the horizontal. This coherent reflection

comes from an area around the intercept point the size of a few Fresnel zones. Its strength, relative phase shift, and polarization depend on the roughness and dielectric properties of the ground and are elevation angle sensitive. In a system utilizing a low-gain antenna (e.g., a dipole) which can geometrically see the specular point and also has gain in that direction, destructive interference between the specular reflection and the direct wave can produce deep fades [CCIR, 1986a (Report 1008); Flock, 1986].

The antennas contemplated for use in LMSS are either low-cost, medium gain, fixed pointed or higher-cost, high gain, tracking antennas. A typical medium gain antenna is a crossed drooping dipole, which has azimuthally omni-directional gain of about 4 dB from 15° to 60° elevation. At lower elevation angles its gain decreases rapidly, thus providing protection against both specular reflection from the ground near the vehicle as well as multipath scatter from elevated objects at larger distances. A high-gain antenna, typically a mechanically or electronically scanned array, achieves even greater rejection of multipath power and a concomitant narrowing of the Doppler spectrum. Isolation from ground specular scatter is further enhanced by placing the antenna on the center of the vehicle roof which acts as a ground plane and helps to direct the pattern upward.

Some additional rejection of the specular reflection can be achieved because circular polarization is reversed when the grazing angle of reflection is larger than the grazing Brewster angles. In particular, these grazing angles are in the range of 15° to 35° for very wet to very dry land, respectively [Reed and Russel, 1966].

8.3 Empirical Regression Models

Empirical regression models correspond to fade distributions derived from experimental measurements at different frequencies, elevation angles, vehicle headings, sides of road, types of terrain, and extent of shadowing. They all have the common advantage of being based on actual data and hence they may be used with a certain degree of confidence for the prediction of fade distributions over similar types of roads. Although they are derived from "time-series" of fading events, this information is lost in the derivation of the distributions. The physics associated with the empirical models exist to the extent that the models are based on the categorized measureables, such as frequency, elevation angles, heading, and percentage of shadowing due to trees.

The common disadvantage associated with these models is that difficulties may exist in extrapolating these models to cases not considered; such as other “road-types” and frequencies outside the interval of scaling.

8.3.1 Large Scale - Small Scale (LS-SS) Coverage Model

The first propagation experiments targeted towards land mobile satellite communications were conducted by observing 860 MHz and 1550 MHz transmissions emanating from NASA's ATS-6 spacecraft [Hess, 1980]. Using the data base from measurements taken over about 1200 km in or near nine cities of the Western and Midwestern United States, an empirical model was derived relating the probabilities of exceeding fades for large scale (LS) and small scale (SS) “coverages.” Coverage in broadcasting is defined either in terms of percentage of locations within an area or percentage of time at a particular location that there exists satisfactory service. For LMSS scenarios, signal level variations as a function of time are produced by vehicular motion. The model under discussion (denoted by LS-SS) describes statistics from measured data for small and large spatial scales. Small scale coverage (as defined by Hess) represents a driving interval of 100 m. For a vehicle speed of 25 m/s (≈ 55 mi/h), this converts to a time interval of 4 seconds or the time interval of a short conversational sentence. For each 100 m interval, Hess derived a cumulative fade distribution given by

$$P_{Si}(A, A_q) = P_{Si} [A < A_q] \quad (8.7)$$

where the right hand side of (8.7) is read as “the probability that the attenuation A is smaller than a designated attenuation level A_q for the i th small scale distribution.” The “large scale” distribution function P_L may be derived as follows. We first construct a large family of small scale distributions of the type depicted by (8.7) on a graph. We next intersect each of these distributions by a fixed percentage (e.g., $P_S = 90\%$) and arrive at a family of fade levels A_q from which a new cumulative fade distribution may be derived. We call this new cumulative distribution the “large scale” case and represent it by

$$P_L(A) = P_L [A < A_q | P_S] \quad (8.8)$$

The right hand side may be read as “the probability that the attenuation A exceeds a designated threshold level A_q given the condition that the small scale probability P_S assumes a particular value ($P_S = 90\%$ for the given example). The physical significance that may be attributed to (8.8) is that it predicts the probability that the fade will be less than a

particular fade level over many kilometers of driving, assuming a given P_S which denotes the likelihood of successful reception over a 100 m driving distance.

Families of distributions of the type given by (8.7) and (8.8) were derived from data collected for different vehicle environments and path geometries. A normal distribution was fit to (8.8) from which a "mean excess path loss, μ ," and "standard deviation, σ " were derived. The model equations of Hess for $P_S = 90\%$ valid in the range of P_L from 50% to 90% are given by:

$$A(P_L) = \mu + k(P_L) \sigma \quad (8.9)$$

where

$$\mu = a_0 + a_1 \text{ ENV} + a_2 \text{ HEAD} + a_3 \text{ FREQ} + a_4 \text{ SIDE} + a_5 \text{ ELEV} \quad (8.10)$$

$$\sigma = b_0 + b_1 \text{ ENV} + b_2 \text{ HEAD} + b_3 \text{ FREQ} + b_4 \text{ SIDE} + b_5 \text{ ELEV} \quad (8.11)$$

In (8.9), k is the number of standard deviations for various values of P_L and are given by

$$k = \begin{cases} 0 & P_L = 50\% \\ 1.28 & P_L = 90\% \\ 1.65 & P_L = 95\% \\ 2.33 & P_L = 99\% \end{cases} \quad (8.12)$$

The model parameters ENV, HEAD, FREQ, SIDE, and ELEV are defined in Table 8.1. We note that the model contains the following elements: (1) the local environment (ENV), such as urban, semi-urban (commercial) and suburban, (2) the vehicle heading (HEAD) with respect to the satellite azimuth, (3) the frequency (FREQ); UHF or L-Band, (4) the side (SIDE) of the road driven (satellite located across opposing lane or not), and (5) the elevation angle (ELEV) to the satellite. The downtown area of a city, with many tall buildings and a rectangular street grid would be characterized as urban. Streets lined by shopping centers as well as by businesses with off-street parking lots are classified as commercial, and areas with small one- or two-story houses along moderately tree-lined roads define suburban environment. Data acquired in rural surroundings are included in the suburban category. The coefficients for the mean fade μ and slope σ given in (8.10) and (8.11), respectively, are summarized in Table 8.2, along with their standard errors.

The overall standard errors of μ and σ are

$$\text{S.E.}(\mu) = 3.65 \text{ dB} \quad (8.13)$$

Table 8.1: Parameter Definition and Values for Hess Model

Parameter	Range of Values
ENVironment	1 = Urban, 0 = Commercial, -1 = Suburban/Rural
HEADing	$-\cos 2(Az_{\text{vehicle}} - Az_{\text{satellite}})$
FREQuency	1 = UHF, 1.8 = L-Band
SIDE of road	+1=Satellite across road, -1=On same side
ELEVation	15° to 50°

$$\text{S.E.}(\sigma) = 2.5 \text{ dB} \quad (8.14)$$

In order to extend the small-scale coverage from the modeled value of $P_s = 90\%$ as given by (8.9)-(8.11) and Table 8.2 to other values of P_s , we use the following formulation:

Urban and Commercial

$$A(P_L, P_s) = \begin{cases} (P_s - 90) \times 0.6 + A(P_L) & 95\% \geq P_s \geq 90\% \\ (P_s - 90) \times 0.2 + A(P_L) & 50\% \leq P_s < 90\% \end{cases} \quad (8.15)$$

Suburban-Rural

$$A(P_L, P_s) = (P_s - 90) \times 0.1 + A(P_L) \quad 50\% \leq P_s \leq 95\% \quad (8.16)$$

Table 8.2: Coefficients In LS-SS Fade Model

Mean Fade, μ			Standard Deviation, σ		
Coeffic.	Value (dB)	Std Error (dB)	Coeffic.	Value (dB)	Std Error (dB)
a_0	9.55		b_0	3.75	
a_1	4.46	0.42	b_1	2.62	0.29
a_2	3.41	0.61	b_2	0.98	0.42
a_3	1.66	0.91	b_3	0.046	0.62
a_4	-0.35	0.36	b_4	-0.24	0.25
a_5	-0.052	0.045	b_5	0.04	0.031

Example: LS-SS Model

To illustrate the procedures by which we execute the LS-SS model, consider the following example. Assume that a receiver can recover the LMSS coded errors as long as the small-scale coverage is at least $P_S = 70\%$. The system operates at L-Band in a suburban area with an elevation angle to the satellite of 45° . It is desired to determine the required fade margin to achieve a large scale probability of $P_L = 95\%$.

We assume a worst case heading and condition of roadside, with the satellite at a right angle to and right of the vehicle. Hence, we employ the following parameter values from Table 8.1:

$$\begin{aligned} \text{ENV} &= -1 && \text{(Suburban/Rural)} \\ \text{HEAD} &= +1 && (\alpha z_{\text{vehicle}} - \alpha z_{\text{satellite}} = 90^\circ) \\ \text{FREQ} &= 1.8 && \text{(L - Band)} \\ \text{SIDE} &= -1 && \text{(Satellite Same Side)} \\ \text{ELEV} &= 45^\circ \end{aligned} \quad (8.17)$$

Substituting the above into (8.10) and (8.11), we obtain

$$\mu = 9.5 \text{ dB} \quad (8.18)$$

$$\sigma = 4.23 \text{ dB} \quad (8.19)$$

Substituting (8.18), (8.19) and $k = 1.65$ (from (8.12) for $P_L = 95\%$) into (8.9) results in

$$A = 16.5 \text{ dB} \quad P_S = 90\% \quad (8.20)$$

The fade given by (8.20) corresponds to a large scale probability of $P_L = 95\%$ and small scale probability of $P_S = 90\%$. To convert the above to the desired small scale probability $P_S = 70\%$, substitute (8.20) into (8.16). Hence,

$$A = 14.5 \text{ dB} \quad P_S = 70\% \quad (8.21)$$

An estimate of the standard deviation associated with (8.20) may be derived by substituting (8.13) for μ and (8.14) for σ in (8.9) and calculating the square root of the sum of the squares of each of the terms (with $k = 1.65$). This gives a prediction error of 5.5 dB.

In Figure 8.1 is given a family of curves of the large-scale cumulative distributions P_L for elevation angles of 20° , 30° , and 45° with small-scale probabilities of $P_S = 90\%$, 70% , and

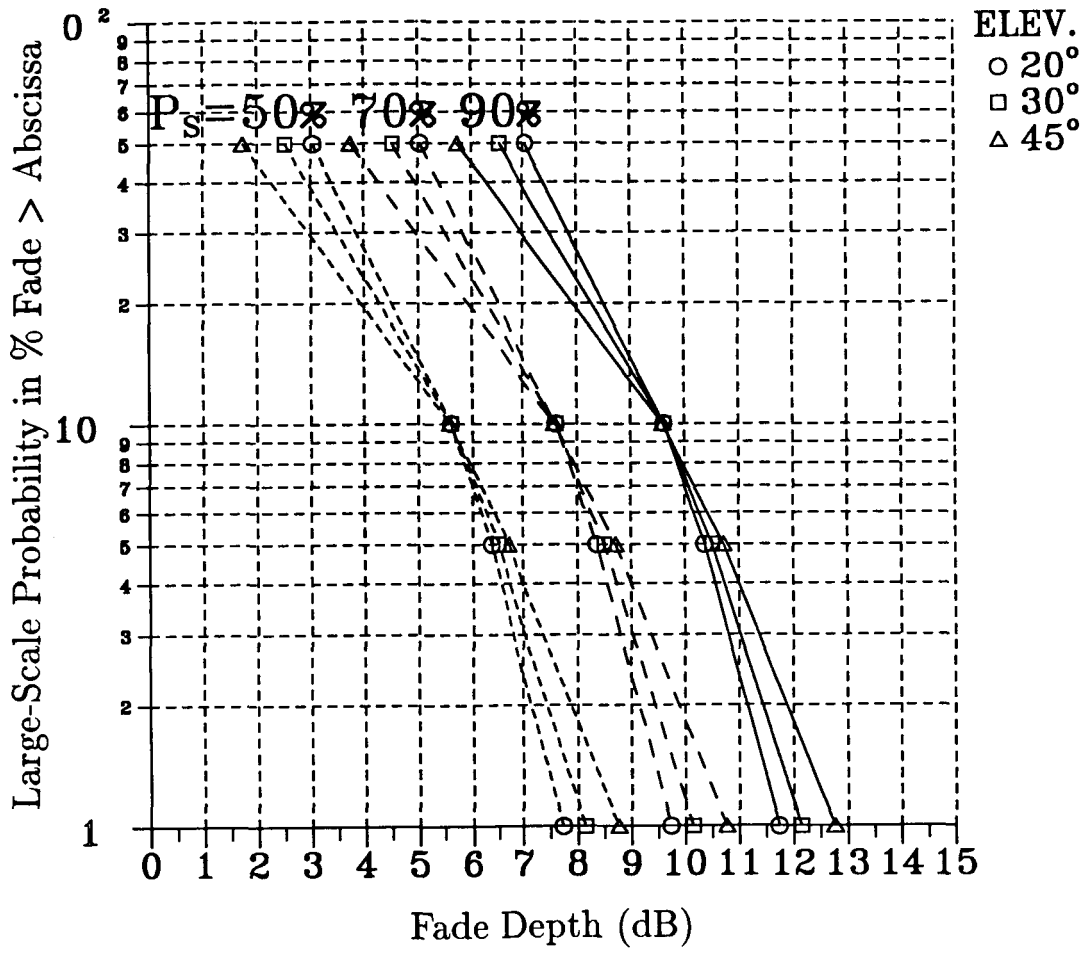


Figure 8.1: Probability distributions for LS-SS model for family of elevation angles and indicated small scale probabilities P_s .

50%. These depict an overall driving condition as each curve represents the average of four distributions; right side of road, left side of road, and difference in vehicle-satellite azimuth directions of 90° and 0° . We note that P_L is relatively insensitive to elevation angle but is highly sensitive to P_S .

Discussion

The LS-SS model of Hess is derived from an extensive data base of measurement results, which is especially weighted for urban to suburban environments. It is simple to use and has realistic parameterization for the most important environmental variables.

The model was derived from data taken with linearly polarized quarter wavelength whip antennas. Such a system will not provide isolation from ground specular reflections as do low gain LMSS type antennas previously described. While shadowing loss measurements were not affected by the antenna choice, multipath and specular effects were most likely enhanced. This may have caused overprediction of signal variations especially in open rural areas where shadowing is statistically less significant than multipath. It is also important to note that the experiment emphasized urban over rural areas, making predictions from the data base for rural areas less reliable.

8.3.2 Empirical Roadside Shadowing Model

Since the empirical roadside shadowing model was addressed in Section 3.3, the model details will not be described here. A short summary discussion is presented in the following paragraphs.

Discussion

The ERS model is based on extensive measurements in rural and suburban environments in central Maryland using a realistic LMSS antenna comprised of a crossed drooping dipole (previously described). The model is based on systematically repeated measurements (at UHF and L-Band) along the same system of roads at different elevation angles ranging from 20° to 60° . The fade distributions are simple to calculate. They are a manifestation of an

overall average fade condition for both left and right side driving and various degrees of roadside shadowing (55% to 75%). It has been independently validated to within a few dB employing measurements in Australia.

Because of the limited dynamic range of the measurements, only the median distribution of many 90 second intervals could be determined and modeled. The higher percentile distributions (e.g., 90th or 95th) were beyond the measurement range of the equipment in the 20% to 1% range of fade exceedance. The variability of the distributions could therefore not be modeled. As is the case with the LS-SS model, the ERS model does not provide information about fade dynamics and therefore cannot be used to generate simulated data. This model is also biased in favor of the geometric condition where maximum shadowing occurs; namely, the line-of-sight path is dominantly directed perpendicular to the line of roadside trees. The model is only valid in the range of elevation angles 20° to 60° .

8.4 Probability Distribution Models

Probability functions used to describe LMSS propagation are the Rayleigh and Rician for multipath effects and the lognormal for shadowing. These statistics are useful to the extent that they accurately describe the shadowing and multipath scenarios.

Models of these type correspond to homogeneous cases for which line-of-sight fading and multipath are simultaneously present, or only multipath is present under the conditions of no shadowing or complete blockage. They do not account for scenarios in which the vehicle may pass from shadowing to non-shadowing conditions (causing bursts of fading and non-fading) typical at higher elevation angles (e.g., 45°) in rural and suburban environments.

Their usefulness is also based on the ability to tailor parameters of the distributions to actual measurements. The parameters of importance are standard deviation, mean, percentage of shadowing, and ratio of line of sight to multipath power. These parameters are however tuned to "light" or "heavy" shadowing, "zero to frequent" percentage of shadowing, and "urban", "suburban", or "highway scenes." They represent a "rough" tuning to the model which is based on measurements at fixed elevation angles. It is, for example, difficult to relate these models to other elevation angles which are known to critically influence fading. Furthermore, it is difficult to extract from these statistics "time-series" of fading events for simulation purposes without the employment of experimental data.

In the following section is given an overview of the density functions used in modeling procedures. A further characterization is given by the CCIR [CCIR, 1986a (Report 1007)].

8.4.1 Density Functions Used In Propagation Modeling

Rician or Nakagami-Rice Density Function

The voltage phasors from all the reflection sources can be combined into two independent orthogonal vectors x and y , the in-phase and quadrature components, having normal envelopes and uniform phase distributions. When received together with a direct signal voltage a , the two-dimensional probability density of the received voltage can be expressed as

$$f_{xy}(x, y) = \frac{1}{2\pi\sigma^2} \exp \left[-\frac{(x - a)^2 + y^2}{2\sigma^2} \right] \quad (8.22)$$

where σ is the standard deviation of the voltage. The signal envelope represents the length of the voltage vector z . It is given by

$$z = \sqrt{x^2 + y^2} \quad (8.23)$$

from which we derive the Rician density $f_z(z)$ [Papoulis, 1965]

$$f_z(z) = \frac{z}{\sigma^2} \exp \left[-\frac{(z^2 + a^2)}{2\sigma^2} \right] I_0 \left(\frac{za}{\sigma^2} \right) \quad (8.24)$$

where I_0 is the zeroth order modified Bessel function.

The normalized line-of-sight power is given by

$$P'_{\text{los}} = \frac{a^2}{2} \quad (8.25)$$

and the average (normalized) multipath power is given by

$$P'_{\text{mp}} = \sigma^2 \quad (8.26)$$

where we denote the powers by a prime to distinguish it from probability. The ratio of these two powers defines the K value which characterizes the influence of multipath scattering on the signal distribution. Hence,

$$K = \frac{P'_{\text{los}}}{P'_{\text{mp}}} = \frac{a^2}{2\sigma^2} \quad (8.27)$$

Usually, the K factor is quoted in terms of dB. That is,

$$K(\text{dB}) = 10 \log \left(\frac{P'_{\text{los}}}{P'_{\text{mp}}} \right) = 10 \log \left(\frac{a^2}{2\sigma^2} \right) \quad (8.28)$$

It is apparent from (8.27) that the lower the relative level of the multipath power, the larger the K value, and conversely. Further normalizing P'_{los} such that $P'_{\text{los}} = 1$, reduces the Rician density (8.24) to a single parameter density function of the voltage, which can be written as a function of K by

$$f_z(z) = K z \exp \left[-K \left(\frac{z^2}{2} + 1 \right) \right] I_0(Kz\sqrt{2}) \quad (8.29)$$

where

$$K = \frac{1}{\sigma^2} \quad (8.30)$$

Rayleigh Density Function

The Rayleigh density is a special case of the Rician distribution and arises when no line-of-sight power is received. Setting $a = 0$ in (8.24)

$$f_z(z) = \frac{z}{\sigma^2} \exp \left(-\frac{z^2}{2\sigma^2} \right) \quad (8.31)$$

Even though no direct signal is received, the Rayleigh density can also be defined in terms of a \bar{K} -factor

$$\bar{K} \equiv \frac{1}{\sigma^2} \quad (8.32)$$

Substituting (8.32) into (8.31)

$$f_z(z) = \bar{K} z \exp \left(-\bar{K} \frac{z^2}{2} \right) \quad (8.33)$$

Note that the Rayleigh distribution has but a single parameter (namely, σ or \bar{K}). For Rayleigh scattering, the average scattered power is variable, but the standard deviation on a dB scale is constant and equal to 5.57 dB. As a rule of thumb, based on the Central Limit Theorem [Papoulis, 1965], at least six random scattering sources are required to produce a Rayleigh (or Rician) distribution.

Lognormal Density Function

Shadowing is a manifestation of the absorption and scattering of the incident direct wave by roadside trees or other obstacles as it is transmitted via the line-of-sight between the satellite and the vehicle. The cumulative distribution function of the received power expressed in dB can often be fit to a straight line when plotted on a normal probability scale. The voltage variation due to shadowing is then lognormal. The lognormal density function for a random variable z can be derived from the normal density function for x by using

$$x = \ln(z). \quad (8.34)$$

In this case the lognormal density of z has the form

$$f_z(z) = \frac{1}{sz\sqrt{2\pi}} \exp \left[-\frac{(\ln(z) - m)^2}{2s^2} \right] \quad (8.35)$$

where m and s are the mean and standard deviation of $\ln(z)$, respectively. Since the power (x) is usually expressed in dB, the relation between x (in dB) and z is

$$x = 10 \log(z) \quad z = \text{power (watts)} \quad (8.36)$$

or

$$x = 20 \log(z) \quad z = \text{voltage (volts)} \quad (8.37)$$

The lognormal density function of power when z is the power in watts is

$$f_z(z) = \frac{4.343}{sz\sqrt{2\pi}} \exp \left[-\frac{(10 \log(z) - m)^2}{2s^2} \right] \quad z = \text{power (watts)} \quad (8.38)$$

where m and s are the mean and standard deviation of $10 \log(z)$, respectively. The lognormal density function of power when z is voltage is

$$f_z(z) = \frac{8.686}{sz\sqrt{2\pi}} \exp \left[-\frac{(20 \log(z) - m)^2}{2s^2} \right] \quad z = \text{voltage (volts)} \quad (8.39)$$

where m and s are the mean and standard deviation of $20 \log(z)$, respectively.

8.4.2 Loo's Distribution Model

A statistical model for land mobile satellite propagation based on probability density functions of multipath and shadowing propagation has been developed by Loo [1985; 1987]. The following assumptions are made: (a) the receiver voltage due to the diffusely scattered power is Rayleigh distributed, and (b) the voltage variations due to attenuation of the line-of-sight signal are lognormally distributed. The two voltages are considered correlated, as attenuation by trees is caused by both absorption and scattering, some of the latter directed into the receiver. The model employs the parameters \bar{K} as given by (8.32), as well as the mean m and standard deviation s previously defined for lognormal fading. The mean scattered power in the model is set constant at a level that depends on the severity of the shadowing relevant to a particular environment. While the line-of-sight attenuation is constant, a conditional Rician distribution of the signal envelope holds. The overall probability density is found by integration of the conditional density multiplied by the lognormal probability of the line-of-sight envelope. The resulting probability density function of the signal envelope is

$$f_v(v) = \frac{\bar{K}v}{s\sqrt{2\pi}} \int_0^\infty \frac{1}{z} \exp \left[-\frac{(\ln(z) - m)^2}{2s^2} - \frac{\bar{K}(v^2 + z^2)}{2} \right] I_0(\bar{K}vz) dz \quad (8.40)$$

For signal voltages much greater and much less than the standard deviation of the Rayleigh process, the density function is lognormal or Rayleigh, respectively, and can be simplified to

$$f_v(v) = \frac{1}{sv\sqrt{2\pi}} \exp \left[-\frac{(\ln(v) - m)^2}{2s^2} \right] \quad v \gg \frac{1}{\sqrt{\bar{K}}} \quad (8.41)$$

and

$$f_v(v) = \bar{K}v \exp \left(-\frac{\bar{K}v^2}{2} \right) \quad v \ll \frac{1}{\sqrt{\bar{K}}} \quad (8.42)$$

At intermediate values of v , $f_v(v)$ is found by numerical integration.

Table 8.3: Parameters for Loo's Model

Shadowing Class	Rayleigh Scatter	Lognormal Shadowing	
	\bar{K}	m	s
Infrequent light	6.3	0.115	0.115
Frequent heavy	15.8	-3.91	0.805
Overall	4.0	-0.69	0.23

The probability that the received voltage is less than or equal to v is

$$F_v(v) = \int_0^v f_v(u) du \quad (8.43)$$

from which the cumulative distribution function A in dB is found using

$$A = 20 \log(v) \quad (8.44)$$

Values of the model parameters were derived by Loo from propagation data measured over a helicopter to vehicle link with 15° elevation angle in a rural environment with two classes of shadowing: infrequent light and frequent heavy. The parameters are summarized in Table 8.3.

Level Crossing Rate and Average Fade Duration

In addition to describing the fade cumulative distribution function, Loo's model also provides insight into the dynamics of fading by deriving statistical relations for the level crossing rate

Table 8.5: Parameter Values for the Lognormal Shadowing Model

Parameter	Range of Values	Remarks
K	22 to 13 dB	low to high multipath unshadowed
\bar{K}	21 to 18 dB	low to high multipath shadowed
m	-1 to -10 dB	light to heavy shadowing
s	0.5 to 3.5 dB	light to heavy shadowing
S	0.0 to 1.0	zero to frequent shadowing

section.

The parameters given in Table 8.5 were determined by a least square error fit of the statistical model to propagation data collected using a helicopter as the source platform.

Discussion

As was the case for the other statistical models, the lognormal shadowing model has been fit to measured cumulative fade distributions quite well. One would expect an increased multipath power level to go hand-in-hand with shadowing conditions. The small range and low level found for \bar{K} seem to indicate that the model does not adequately decouple shadowing and scattering. The range of applicability of the model vis a vis elevation angle has also not been specified.

Because of the complexities in evaluating (8.55), a much simpler empirical model (in the next section) was derived from the statistical results by curve fitting procedures.

8.4.5 Simplified Lognormal Shadowing Model

This model [Barts and Stutzman, 1991; Bartz et al., 1987] has the inputs K , \bar{K} , m , s , and S which have been defined in the previous two sections and assume the values summarized in Table 8.5. The resultant probability distribution model is expressed in terms of the contributions for the “no shadowing” and “shadowing” cases in the following way

$$P(A > A_q) = P_{ns} (1 - S) + P_s S \quad (8.56)$$

where P_{ns} is the probability distribution for the case of no shadowing of the line of sight and is given by,

$$P_{ns}(A > A_q) = \exp \left[-\frac{(A + U_1)}{U_2} \right] \quad (8.57)$$

where the parameters U_1 and U_2 are functions of K and are given by

$$U_1 = 0.01 K^2 - 0.378 K + 3.98 \quad (8.58)$$

$$U_2 = 331.35 K^{-2.29} \quad (8.59)$$

In (8.56), P_s is the probability distribution for the case of shadowing of the line of sight and is

$$P_s(A > A_q) = (50 - A_q) \frac{V_2}{V_1} \quad (8.60)$$

where the parameters V_1 and V_2 are given by the following functions of \bar{K} as well as the mean m and standard deviation s of the lognormal signal

$$V_1 = -0.275 \bar{K} + 0.723 m + 0.336 s + 56.979 \quad (8.61)$$

$$V_2 = (-0.006 \bar{K} - 0.008 m + 0.013 s + 0.121)^{-1} \quad (8.62)$$

Typical fade predictions calculated from (8.56) have been plotted in Fig. 8.2 for light and heavy as well as in Fig. 8.3 for medium heavy shadowing, for infrequent ($S=0.25$), moderate ($S=0.5$) and frequent ($S=0.75$) shadowing occurrences. In the worst case scenario: heavy and frequent shadowing, the calculated fade probabilities may exceed 1.0, but should be limited to that value.

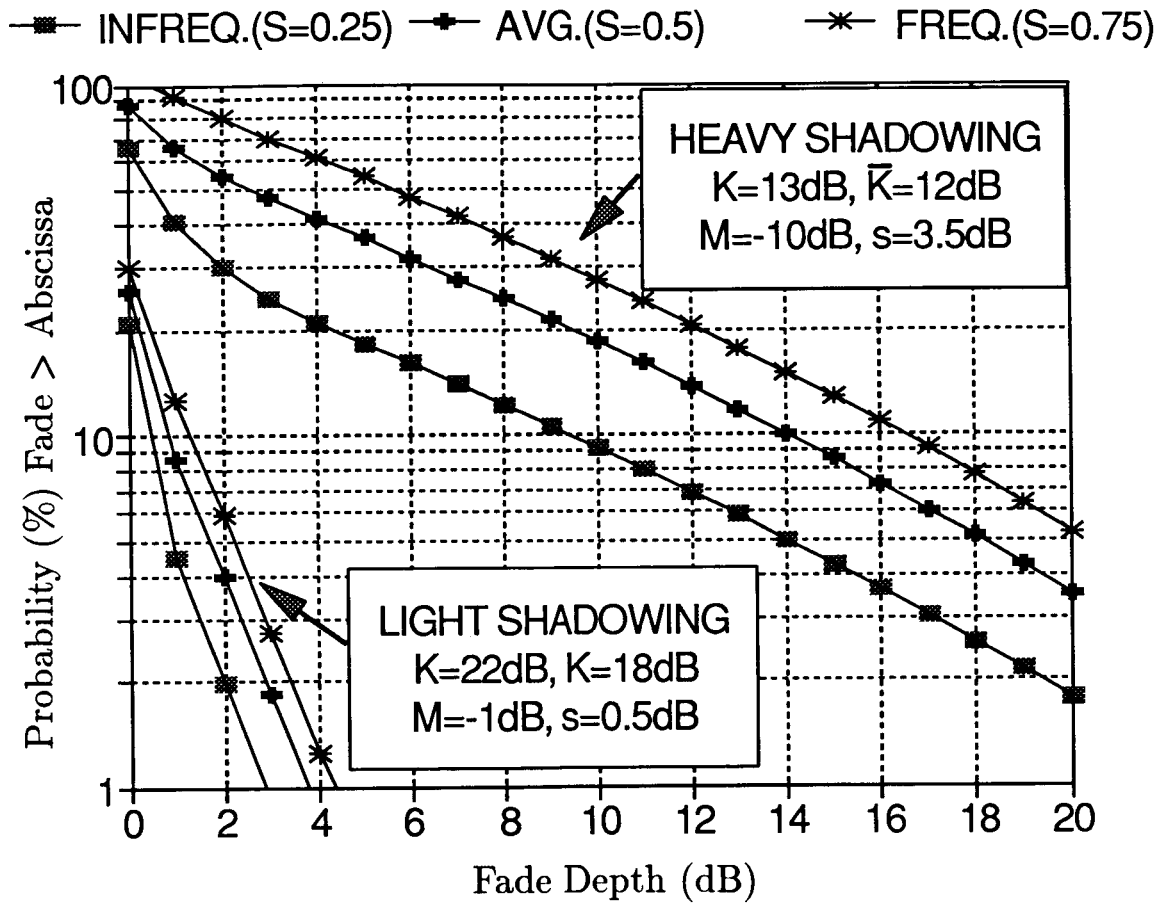


Figure 8.2: Typical fade distributions calculated from the Simplified Lognormal Shadowing Model for light (L), and heavy (H) shadowing, and for infrequent (I; $S = 0.25$), moderate (M; $S = 0.5$), and frequent (F; $S = 0.75$) shadowing occurrences.

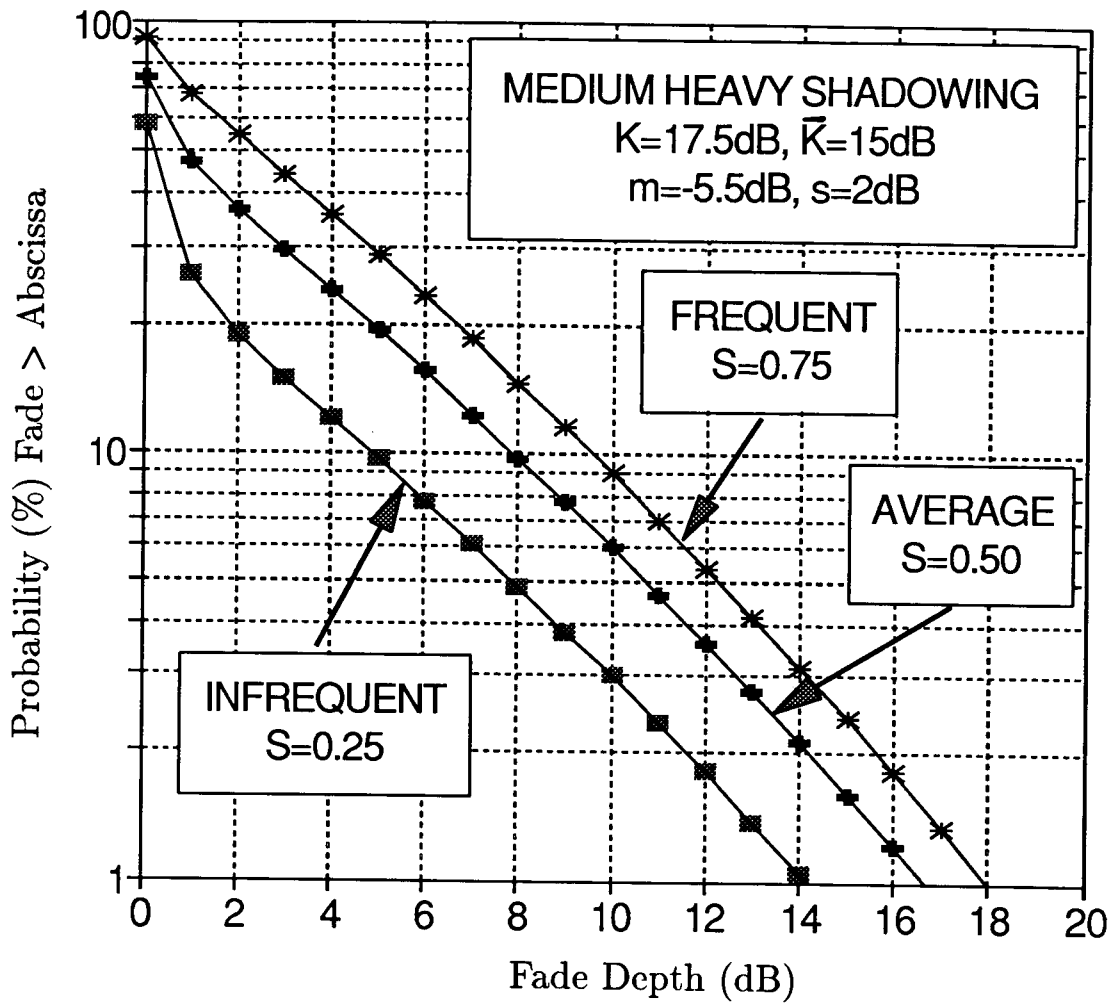


Figure 8.3: Typical fade distributions calculated from the Simplified Lognormal Shadowing Model for medium shadowing (M), and for infrequent (I; $S = 0.25$), moderate (M; $S = 0.5$), and frequent (F; $S = 0.75$) shadowing occurrences.

(LCR) and the average fade duration (AFD). The level crossing rate is the expected rate at which the signal envelope crosses a specified signal level with a positive slope. The average fade duration is the expected time or distance the signal envelope is below the specified signal level. The inverse of the level crossing rate is the sum of the average fade and non-fade durations. The derivation, based on earlier work by Rice and Jakes, hinges on the statistical independence between the signal envelope and its time derivative, which is assumed to be a Gaussian process both for Rician and lognormal fading. The LCR is normalized by the maximum possible Doppler shift

$$f_{\max} = \frac{v}{\lambda} \quad (8.45)$$

where v is the vehicle speed and λ is the wavelength. The normalized level crossing rate LCR_n is based on the wavelength, independent of speed, and can be written as

$$\text{LCR}_n = \frac{\text{LCR}}{f_{\max}} = \sqrt{2\pi} \sqrt{(1 - \rho^2)} \sigma^2 \frac{\sqrt{\sigma^2 + 2\rho\sigma s + s^2}}{\sigma^2 (1 - \rho^2) + 4\rho\sigma s} f_v(v) \quad (8.46)$$

where ρ , now a fourth parameter of Loo's model, is the correlation coefficient for the rate of change of the envelope due to multipath and shadowing effects. Typically, the correlation coefficient ρ was in the range from 0.5 to 0.9 for the data set used by Loo.

The AFD can be found from LCR_n by

$$\text{AFD} = \frac{1}{\text{LCR}_n} \int_0^L f_v(v) dv \quad (8.47)$$

With supporting helicopter data at 870 MHz and satellite data at 1542 MHz and for elevation angles from 5° to 30°, it was shown that the signal phase and the rate of change of the phase can be treated as Gaussian processes [Loo, 1987]. Values of the mean and standard deviation were 7.5° and 12.6° at 870 MHz, and 7.5° and 26° at 1542 MHz, respectively.

Discussion

The Loo model provides a description of primary and secondary fade statistics for LMSS scenarios based on four parameters derived from measurements performed in Canada. As all of the measurements were made at elevation angles below 30°, model parameters for higher elevation angles are not available.

8.4.3 Total Shadowing Model

Another statistical model characterizing the fade distribution applicable to LMSS propagation has been devised by Lutz et al. [1986]. As in Loo's model, Rician, Rayleigh, and lognormal probability densities are combined and model parameters are derived from least-square error fits to measured data. However, there are significant differences in the way the three distributions are assigned to the two major propagation phenomena, scattering and shadowing. As described in the previous section, Loo combines a constant intensity Rayleigh distributed scattering voltage with a lognormally shadowed line-of-sight signal voltage. Lutz et al., on the other hand, consider two distinct propagation link states; shadowing, and no shadowing. In the unshadowed state, the envelope statistics are assumed to be Rician with constant K-factor due to the superposition of the direct wave with constant intensity multipath echoes. When the propagation link is shadowed by roadside trees, the line-of-sight is assumed to be totally obscured and most of its power converted into scattered waves, leaving only multipath signals with Rayleigh statistics, but their average strength is modeled as lognormally distributed. Loo modulates the Rician K-factor by shadowing the line-of-sight component. Lutz, in the shadowed state, varies the intensity of the Rayleigh scattering process, or the \bar{K} factor, in the absence of any line-of-sight signal. In Lutz's model, the probability density of the received voltage for the unshadowed fraction (1-S) of the driving distance is Rician. When expressed in terms of the received power P' , it has the form

$$f_{P',\text{Rice}}(P') = K \exp[-K(P' + 1)] I_0(2K\sqrt{P'}) \quad (8.48)$$

where unity line-of-sight power is assumed and K is the ratio of line-of-sight to average multipath power. That is

$$K = \frac{1}{P'_{\text{mp}}} \quad (8.49)$$

For the shadowed fraction S of the total distance, it is Rayleigh distributed and has the following form when expressed in terms of the received power, P'

$$f_{P',\text{Rayleigh}}(P') = \bar{K} \exp(-\bar{K} P') \quad (8.50)$$

where \bar{K} is the reciprocal of the average multipath power as given by (8.32). Lutz et al. postulate this multipath power Rayleigh intensity $1/\bar{K}$ to be lognormally distributed. The

density can be expressed in terms of the \bar{K} -factor, the mean m , and the standard deviation s of $10 \log(\bar{K})$ as

$$f_{\bar{K}}(\bar{K}) = \frac{4.343}{\bar{K} s \sqrt{2\pi}} \exp \left[-\frac{(10 \log(\bar{K}) - m)^2}{2 s^2} \right] \quad (8.51)$$

where

$$m = E [10 \log(\bar{K})] \quad (8.52)$$

and

$$s = \left\{ E \left[(10 \log(\bar{K}))^2 \right] - m^2 \right\}^{1/2} \quad (8.53)$$

where E denotes the "expected value."

The overall probability density of the received power follows by combining (8.48) and (8.50) with (8.51)

$$f_{P'}(P') = (1 - S) f_{P',\text{Rice}}(P') + S \int_0^{\infty} f_{P',\text{Rayleigh}}(P' | \bar{K}) f_{\bar{K}}(\bar{K}) d\bar{K} \quad (8.54)$$

The cumulative distribution of the fractional distance the fade exceeds A dB is found by evaluating (8.54). Model parameters were determined by Lutz et al. from regressions to satellite measurements performed in various environments with a 24° elevation angle. They are summarized in Table 8.4 for a vehicle antenna with a hemispherical pattern. Good fits of the model to the measured cumulative distribution functions of the attenuation were obtained.

Discussion

The Lutz et al. experiments were carried out using three different receiving antennas. The shadowing parameter S derived from the corresponding data sets was found to be dependent on the antenna, which indicates a coupling of S to multipath propagation. Had the model been a true representation of LMSS propagation, S should have been independent of the antenna pattern.

Table 8.4: Typical Parameters for Total Shadowing Model of Lutz et al. [1986]

Environment	S	K(dB)	m(dB)	s(dB)
Urban	0.60	3.0	-10.7	3.0
Suburban	0.59	9.9	-9.3	2.8
Highway	0.25	11.9	-7.7	6.0

8.4.4 Lognormal Shadowing Model

Smith and Stutzman [1986] incorporated the idea into a model that different statistics should be used to describe LMSS signal variations depending on whether the propagation path is shadowed or unshadowed. They developed a model which assigns Rayleigh, Rician and lognormal behavior of the received signal voltage in a manner similar to Loo's model. In the unshadowed state, the received signal consists of the sum of the direct signal and a constant average intensity Rayleigh voltage due to the diffusely scattered multipath echoes. The resulting signal amplitude has a Rician probability density characterized by a constant ratio of direct to scattered power. In the shadowed state, the amplitude of the line-of-sight signal is assumed to have lognormal statistics. When combined with constant level diffuse multipath, the probability density (8.40) derived by Loo applies.

The overall probability density of the received voltage is developed in analogy to the derivation of (8.54) as

$$\begin{aligned}
 f_v(v) = & (1 - S) K v \exp \left[-K \left(\frac{v^2}{2} + 1 \right) \right] I_0(K v) + S \frac{8.686 \bar{K} v}{s \sqrt{2\pi}} \\
 & \times \int_0^\infty \frac{1}{z} \exp \left[\frac{-(20 \log(z) - m)^2}{2 s^2} - \frac{\bar{K} (v^2 + z^2)}{2} \right] I_0(\bar{K} v z) dz \quad (8.55)
 \end{aligned}$$

where S, K, \bar{K} , m, and s are the five model parameters already described in the previous

Discussion

The model has been shown to fit measured fade distributions when the propagation parameters were determined by tailoring the data to the model. Calculation procedures are straightforward.

8.4.6 Models With Fade State Transitions

Two- and Four-State Markov Modeling

A 2-state Markov model (Gilbert-Elliott model) for non-shadowed (good) and shadowed (bad) channel conditions and a 4-state Markov model, also with good and bad states and qualified by either short or long duration, have been used to predict error rates in the land mobile satellite channel [Cygan et al., 1988]. Channel states are related to the presence or absence of shadowing conditions and both models describe the transition probabilities between states. Model parameters are determined from data collected in L-Band satellite propagation experiments carried out in a variety of environments at elevation angles between 21° and 24° . The data set on which the parameters are based is the same as the one used for the derivation of the total shadowing model.

The 2-state model has a total of four parameters, of which two are signal level dependent error rates and two are state transition probabilities. A summary of its parameters for three propagation scenarios is given in Table 8.6. The derived bad lengths appended to the table may be reasonable in the urban environment where much of the shadowing is due to blockage by buildings. For tree shadowing prevalent in the suburban environment, the 2-state model is lacking in predicting the effects of many short fades observed in real channel measurements.

At the price of being more calculation intensive, the 4-state model is capable of providing a more realistic statistical simulation of error bursts. It has a total of thirteen parameters, of which eight are state transition probabilities, two express the transitional durations between short and long good or bad states, and three are measures for the error probabilities in all good and short and long bad states. Typical values of the transitional durations for good/bad states are 0.46/1.85 m for urban, 0.92/0.65 m for suburban, and 5.2/2.5 m for highway driving, respectively. Error probabilities range from 1×10^{-4} – 3.5×10^{-4} for the good states to 0.16 – 0.37 for the bad states, with the short bad state's error rate about 30%

Table 8.6: Parameters for 2-State Model

Parameter	Remark	Urban	Suburban	Highway
P_{GB}	Transition probability from "good" to "bad" state	3.95×10^{-4}	2.1×10^{-4}	2.96×10^{-5}
P_{BG}	Transition probability from "bad" to "good" state	1.05×10^{-4}	1.54×10^{-4}	1.29×10^{-4}
ε_G	Error rate in "good" state	2.1×10^{-4}	3.4×10^{-4}	1.1×10^{-4}
ε_B	Error rate in "bad" state	0.317	0.298	0.194
L_G	Derived "good" length (m)	24	45	704
L_B	Derived "bad" length (m)	88	60	161

below the long bad state. While the discussion of error probabilities is beyond the scope of this text, these models give an indication of the level of complexity that may be required for successfully modeling the LMSS channel.

Markov Transitions, Multipath, and Fade Depth Model

By combining three distinct concepts into one LMSS propagation model, Wakana [1991] has modeled fading and its spatial characteristics. Fading due to multipath is rendered by Rician statistics (8.29), while fading of the line-of-sight signal due to tree shadowing is described in terms of a Markov model for the transitions between fade states and an attenuation algorithm for the fade depth. Like the 4-state model described above, this Markov model considers transition probabilities between four fade states: fade or non-fade, short or long, but with a total of only six as opposed to eight independent parameters. Of two attenuation models introduced, one linking the attenuation to the fade state, the other to the fade duration, the former alternative was used. Besides the six state transition probabilities, four other parameters are required. They are the Rician K-factor for the multipath scattering, attenuation levels for short and long fades, and a lowpass filter time constant to smooth the transitions between fade and non-fade states. The ten model parameters were determined for one particular suburban propagation path geometry with an optimization procedure performed on data collected in a helicopter experiment. Simulated data produced using these parameters are qualitatively similar to real data when time series are compared and have, of course, similar cumulative distributions of fades, fade durations, and non-fade durations. Typical parameter values are in the range of 0.13 – 0.97 for the transition probabilities, 10.7 dB attenuation for both fade states, a 13 dB K-factor, and a 22 Hz lowpass filter cut-off frequency, corresponding to a spatial filter of about 1 m.

Variations of the signal level at near line-of-sight power, which may be due to diffraction at the fade state transition zone and specular reflection from the ground near the vehicle have not been considered in the model development and therefore are not replicated by the simulator. Until parameters are determined for a variety of environments and elevation angles, the modeling results cannot readily be applied to other propagation geometries.

8.5 Geometric Analytic Models

Geometric analytic models are useful for gaining physical insight of the mechanism of fading and characteristics of signal retrieval. They may also be used to achieve time-series fades which may be interfaced with simulation techniques. Unfortunately, the complexities of "real life" scenarios do not lend themselves to analytic models and only simplified and idealized scenarios are considered.

8.5.1 Single Object Models

Point Scatterer Multipath

Frequently, signal variations observed in satellite land-mobile propagation experiments can be correlated with the receiving vehicle passing in the vicinity of a generator of multipath scattering, such as a utility pole or roadside sign. To increase understanding of these multipath reflections observed from a moving platform, a physical model based on the geometry of a single point scatterer has been developed [Vogel and Hong, 1988]. While the model does not address the major limitation of LMSS, shadowing, it provides a tool to study the dependence of signal variations observed under clear line-of-sight conditions on parameters such as antenna pattern, path azimuth and elevation angles, distance of multipath sources, and bandwidth.

A sketch of the propagation scenario considered is shown in Fig. 8.4, in which a vehicle carries an antenna with a given pattern along the x-axis with speed v . A plane wave transmitted from a satellite propagates into the direction (Θ_t, Φ_t) . In addition to the line-of-sight wave, the vehicle also receives one multipath component scattered by an object at (x_s, y_s, z_s) . The vectorial sum of the two waves constitutes the received signal. In order to achieve simplicity in the numerical evaluation of the model, the following assumptions were made: 1) there is only one scatterer, 2) it scatters isotropically, and 3) the receiving antenna's gain is azimuthally omnidirectional. The formula developed by Vogel and Hong [1988] for the received electric field strength E_r is

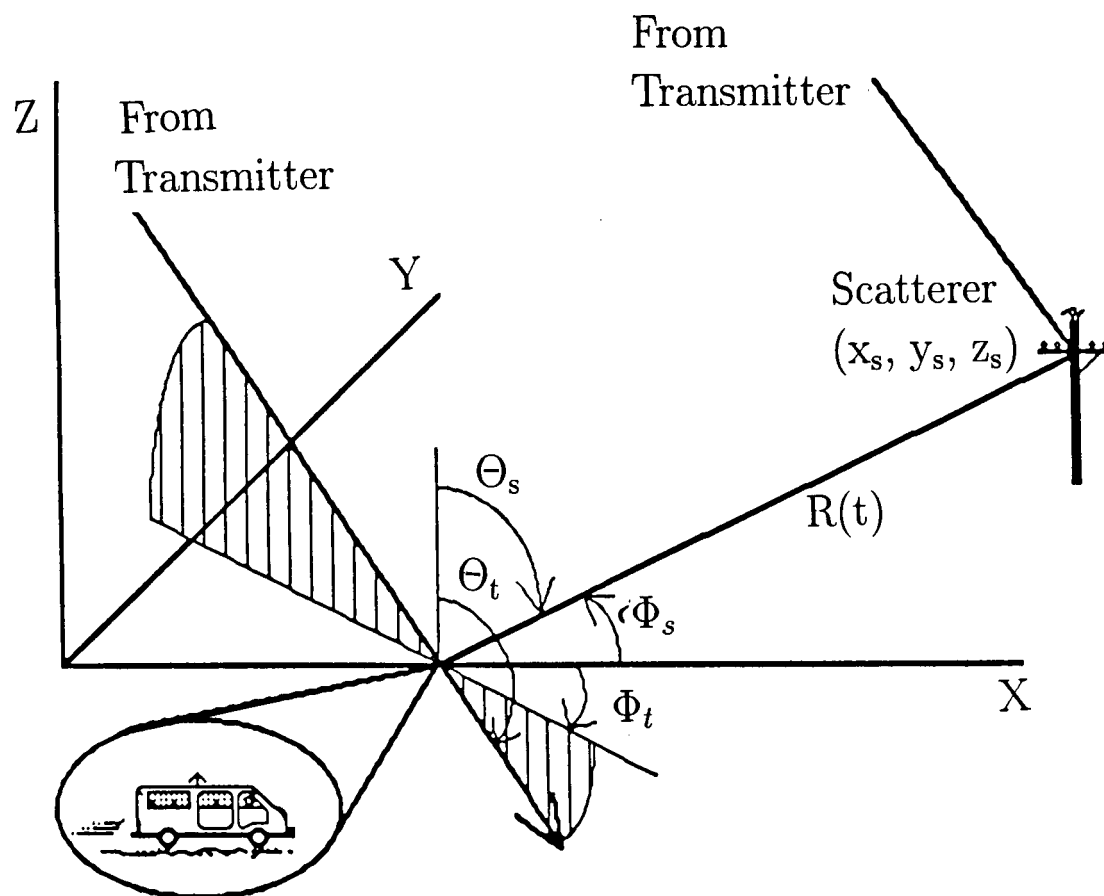


Figure 8.4: Propagation geometry for single object scattering in which a vehicle traveling at a speed v carries an antenna with a given pattern along the x-axis

$$E_r(t) = E_o D(\Theta_t) \exp [j\omega_o t - \beta] \times \left\{ T + \frac{\sqrt{\sigma} D(\Theta_s)}{2\sqrt{\pi} R(t)D(\Theta_t)} \exp \left[j\frac{2\pi}{\lambda} (a(t) - p - R(t)) \right] \right\}, \quad (8.63)$$

where β is the phase shift given by

$$\beta = \frac{2\pi}{\lambda} vt \sin(\Theta_t) \cos(\Phi_t), \quad (8.64)$$

$a(t)$ is the path length from the wave through the origin to the antenna given by

$$a(t) = t \sin(\Theta_t) \cos(\Phi_t), \quad (8.65)$$

p is the path length from the wave plane through the origin to the scatterer given by

$$p = x_s \sin(\Theta_t) \cos(\Phi_t) + y_s \sin(\Theta_t) \sin(\Phi_t), \quad (8.66)$$

and where

E_o	line-of-sight field strength,
$D(\Theta_t)$	antenna voltage directivity versus elevation Θ_t ,
ω_o	transmitter frequency,
T	transmission of direct wave: 1 = no shadowing, 0 = complete blockage,
σ	bistatic cross section of scatterer,
$R(t)$	path length between antenna and scatterer,
λ	wavelength.

This model has been shown to produce time series of received data that closely match those observed, if appropriate parameters are used. One such example is shown in Fig. 8.5 and Fig. 8.6, which respectively depict experimentally received and calculated signal level and phase for an L-Band receiver using a crossed drooping dipole antenna and moving at 24 m/s. The transmitter azimuth and elevation angles are 150° and 35°, respectively. The

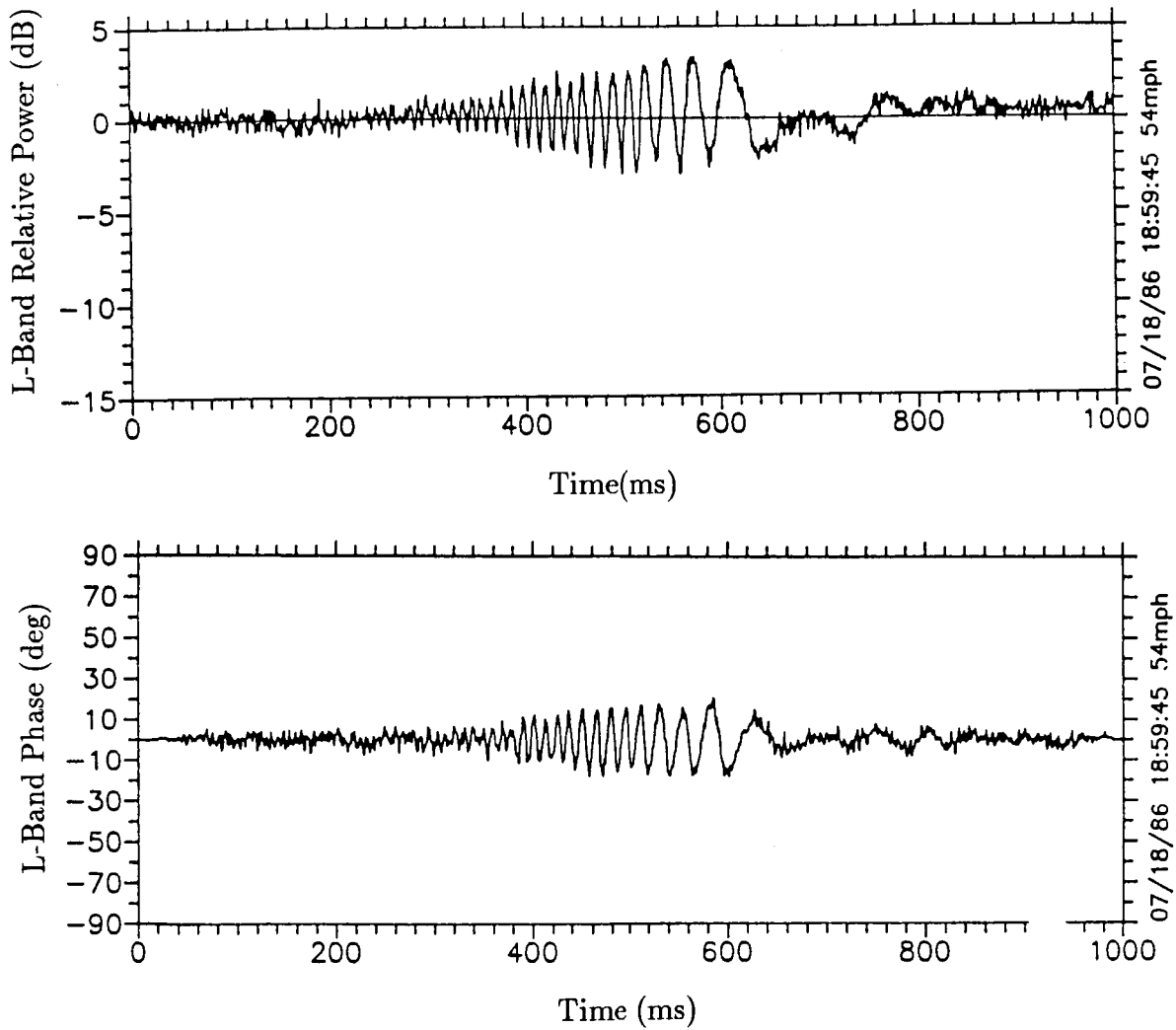


Figure 8.5: Measured L-Band signal level and phase fluctuations as a function of time relative to arbitrary reference as receiving vehicle passes by a wooded utility pole with a metal cross bar. The vehicle closest approach to the pole occurs at 540 ms.

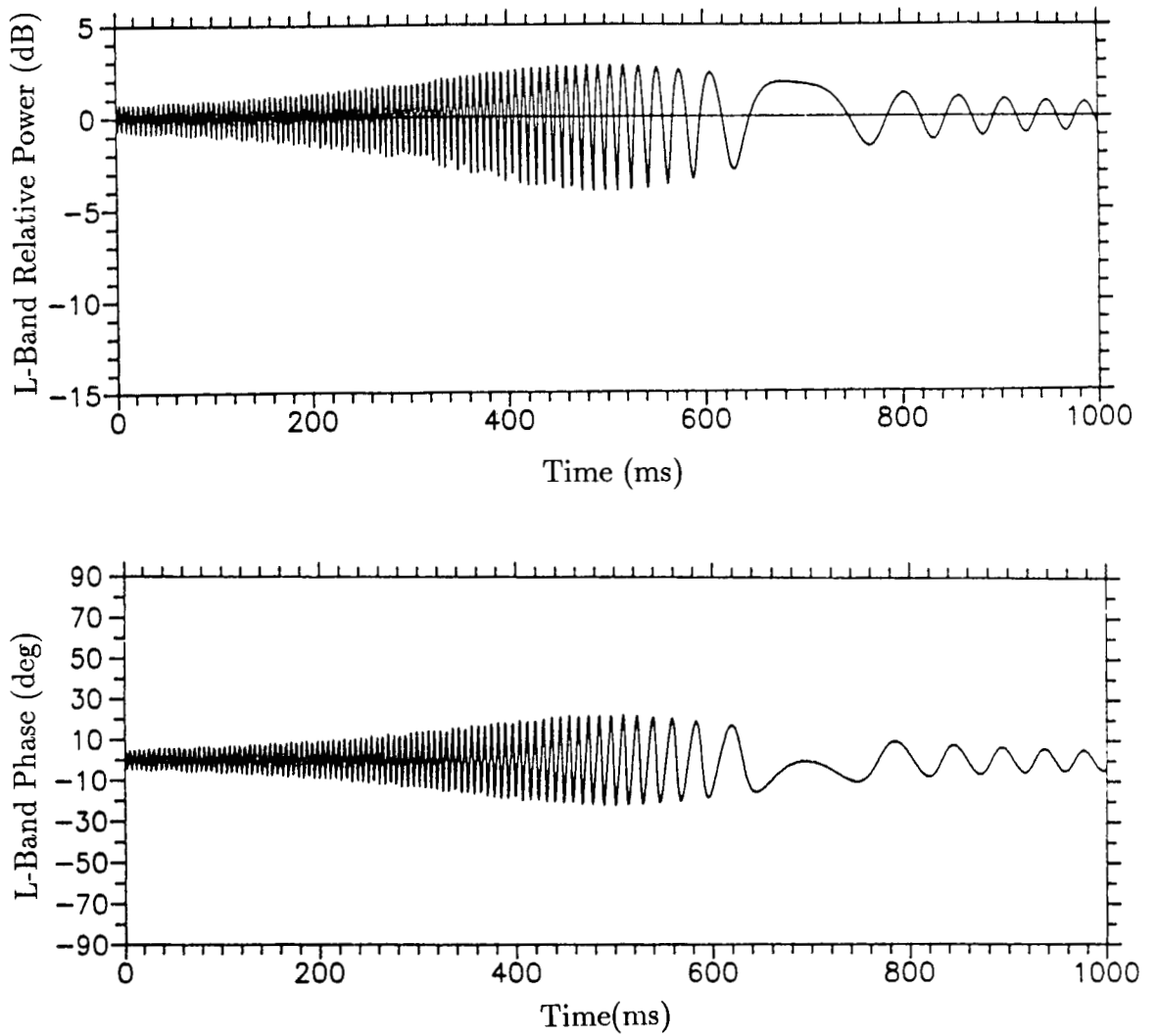


Figure 8.6: Calculated L-Band signal level and phase fluctuations as a function of time for geometry of Figure 8.5

scattering object is a wooden utility pole about 3 m to the right of and 4 m above the vehicle with a 32 m² radar cross section. The model predicts higher fluctuations before and after passing the pole, an indication that the scattering is in reality not isotropic.

Evaluating the model over a range of parameters, the following has been empirically determined:

1. The peak-to-peak fluctuations of the received signal level (dB) due to multipath vary with the inverse of the square root of the satellite elevation angle.
2. The multipath power (dB) varies as the inverse distance to the scatterer taken to the 4/3 power.
3. Assuming two frequencies (at L-Band) are simultaneously received, the rms deviation of the dB power difference between signal levels at the respective frequencies is proportional to the frequency difference. Employing this result, amplitude dispersion is found to be negligible for narrow band (bandwidth < 10 kHz) LMSS systems.

Fresnel Approaches to Tree Shadowing

Several simplifying methods have been used to assess the effect of shadowing by a single tree. Modeling a tree trunk as a very long opaque strip of equal width, a diffraction pattern was obtained by LaGrone and Chapman [1961] and compared to measurements at UHF frequencies. Taking account of the tree crown, two different two-dimensional tree models have been studied, both capable of achieving rough quantitative agreement with observations of tree shadowing. One assumed a tree to be composed of a number of finite, canted opaque strips of varying width and length, representing the silhouette of a tree with branches of various sizes [Vogel and Hong, 1988]. Attenuations of up to about 12 dB were calculated at L-Band versus 8 dB at UHF. Spatial fluctuations in the shadow of the tree were found to be faster with higher signal frequency and closer proximity to the tree during a simulated drive-by scenario. The maximum fade was proportional to the logarithm of the number of limbs. In the second approach [Yoshikawa and Kagohara, 1989], the tree crown was modeled as a triangle which obscures a wedge of the first Fresnel zone. By comparisons with measurements, the results have been shown to correctly explain the average decrease of attenuation with increasing distance of the receiver from the tree.

8.5.2 Multiple Object Scattering Models

Two-Dimensional Model

A two-dimensional geometric LMSS propagation model by Amoroso and Jones [1988] considered 1000 scatterers randomly distributed in an annular region with an outer radius of 2000 m and an inner radius of 400 m, corresponding to an average scatterer density of 12,000 m²/scatterer. The model has been used to correctly predict multipath Doppler spectra, both for omnidirectional and directive antennas. The simulated fading record of unmodulated carrier power for an omni-directional antenna shows unrealistic peak-to-peak variations of over 20 dB, however. This is the consequence of (1) using a two-dimensional approach, which eliminates realistic elevation angle and antenna effects, and (2) the avoidance of any scatterers in proximity to the vehicle, which in field measurements have been shown to dominate the signal variations in the absence of shadowing. The model therefore also overestimates delay spread.

Three-Dimensional Model

An extension to the single scatterer multipath model of Vogel and Hong [1988] allows a vehicle to be driven through a region with many randomly distributed, point-source multipath scatterers [Vishakantaiah and Vogel, 1989]. The output of the drive simulator yields time series of signal amplitude and phase as well as Doppler spectra, all for user-specified conditions. These outputs, in turn, can be used to calculate system performance parameters. The simulator does not consider shadowing, and this limits its application to very low fade margin systems, where multipath fading effects determine system performance most of the time.

In order to obtain the total field at the receiver due to many scatterers, the vector sum of the constant incident field and all the scattered fields e is formed similarly to (8.63) and the relative total power and phase are calculated from

$$P'_{\text{total}} = \sqrt{\left(1 + \sum e_{\text{real}}\right)^2 + \left(\sum e_{\text{imag}}\right)^2} \quad (8.67)$$

$$\text{Phase}_{\text{total}} = \arctan \left(\frac{\sum e_{\text{imag}}}{1 + \sum e_{\text{real}}} \right) \quad (8.68)$$

where the summation includes the real or imaginary parts of each scatterer's response e to the incident wave.

The model was validated by comparing the predicted power and phase assuming a single scatterer to the results from measurements, both with similar parameters as well as by comparing the calculated power spectral density to the one expected [Clarke, 1968]. Figure 8.7 demonstrates that the model produces the correct Doppler spectrum, centered on the received carrier frequency. The shape shows the typical signature of mobile multipath propagation, a sharply bandlimited spectrum with maximum power at the edges. The frequency deviation of the scattered wave (± 120 Hz) agrees with the value expected from the geometry. The signal level output of the model, assuming 1000 scatterers located in an annular region with radii of 400 and 2000 m, a drooping dipole antenna, and the height of the scatterers randomly distributed between 0 and 10 m, shows a peak-to-peak variation of less than 1.5 dB, a value in agreement with measurements made in locations where no scatterers are in the vicinity of the vehicle.

Similar cases to the one above, except for an outer radius of 500 m and the much higher average scatterer density of $625 \text{ m}^2/\text{scatterer}$, were examined with inner clearance radii from 30 to 400 m. The result demonstrates that multipath phenomena for LMSS scenarios are significant only if the scatterers are located close to the vehicle. The standard deviation of the logarithmic amplitude decreases monotonically with increasing inner clearance from 0.22 dB to 0.07 dB.

As an outgrowth of geometric modeling, it has been ascertained that when higher gain antennas are employed, the side of the road the scatterer is located influences the multipath fading [Vishakantiah and Vogel, 1989]. For example, assuming an antenna having an 80° half power beamwidth in both the azimuth and elevation planes, the multipath fading was 10 dB when a simulated scatterer (e.g., a utility pole) was placed between the vehicle and the satellite. Only 1 dB multipath fading occurred when the vehicle was between the scatterer and the satellite. This diminished fading for the latter case was caused by filtering of the signal by the antenna pattern. On the other hand, when an azimuthal omni-directional antenna was used, no change in the multipath fading (e.g., 10 dB) was observed for the two cases. In an environment with many scatterers at random heights and cross sections, the reduction of the fade fluctuations arising from lower versus higher gain antennas is not as extreme, but still significant. For the case of 500 scatterers (having random heights and cross

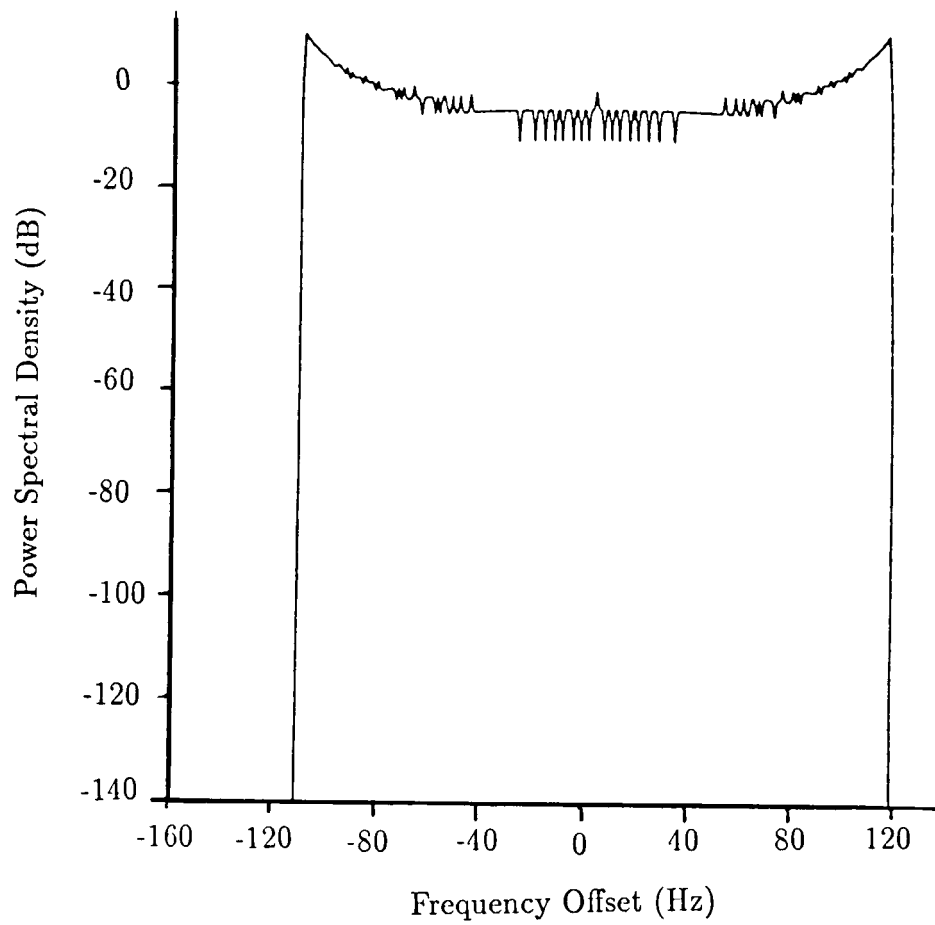


Figure 8.7: Calculated Doppler spectrum due to single multipath reflector averaged over one second, while the vehicle is driving past the scatterer.

sections) located at distances between 10 m to 300 m, the peak-to-peak fade fluctuations were reduced from 3.6 dB (for the lower gain antenna) to 0.8 dB (for the higher gain antenna).

Discussion

Two-dimensional simulation models overestimate multipath, because the elevation angle selectivity of the receiving antenna is neglected. Therefore they cannot be used to predict either amplitude, phase, or bandwidth effects realistically. The three-dimensional simulator demonstrates that only scatterers in the immediate vicinity of the receiver matter. As a consequence, the delay spread spectrum is narrow and has no detrimental impact on contemplated systems with channel bandwidths of 5 kHz.

Time-series produced with this model will give more realistic inputs to systems which analyze bit error performance than those based on statistical assumptions only as long as the no shadowing condition holds.

8.6 General Conclusions

The salient conclusions associated with model execution and development may be summarized as follows:

1. When the propagation path is unshadowed, Rician statistics apply most of the time, although the K-factor cannot strictly be assumed constant.
2. Signal variations in the clear path case are due to scattering from objects such as trees and utility poles in the vicinity of the vehicle, as weighted by the vehicle antenna pattern. Where these objects recede from or come closer to the vehicle, the K-factor decreases or increases, respectively.
3. When a single scatterer dominates, as might be the case with a utility pole, Rician statistics are no longer applicable and a geometrical analytical model must be used. This case is treated in Section 8.5.1.

4. Statistics of clear path K-factor variations have not been considered in any of the models.
5. Signal fluctuations for LMSS scenarios which are solely due to multipath scattering at path elevation angles above about 15° are less than 2 or 3 dB for 99% of the distance, consequently there may not be a need to have a more accurate description of "unshadowed propagation" than that given by applying Ricean multipath scattering models as given by (8.29) or by using geometric-analytic models of the type described in Section 8.5.
6. When the line-of-sight is completely blocked by continuous obstacles such as mountains, buildings, or overpasses, not enough power is contributed by multipath scattering to enable any communication through a satellite system with a commercially feasible fade margin of around 6 to 12 dB. In this case LMSS cannot be functional at all and what is required is some knowledge of the probability of blockage and its duration for specific path geometry. No separate statistical evaluations for the incidence of blockage are currently available.
7. In view of items 5 and 6, the major propagation model of interest should describe the condition of shadowing of roadside trees where complete blockage does not occur.
8. Simulation of time series of fade data for various conditions of tree shadowing is a requirement for analytically addressing fade mitigation techniques such as antenna diversity and error correction schemes.

8.7 Recommendations and Follow-On Efforts

Based on the results to date as examined in this text, the following represents a list of recommendations to fill the present modeling gaps for LMSS scenarios.

1. A comparative assessment of the various statistical models described in this Chapter is recommended.
2. In the absence of 1, the authors recommend the following:

* Designers interested in cumulative fade distributions should employ empirical models such as ERS (Section 3.3) or the Simplified Lognormal Model (Section 8.4.5) which are derived directly from measured data.

* Designers interested in fade durations and fade rates should employ Loo's model (Section 8.4.2) which appears to be the most mature.

3. Empirical models describing cumulative fade distributions should be developed from data bases associated with the following locations:

* regions in which elevation angles range between 0° to 20° . At angles near grazing, (e.g., northern latitudes), scintillations and refractive effects due to the troposphere may influence the fade statistics.

* regions where ionospheric scintillations are prevalent such as in the tropics (e.g., geostationary satellite communications) or auroral regions for cases in which communications exist with polar orbiting satellites.

4. Systematic measurements and modeling of wideband delay spread characteristics should be executed.

References

- Amoroso, F. and W. W. Jones [1988], "Modeling Direct Sequence Pseudonoise (DSPN) Signaling with Directional Antennas in the Dense Scatterer Mobile Environment," *38th IEEE Vehicular Technology Conference*, Philadelphia, PA, pp 419-426, 15-17 June.
- Barts, R. M. and W. L. Stutzman [1991], "Modeling and Simulation of Mobile Satellite Propagation," *IEEE Trans. Antennas Propagat.*, (in press).
- Barts, R. M., W. L. Stutzman, W. T. Smith, R. S. Schmier, and C. W. Bostian [1987], "Land Mobile Satellite Propagation Modeling," *Proc of the 1987 IEEE A&P Society International Symposium*, Vol. 1, pp 20-23.
- Bell, T.E. [1988], "Technology 88 - Communications," *IEEE Spectrum*, pp 41-43, Jan.
- Bundrock, A. and R. Harvey [1988], "Propagation Measurements for an Australian Land Mobile-Satellite System," *Proc. of Mobile Satellite Conference*, pp 119-124.
- Butterworth, J. S. [1984a], "Propagation Measurements for Land-Mobile Satellite Systems at 1542 MHz," *Commun. Res. Cent.*, Ottawa, Canada Tech. Note 723, Aug.
- Butterworth J. S. [1984b], "Propagation Measurements for Land-Mobile Satellite Services in the 800 MHz Band," *Commun. Res. Cent.*, Ottawa, Canada Tech. Note 724, Aug.
- Butterworth, J. S. and E. E. Matt [1983] "The Characterization of Propagation Effects for Land Mobile Satellite Services," *IEE 3rd International Conference on Satellite Systems*

- for Mobile Communications and Navigation; Conference Publication No. 222*, London, U.K., June 7-9, pp 51-54.
- CCIR [1986a], *Recommendations and Reports of the CCIR*, Volume V, Propagation in Non-Ionized Media, International Telecommunications Union, Geneva, Switzerland.
- CCIR [1986b], *Recommendations and Reports of the CCIR*, Volume VI, Propagation in Ionized Media, International Telecommunications Union, Geneva, Switzerland.
- Clarke, R. H. [1968], "A Statistical Theory of Mobile-Radio Reception," *Bell System Technical Journal*, Vol. 47, No. 6, July-August, pp 957-1000.
- Cygan, D., M. Dippold and J. Finkenzeller [1988], "Kanalmodele fuer die Satellitengestuetzte Kommunikation Landmobiler Teilnehmer," *Archiv fuer Elektronik und Uebertragungstechnik*, Vol. 42, No. 6, pp 329-339.
- Davies, K. [1990], *Ionospheric Radio*, IEE/Peter Peregrinnus Ltd, London, U.K.
- Flock, W. L. [1987], "Propagation Effects on Satellite Systems at Frequencies Below 10 GHz; A Handbook for Satellite System Design (Second Edition)," *NASA Reference Publication* 1108 (02), December.
- Goldhirsh, J. and W. J. Vogel [1987], "Roadside Tree Attenuation Measurements at UHF for Land-Mobile Satellite Systems," *IEEE Trans. Antennas Propagat.*, Vol. AP-35, pp. 589-596, May.
- Goldhirsh, J. and W. J. Vogel [1989], "Mobile Satellite System Fade Statistics for Shadowing and Multipath from Roadside Trees at UHF and L-band," *IEEE Trans. Antennas Propagat.*, Vol. AP-37, No. 4, pp. 489-498, April.
- Hase, Y., W. J. Vogel, and J. Goldhirsh [1991], "Fade-Durations Derived from Land-Mobile-Satellite Measurements in Australia," *IEEE Trans. Communications*, Vol. 39, No. 5, pp. 664-668, May
- Hess, G. C. [1980], "Land-Mobile Satellite Excess Path Loss Measurements," *IEEE Trans. on Vehicular Tech.*, Vol. VT-29, No. 2, pp. 290-297, May.
- Hodge, D. B. [1978], "Path Diversity for Earth-Space Communication Links," *Radio Sci.*, Vol. 13, No. 3, pp. 481-487.

- Huck, R. W., J. S. Butterworth, and E. E. Matt [1983], "Propagation Measurements for Land Mobile Satellite Services," *33rd IEEE Vehicular Technology Conference*, Toronto, pp 265-268.
- Jakes, W. C., Jr. (Editor) [1974], *Microwave Mobile Communications*, Wiley, New York.
- Jongejans, A., A. Dissanayake, N. Hart, H. Haugli, C. Loisy, and R. Rogard [1986], "PROSAT-Phase 1 report," *European Space Agency Tech. Rep. ESA STR-216*, May (European Space Agency, 8-10 Rue Mario-Nikis, 75738 Paris Cedex 15, France.)
- LaGrone, A. H. and C. W. Chapman [1961], "Some Propagation Characteristics of High UHF Signals in the Immediate Vicinity of Trees," *IRE Trans. on Antennas and Propagat.*, Vol. AP-9, September, pp. 487-491.
- Lee, W. C. Y. [1986], *Mobile Communications Design Fundamentals*, H. W. Sams and Co., Indianapolis, Indiana.
- Loo, C. [1985], "A Statistical Model for A Land Mobile Satellite Link," *IEEE Trans. on Vehicular Technol.*, Vol. VT-34, No. 3, August, pp. 122-127.
- Loo, C. [1987], "Measurements and Models of A Land Mobile Satellite Channel and Their Applications to MSK Signals," *IEEE Trans. on Vehicular Technol.*, Vol. VT-35, No. 3, August, pp. 114-121.
- Lutz, E., W. Papke, and E. Ploechinger [1986], "Land Mobile Satellite Communications - Channel Model, Modulation and Error Control," *Seventh International Conference on Digital Satellite Communications*, 12 - 16 May, pp. 537-543.
- Papoulis, A. [1965], *Probability, Random Variables, and Stochastic Processes*, McGraw-Hill, New York.
- Reed, H. R., and C. M. Russel [1966], *Ultra High Frequency Propagation*, Boston Technical Publishers, Inc., Cambridge, MA.
- Renduchintala, V.S.M., H. Smith, J.G. Gardiner, and I. Stromberg [1990], "Communications Service Provision to Land Mobiles in Northern Europe by Satellites in High Elevation Orbits - Propagation Aspects," *40th International Conference on Vehicular Technology*, May 6-9, Orlando, Florida (IEEE VTC '90).

- Saruwatari, T., and H. Ryuko [1989], "Propagation Characteristics For Land Mobile Satellite Systems in 1.5 GHz Band," *Proc. of 1989 International Symposium on Antennas and Propagation (ISAP '89)*, Tokyo, Japan, pp 769-772.
- Smith, H., V. S. M. Renduchintala, and J. G. Gardiner [1990], "Assessment of the Channel Offered by A High Elevation Orbit Satellite to Mobiles in Europe - Narrowband Results, Wideband Experiments," *IEE Conference on Radio Receivers and Associated Systems*, Churchill College, Cambridge, UK, July.
- Smith, W. T. and W. L. Stutzman [1986], "Statistical Modeling for Land Mobile Satellite Communications," Virginia Tech Report EE Satcom 86-3 Virginia Tech, Blacksburg, VA, August.
- Ulaby, F. T., M. W. Whitt, and M. C. Dobson [1990], "Measuring the Propagation Properties of A Forest Canopy Using A Polarimetric Scatterometer," *IEEE Trans. Antennas Propagat.*, Vol. AP-38, No. 2, pp. 251-258, Feb.
- Vishakantaiah, P. and W. J. Vogel [1989], LMSS Drive Simulator for Multipath Propagation," *Proc. of NAPEX XIII*, San Jose, CA, 29-30 June, pp 42-47 (Jet Propulsion Laboratory Publication JPL 89-26).
- Vogel, W. J., and J. Goldhirsh [1986], "Tree Attenuation at 869 MHz Derived from Remotely Piloted Aircraft Measurements," *IEEE Trans. Antennas Propagat.*, Vol. AP-34, No. 12, pp. 1460-1464. Dec.
- Vogel, W. J., and U.-S. Hong [1988], "Measurement and Modeling of Land Mobile Satellite Propagation at UHF and L-band," *IEEE Trans. Antennas Propagat.*, Vol. AP-36, No. 5, pp 707-719, May.
- Vogel, W. J., and J. Goldhirsh [1988], "Fade Measurements at L-band and UHF in Mountainous Terrain for Land Mobile Satellite Systems," *IEEE Trans. Antennas Propagat.* Vol. AP-36, No. 1, pp. 104-113, June.
- Vogel, W. J., and J. Goldhirsh [1990], "Mobile Satellite System Propagation Measurements at L-Band Using MARECS-B2" *IEEE Trans. Antennas Propagat.*, Vol. AP-38, no 2, pp 259-264, Feb.
- Vogel, W. J., J. Goldhirsh, and Y. Hase [1991], "Land-Mobile-Satellite Fade Measurements in Australia," *AIAA Journal of Spacecraft and Rockets*, July-August.

- Wakana, H. [1991], "A Propagation Model for Land-Mobile-Satellite Communication," *1991 North American Radio Science Meeting and IEEE/APS Symposium*, The University of Western Ontario, London, Ontario, Canada June 24-28, 1991.
- Weissberger, M. A. [1981], "An Initial Critical Summary of Models for Predicting the Attenuation of Radio Waves by Foliage," ECAC-TR-81-101, *Technical Report of Electromagnetic Compatibility Analysis Center*, Annapolis, Maryland.
- Yoshikawa, M., and M. Kagohara [1989], "Propagation Characteristics in Land Mobile Satellite Systems," *39th IEEE Vehicular Technology Conference*, 1-3 May, pp. 550-556.

Index

- absorption, 5
- AFD (average fade duration), 91
- aircraft platform, 8
- Amoroso, F., 109, 115
- antennas**
 - crossed drooping dipole, 78, 84
 - diversity spacing, 55
 - gain pattern effects, 34, 51, 52
 - high versus low gain, 52, 54
 - low gain, 78
 - quarter wave, 85
 - separation (diversity), 51, 56
- ATS-6 (measurements with), 70, 79
- attenuation (mobile)**
 - angle dependence, 19-27
 - cross polarization effects, 52-53
 - diversity operation, 55-60
 - Empirical Roadside Shadowing (ERS)
 - model, 16-27
 - fade duration, 40-46
 - frequency (effects of), 27
 - high-gain versus low gain antennas, 52-54
 - investigations from different countries, 61-73
 - INMARSAT (with), 4, 15, 24, 26, 63
 - Japanese ETS-V (with), 2, 4, 11, 15, 16, 23, 26, 40, 63, 72
 - L-Band (measurements at), 15
 - L-Band versus UHF, 25, 28
 - line-of-sight, 34-39
 - MARECS A (with), 68
 - MARECS-B2 (with), 4, 15, 66
 - modeling, 74-114
 - non-fade duration, 46, 47
 - phase fluctuations, 48-50
 - roadside trees, 15-33
 - season (effects of), 28, 29
 - side of road (effects of), 29-33
 - time-series, 16-18
 - UHF (measurements at), 15
- attenuation (static)**
 - bare trees (effects of), 12
 - Burr Oak, 9
 - Callery Pear, 9, 12, 13
 - canopy, 6
 - coefficients, 7-9, 11
 - elevation angle (effects of), 12, 14
 - frequency scaling, 11
 - full foliage (effects of), 12
 - grove of trees, 7
 - grove path length, 6
 - Holly, 9
 - individual trees, 5-14
 - L-Band, 15
 - Norway Maple, 9
 - path length, 6-8
 - Pin Oak, 9

- pine grove, 9
- Sassafras, 9
- Scotch Pine, 9
- seasonal effects (static case), 11
- single tree, 7
- static, 5-14
- summer, 12
- trees (full foliage), 8
- tree types, 8, 9
- UHF, 15
- White Pine, 9
- winter, 12
- Australian campaign, 15, 16, 23, 40, 41, 56, 86
- average fade duration (AFD), 91
- balloons (stratospheric), 71
- bandwidth, 3
- Barts, R. M., 97, 115
- Belgium (measurements in), 68, 69
- Bell, T. E., 3, 115
- Big Thompson Canyon (measurements in), 35
- Boulder Canyon (measurements in), 35
- Brewster angle, 78
- Bundrock, A., 1, 27, 63-65, 115
- Burr Oak, 9
- Butterworth, J. S., 1, 6, 8, 63, 66-68, 115
- Callery Pear, 9, 12
- campaigns, 4
- Canada (cumulative distributions), 63, 66-68
- canopy shadowing, 20, 42
- CCIR; 1986a**
 - Report 1008, 78, 116
 - Report 1007, 87, 116
- CCIR: 1986b**
 - Report 263-6, 77, 116
- cellular communications, 2, 3, 12
- Central Limit Theorem, 88
- Central Maryland (measurements in), 8, 15, 40
- Chapman, C. W., *see* LaGrone, A. H., 108, 117
- circular polarization, 7, 77,
- Clarke, R. H., 110, 116
- Colorado (measurements in), 15
- co-polarization, 52
- crossed drooping dipole, 78, 84
- cross polarization, 52, 53
- cumulative distributions**
 - Canada (fade measurements in), 63
 - canyons (fade measurements in), 35
 - England (fade measurements in), 68, 70
 - Empirical Roadside Shadowing Model (ERS), 16-27
 - fade durations, 41
 - Japan (fade measurements in), 72
 - joint (diversity gain), 56, 57
 - modeling of, 86-102
 - non-fade durations, 46
 - phase fluctuations, 48, 49
 - rural/farmland (fade measurements), 67, 68
 - rural/forested (fade measurements), 67, 68
 - seasonal effects (fade measurements), 29
 - suburban (fade measurements), 67, 68
 - roadside trees (fade measurements), 38
 - United States (measurements in), 4, 16-27, 71, 79-85
- Cygan, D., 100, 116
- Davies, K., 77, 116

- deciduous trees, 19, 28
delay spread, 114
density functions
 lognormal, 89
 Nakagami-Rice, 87
 Rayleigh, 75, 86, 88, 90
Denver (measurements in), 71
diffuse scattering, 76
digital filtering, 41
dipole (crossed drooping), 78
distribution fits
 exponential (fade), 39, 43
 logarithmic (fade), 17
 lognormal (fade duration), 45
 polynomial (phase), 50
 power fits (fade, non-fade duration) 36,
 47
diversity gain, 56, 58, 60
diversity improvement factor, 56, 59
diversity operation, 55-60
Doppler
 shift, 41, 48, 76, 92
 spectrum, 78, 110, 11
drooping dipole, 110
durations (fade), 40, 41, 44, 45
elevation angle (attenuation effects of), 12,
 16, 20, 80
empirical regression models, 78-86
Empirical Roadside Shadowing model (ERS),
 16-27, 63, 71, 85
England (measurements in), 68, 70
ESA (European Space Agency), 68
ETS-V (measurements with), 2, 4, 11, 15,
 16, 23, 26, 40, 63, 72
Eucalyptus tree, 23, 63
experimental campaigns, 4, 61-73
experimental parameters, 4, 10, 24, 55
extreme shadowing, 42
fade
 bursts, 86
 durations, 23, 40, 40-46
 frequency scaling (static case), 11
 median, 8
 non-fade durations, 46, 47
 reduction, 31, 29, 58
 time-series, 17, 18
fade state transition models, 100-102
Faraday rotation, 77
Flock, W. L., 1, 77, 78, 116
fluctuations (signal level), 106
foliage, 8, 12
follow-on efforts, 113
frequency
 re-use, 52, 53
 scaling (dynamic case), 27
 scaling factor, 11
 scaling (static case), 11
Fresnel region, 7, 76, 78
Gaussian processes, 92
geographic regions, 61
geometric-analytic models, 103-114
geostationary satellites, 2, 4, 11, 15, 16, 23,
 24, 26, 40, 63, 67, 68, 72
Gilbert-Elliott model, 100
Goldhirsh and Vogel, 6, 7, 12, 29, 116
Goldhirsh, J. *see* Vogel et al., 7, 15, 16, 118
ground reflected waves, 77, 78
grove of trees, 5-7
Harvey, R., *see* Bundrock, A., 27, 63-65,
 115
Hase et al., 15, 40, 48, 116
Hase, Y., *see* Vogel et al., 15, 16, 118
helicopter (measurements with), 2, 7, 15,
 16

- Hess, G. C., 1, 70, 79, 116
high versus low gain antennas, 52, 54
Hodge, D. B., 58, 116
Holly, 19
Hong, U. S., *see* Vogel, W. J., 71, 103, 108, 118
Huck, R. W., 63, 116
INMARSAT Pacific (measurements with), 2, 15, 26, 63
investigations (different countries), 61–73
ionosphere, 77, 114
isolation, 52, 78, 84
Jakes, W. C., 74, 92, 117
Jones, W. W., *see* Amoroso, F. 109, 115
Jongejans et al., 1, 117
Japan (cumulative distributions), 72
Japanese ETS-V, 15, 16, 26, 40, 72
joint probabilities, 56, 57
Jones, W. W., *see* Amoroso, F., 109, 115
Jongejans et al., 1, 68, 117
K factor, 87
Kagohara, M., *see* Yoshikawa, M., 6, 11, 108, 117
LaGrone, A. H., 108, 117
lane diversity, 29
large scale–small scale model, 79–86
L-Band (measurements at), 15
L-Band versus UHF, 11, 27, 28
Lee, W. C. Y., 74, 117
level crossing rate (LCR), 91
line-of-sight, 7, 34–39
LMSS scenarios, 6
lognormal fade distribution, 41, 75, 44, 86, 89
Lognormal Shadowing Model, 95
Loo, C., 49, 90, 91, 117
Loo's distribution model, 90–92
Lutz, E. W., 93, 117
MARECS A (measurements with), 63
MARECS-B2 (measurements with), 15, 16, 66
maritime, 3
Markov model, 100
Markov transitions, 102
mobile attenuation, 15–33
Maryland (measurements in) 8, 15, 40
Matt, E. E., *see* Butterworth, J. S., 63, 115
measurements in
 Australia, 63
 Belgium, 69
 Big Thompson Canyon, 35
 Boulder Canyon, 35
 Canada, 8, 63, 92
 Colorado, 15
 Denver, 71
 England, 70
 Japan, 72
 Maryland, 8, 15, 40
 New Mexico, 15
 Texas, 15
median fade level, 8
mobile van, 10, 35, 55
models
 cumulative distributions *see* cumulative distributions
 empirical regression fits, 78–86
 Empirical Roadside Shadowing Model (ERS), 16–27, 63, 85
 fade-state transitions, 100–102
 geometric-analytic, 75, 103–114
 Hess, 79–84
 large scale–small scale (LS-SS), 79–85
 Lognormal Shadowing, 95, 96
 Loo's distribution, 90–92

- multiple object scattering, 109–112
- probability distribution, 75, 86–102
- Simplified Lognormal, 97
- single object, 103–108
- Total Shadowing, 93–95
- modeling for LMSS, 74–114
- moderate shadowing, 42
- mountain (multipath effects), 34–37
- multipath**
 - canyons, 35
 - elevation angle dependence, 38
 - mountains, 34–37
 - roadside trees, 34, 37–39
 - scattering, 5, 7
 - power, 88
- multiple object models, 109–112
- Nakagami-Rice density function, 87
- New Mexico (measurements in), 15
- non-fade durations, 40, 46
- Norway Maple, 9
- Ottawa, Canada (measurements in), 8
- overhanging tree canopies, 42
- Papoulis, A., 87, 88, 117
- path length, 6–8, 12
- percentage of optical shadowing (POS), 19
- phase fluctuations, 48–50
- phase shifts, 16–18, 40, 41, 106, 107
- Pin Oak, 8, 9
- Pine grove, 9
- point scatterer, 103
- polarization**
 - circular, 7, 77, 78
 - Faraday rotation, 77
 - frequency re-use, 52, 53
- probability distributions *see* cumulative distributions
- probability distribution models, 86–102
- PROSAT, 66
- Rayleigh distribution, 75, 86, 88, 90
- receiver (characteristics of), 7, 10, 55
- recommendations, 113
- Reed, H. R., 78, 117
- references, 115–118
- remotely piloted aircraft (measurements with)
 - 2, 7, 8
- Renduchintala et al., 1, 70, 117
- Ricean density function, 75, 86–88, 92
- roadside trees, *see* attenuation (mobile)
- Russel, C. M. *see* Reed, H. R., 78, 117
- Ryuko, H., *see* Saruwatari, T., 72, 117
- sampling rate, 8
- sample size, 8
- Saruwatari, T., 72, 117
- Sassasafras tree, 9
- scattering**
 - diffuse, 76
 - ground, 76
 - multiple, 5
 - multipath, 7
 - tree canopies 5, 37
 - tree trunks, 5
- scintillations, 114
- Scotch Pine, 9
- seasonal effects (on attenuation), 12, 28, 29
- shadowing, 7, 16, 20, 19, 42, 45, 86
- signal fluctuations, 106
- Simplified Lognormal Shadowing model, 97–100
- single object models, 103–108
- single tree attenuation, 7, 9
- Smith, H., 70, 118
- Smith, W. T., 95, 118
- space diversity, 55
- specular reflection, 77, 78

- speed of van, 41
static attenuation, 5-14
static attenuation coefficient, 7
stratospheric balloons (measurements with)
 2, 15, 71
Stutzman, W. L., *see* Smith, W. T., , 95,
 118
suburban-rural measurements, 81
summer attenuation, 28
Texas (measurements in), 77
The Johns Hopkins University, 1
The University of Texas, 1, 71
time-series of fades, 16, 17
time-series of phases, 17, 18
total electron content (TEC), 77
Total Shadowing model, 93-95
transmitter characteristics, 7, 8, 10, 16, 25
Trees
 bare (attenuation of), 12
 branches (attenuation of), 12
 Burr Oak, 9
 canopies 5, 20, 42
 Callery Pear, 9, 12, 13
 dimensions, 8, 12
 Eucalyptus, 23
 grove of, 5
 Holly, 9
 modeling, 108
 Norway Maple, 9
 Pin Oak, 8
 Sassafras, 9
 Scotch Pine, 9
 trunks, 5
 types (attenuation), 8, 9
 White Pine, 9
tropospheric effects, 114
UHF (measurements at), 15
Ulaby et al., 6, 11, 118
United States (measurements in), 4, 16-27,
 71, 79-85
urban measurements, 79-85
utility poles, 20, 106
validation of ERS model, 23, 25, 26
Vishakantaiah, P., 109, 118
Vogel, W. J. *see* Vishakantaiah, P., 109,
 118
Vogel and Goldhirsh, 7, 15, 118
Vogel and Hong, 71, 103, 108, 118
Vogel et al., 15, 16, 23, 40, 118
Wakana, H., 102, 118
Wallops Island, VA. (measurements in), 8
WARC 1987, 3
Weissburger, M. A., 6, 119
White Pine, 9
winter attenuation, 28
Yoshikawa, M., 6, 11, 108, 119

REPORT DOCUMENTATION PAGE			Form Approved OMB No. 0704-0188	
Public reporting burden for this collection of information is estimated to average 1 hour per response, including the time for reviewing instructions, searching existing data sources, gathering and maintaining the data needed, and completing and reviewing the collection of information. Send comments regarding this burden estimate or any other aspect of this collection of information, including suggestions for reducing this burden, to Washington Headquarters Services, Directorate for Information Operations and Reports, 1215 Jefferson Davis Highway, Suite 1204, Arlington, VA 22202-4302, and to the Office of Management and Budget, Paperwork Reduction Project (0704-0188), Washington, DC 20503.				
1. AGENCY USE ONLY (Leave blank)	2. REPORT DATE February 1992	3. REPORT TYPE AND DATES COVERED Reference Publication		
4. TITLE AND SUBTITLE Propagation Effects for Land Mobile Satellite Systems: Overview of Experimental and Modeling Results			5. FUNDING NUMBERS RTOP 643-10-03	
6. AUTHOR(S) Julius Goldhirsh Wolfhard J. Vogel				
7. PERFORMING ORGANIZATION NAME(S) AND ADDRESS(ES) The Johns Hopkins University Applied Physics Laboratory Johns Hopkins Road Laurel, MD 20707			8. PERFORMING ORGANIZATION REPORT NUMBER	
The University of Texas Electrical Engineering Research Laboratory 10100 Burnett Road Austin, TX 78758				
9. SPONSORING/MONITORING AGENCY NAME(S) AND ADDRESS(ES) National Aeronautics and Space Administration Washington, DC 20546 Office of Commercial Programs			10. SPONSORING/MONITORING AGENCY REPORT NUMBER NASA RP-1274	
11. SUPPLEMENTARY NOTES Goldhirsh: The Johns Hopkins University, Applied Physics Laboratory, Laurel, MD. Vogel: The University of Texas, Electrical Engineering Laboratory, Austin, TX.				
12a. DISTRIBUTION/AVAILABILITY STATEMENT Unclassified-Unlimited Subject Category 32			12b. DISTRIBUTION CODE	
13. ABSTRACT (Maximum 200 words) The period from 1980 to 1990 saw numerous experiments carried out and models developed with the objective of characterizing the propagation environment associated with the provision of land mobile communications using satellites. Experiments were carried out with transmitters on stratospheric balloons, remotely piloted aircraft, helicopters, and geostationary satellites. This text assembles the experimental results in a single source for use by communications engineers, designers of planned Land Mobile Satellite Systems (LMSS), and modelers of propagation effects. The results given here are mostly derived from systematic studies of propagation effects for LMSS geometries in the United States associated with rural and suburban regions. Where applicable, the authors also draw liberally from the results of other related investigations in Canada, Europe, and Australia. Frequencies near 1500 MHz are emphasized to coincide with the frequency bands allocated for LMSS by the International Telecommunication Union although earlier experimental work at 870 MHz is also included.				
14. SUBJECT TERMS Radio Wave Propagation, Land Mobile Satellite Communications Systems, L-band propagation, UHF propagation			15. NUMBER OF PAGES 138	
			16. PRICE CODE A07	
17. SECURITY CLASSIFICATION OF REPORT Unclassified	18. SECURITY CLASSIFICATION OF THIS PAGE Unclassified	19. SECURITY CLASSIFICATION OF ABSTRACT Unclassified	20. LIMITATION OF ABSTRACT	